The role of cellular prion protein on exosomes in the molecular pathogenesis of Alzheimer's disease

Dissertation zur Erlangung des Doktorgrades

an der Fakultät für Mathematik, Informatik und Naturwissenschaften

Fachbereich Biologie

der Universität Hamburg

vorgelegt von Clemens Friedrich Falker-Gieske

Hamburg, 2014

Tag der Disputation: 27.02.2014

Erstgutachter: Prof. Dr. Markus Glatzel

Zweitgutachter: Prof. Dr. Thorsten Burmester

Table of contents

List of figures

List of tables

Abbreviations

aa	Amino acid
αAPP CTF or C83	Small C-terminal APP fragment
Aβ	Amyloid beta
AD	Alzheimer's disease
ADAM	A disintegrin metalloprotease
AICD	APP intracellular domain
Amp	Ampicillin
APH-1	Anterior pharynx-defective 1
APLP1	APP-like protein-1
APLP2	APP-like protein-2
ApoE	Apolipoprotein E
APOE	Gene encoding apolipoprotein E
APP	Amyloid precursor protein
APPsα	Large N-terminal fragment of APP
APPsβ	Large part of the ectodomain of APP
APS	Ammonium persulfate
AV	Apoptotic vesicle
BACE1	b-site APP cleaving enzyme-1
βAPP CTF or C99	APP C-terminal fragment
BSA	Bovine Serum Albumin
BSE	Bovine spongiform encephalitis
C1	Carboxy-terminal part of the cellular prion protein
cDNA	Complementary DNA
CHO	Chinese hamster ovary
C-terminus	Carboxy terminus
DAPI	4',6-diamidino-2-phenylindole
DIC	Differential interference contrast
DMEM	Dulbecco's modified Eagle medium
DMEM-F12	Dulbecco's modified Eagle's F12 medium
DMSO	Dimethyl sulfoxide
DNA	Deoxyribonucleic acid
DSB	Double-strand break
EGCase	Endoglycoceramidase
EDTA	Ethylene diamine tetra-acetic acid
EV	Extracellular vesicle
FACS	Fluorescence-activated cell sorting
FBS	Fetal bovine serum
FDA	Food and Drug Administration
Fyn	Tyrosine-protein kinase

G418	Gentamycin
GPI	Glycophosphatidylinositol
GSLs	Glycosphingolipids
Hpl3-4	*Prnp*$^{0/0}$ hippocampal cells
HPLC	High performance liquid chromatography
hsp70	70 kilo dalton heat shock protein
HW8-1	Wild type hippocampal cells
IPTG	Isopropyl β-D-1-thiogalactopyranoside
IRES	Internal ribosome entry site
kDa	Kilo dalton
LTP	Long term potentiation
MES	2-ethanesulfonic acid
mPrP-KO-Cas	*Prnp* knockout cassette
miRNA	Micro RNA
mRNA	Messenger RNA
MV	Microvesicle
N1	Amino-terminal part of the cellular prion protein
N2a	Murine Neuro 2a neuroblastoma cells
N2a-PrP$^{0/0}$	N2a *Prnp* knockout cells
NHEJ	Non-homologous end joining
NLS	Nuclear localization signal
NMDA	N-methyl-D-aspartate
NTA	Nanoparticle tracking analysis
N-terminus	Amino terminus
O/N	Overnight
PBS	Phosphate buffered saline
PCR	Polymerase chain reaction
PEN-2	Presenilin enhancer 2
PFA	Paraformaldehyde
PLD3	Phospholipase D3
Prnp	Murine gene encoding the cellular prion protein
PrP^{C}	Cellular prion protein
PrP^{Sc}	PrP scrapie
PS	Presenilin
PSEN1	*Presenilin 1* gene
PSEN2	*Presenilin 2* gene
qPCR	Quantitative PCR
RIPA	Radioimmunoprecipitation assay
RNA	Ribonucleic acid
RNAi	RNA interference
RVD	Repeat-variable di-residue
SDS	Sodium dodecyl sulfate

SH-SY5Y-PrP(+)	Human neuroblastoma cells transfected with human PrPC
SH-SY5Y-PrP(-)	Human neuroblastoma cells transfected with empy IRES vector
Spec	Spectinomycin
TAL	Transcription activator-like
TALEN	Transcription activator-like effector nuclease
TEMED	Tetramethylethylenediamine
Tet	Tetracycline
TREM2	Triggering receptor expressed on myeloid cells 2
UTR	Untranslated region
ThT	Thioflavin T
WT	Wild type
X-Gal	5-bromo-4-chloro-3-indolyl-beta-D-galacto-pyranoside

1 Introduction

1.1 Alzheimer's disease (AD)

Alzheimer's disease (AD) is the most common form of dementia affecting more than 25 million people worldwide and is one of the leading causes of death in the elderly in western countries[1,2]. Pathological hallmarks of the disease are cerebellar atrophy as well as the formation of neurofibrillary tangles and the deposition of amyloid plaques in the brain (Figure 1.1)[3]. Neurofibrillary tangles consist of aggregated hyperphosphorylated tau protein[4] and amyloid plaques are mainly aggregates of amyloid beta (Aβ)[5,6].

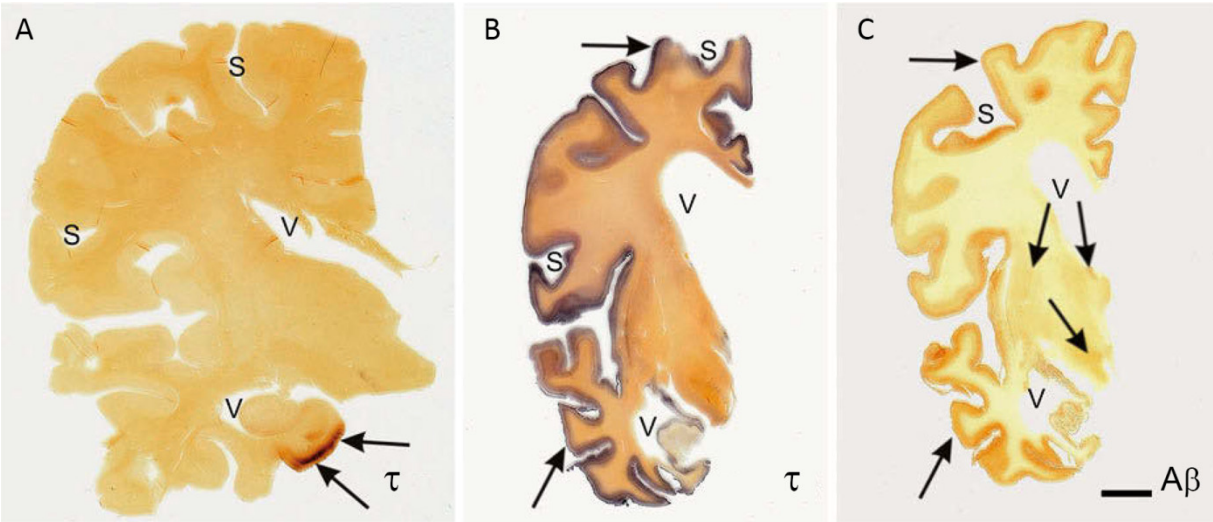

Figure 1.1: Sections of healthy and AD brains.

(A) Healthy brain shows more intact gyri compared to the AD brain and hyperphosphorylated tau (τ) is only detectable in the entorhinal cortex (indicated by arrows). (B) The brain of an AD patient displays shrinkage of the gyri, enlarged sulci, and enlarged ventricles. Hyperphosphorylated tau is detectable throughout the whole cortex (indicated by arrows). (C) Aβ staining of an AD brain shows heavy amyloid plaque load in the cortex (indicated by arrows; S: sulcus, V: ventricle; scale bar=6mm; modified from Klöppel 2012)[7].

Aβ, the product of sequential proteolytic processing of the amyloid precursor protein (APP), is released to the extracellular space[8]. According to the amyloid-hypothesis, generation and extracellular deposition of Aβ leads to neurodegeneration[9,10]. Small soluble pre-fibrillar Aβ species are thought to represent the neurotoxic entity causing synaptic dysfunction and dendritic spine loss[11,12]. The molecular pathways leading to neurodegeneration in AD are not yet fully understood.

1.1.1 History

AD was discovered and firstly described by the German psychiatrist and neuropathologist Alois Alzheimer in 1906[13,14]. Alzheimer described the case of Auguste D., who was suffering from memory loss, unsubstantiated suspicion towards her family, and several other psychological changes. Autopsy of her brain revealed severe cerebral shrinkage and abnormal deposits around nerve cells[15]. The first description of plaque formation in grey matter was done by Blocq and Marinesco in 1892[16]. Teofil Simchowicz, who worked under Alois Alzheimer from 1907 to 1910, postulated an association between these bodies and amyloid dementia[17]. In the eighth edition of his book “Psychiatrie” in 1910, Emil Kraepelin introduced the term “Alzheimer’s disease”[18].

1.1.2 Disease characteristics

The earliest and most prevalent feature of AD is impairment of episodic memory along with deficits in language, semantic memory, executive functioning, visuospatial abilities, and cognitive impairment. Over the course of disease these symptoms worsen until patients are bed-ridden and eventually die due to loss of bodily functions[19]. Biological markers of AD can already be found years before the presentation of clinical symptoms[20]. Furthermore, clinical characteristics of early symptoms of AD could be spatially correlated with brain regions affected in those patients[21]. The earliest neurofibrillary changes are usually observable in medial temporal lobe structures like the hippocampus or the entorhinal cortex - neural networks crucial for episodic memory[22]. This most likely leads to deficits in learning and memory as well as an impairment of long term potentiation (LTP), the clinical hallmarks of AD[19]. Amyloid pathology is thought to occur years before disease onset[23] and mostly affects regions that project numerous axons to medial temporal lobe structures[24,25]. An early symptom in AD patients is a loss of working memory (also called short term memory), which refers to a processing system responsible for temporary memorization of multiple pieces of transitory information, where this information can be manipulated[26]. In late stage AD all aspects of working memory are found to be defective[27] resulting in the inability to memorize new information.

1.1.3 Prevalence, epidemiology, genetics and therapy of AD

Based on the age of onset, AD can be divided in to two subtypes. Early-onset AD comprises cases that become symptomatic before the age of 60-65 whereas patients older than 60-65 years belong to the group of late-onset AD. Only 1% to 6% of AD cases are early-onset and 60% of these cases have a familial history of AD. 13% of these familial cases are inherited, autosomal-dominant and can be identified over at least three generations[28,29] Apart from these few exceptions of autosomal-dominant inherited familial cases, most AD cases present as complex disorders involving multiple causative genes and/or environmental factors (see Section 1.1.7)[30]. More than 25 million people worldwide currently suffer from AD with about 5 million new cases every year[1]. The risk for AD increases with age (Figure 1.2) and with the World population growing older the number of AD cases is expected to rise linearly to over 80 million cases by the year 2040[31,32].

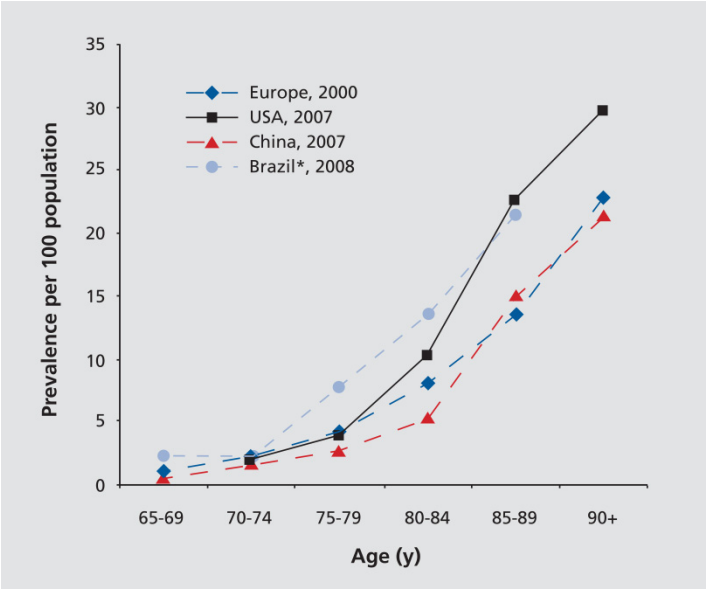

Figure 1.2: Prevalence of AD in different countries or on different continents.

Percentage of AD cases was correlated to the age of patients. AD frequency clearly rises with increasing age (*prevalence of all types of dementia; figure taken from Qiu 2009)[32].

More than 90% of AD cases are classified as sporadic and late onset, which means that multiple causative genes and risk factors are involved and that disease onset is at age 65 or older[33]. *APOE* , the gene encoding apolipoprotein E (ApoE), is the only common risk factor identified in multiple studies of sporadic AD (reviewed in Bekris 2010)[30]. Mutations in app*OE* are thought to affect Aβ clearance[34] and oligomerization[35]. But to carry the *APOE4* allele alone, although it is a risk factor, is not sufficient to cause AD[36]. Other genetic risk factors

that have recently been identified are the genes encoding phospholipase D3 (*PLD3*)[37] and the triggering receptor expressed on myeloid cells 2 (*TREM2*)[38,39].

Familial AD can either be caused by mutations in the genes encoding APP or the enzymes responsible for proteolytic cleavage of APP[40]. There are 37 APP mutations with clinical relevance known[41]. They are mostly located in the middle of the Aβ peptide and increase the tendency of Aβ to aggregate[42,43]. Mutations in the *Presenilin 1* gene (*PSEN1*) have been associated with early onset familial AD and account for 18% to 50% of all familial AD cases[44]. Missense mutations in Presenilin2 (*PSEN2*) also cause early onset familial AD but occur with a much lower frequency and an age of disease onset of 45-88 years[30]. Furthermore, the penetrance of these mutations is much lower compared to *PSEN1* mutations[45].

The treatment options for AD are currently very limited. In the United States the Food and Drug Administration (FDA) have approved only two types of drugs for AD treatment. The neurotransmitter acetylcholine is depleted in AD brains. Thus, Acetylcholine esterase inhibitors are prescribed to help increase acetylcholine levels. N-methyl-D-aspartate (NMDA) receptor antagonists are applied to prevent aberrant neuronal stimulation[46]. These drugs show little beneficial effects and do not prevent or delay disease progression[47]. Drugs that are currently under development, target the production and clearance of Aβ or hyperphosphorylated tau, or ApoE levels and biophysical properties (reviewed in Huang 2012)[47]. Other therapeutic strategies have focused on autophagy, modulators of aging, synaptic dysfunction, oxidative damage, inflammation, exosomes, and mitochondrial stress. None of these have produced a promising course of treatment so far[47].

1.1.4 The amyloid precursor protein (APP)

APP is a type I trans-membrane glycoprotein[48] with an extracellular amino terminus (N-terminus) and a cytosolic carboxy terminus (C-terminus)[49]. It is expressed in a large number of cells in both mammalian and non-mammalian systems[50]. The family of APP proteins in mammals comprises APP, the APP-like protein-1 (APLP1) and the APP-like protein-2 (APLP2)[51]. One of the proteolytic cleavage products of APP is Aβ, which has been shown to be the major protein component of amyloid plaques[52]. The physiological function of APP is not yet clearly defined but a number of potential biological roles have started to

emerge(reviewed in Dawkins 2014)[53]. APP has been linked to mitosis, cell proliferation and cell differentiation[54-56]. Evidence that underscores this theory is an increased expression of APP and APP-like proteins during the development of the rat olfactory system and in neurite outgrowth and synaptogenesis[57]. However, the role of APP in development is not essential since APP loss of function mice are viable and fertile and show only subtle deficits, as well as reduced body and brain mass[58]. After its translation, newly synthesized APP can be subjected to several post-translational modifications including glycosylation, sulphation, phosphorylation, and palmitoylation[59,60]. Following modification in the Golgi network, APP is transported to the cell surface for plasma membrane-insertion[61]. APP can then be transported to the endosomal-lysosomal system by clathrin-mediated endocytosis[62] to undergo degradation in the lysosome[63]. A fraction of endosomal APP might undergo recycling to the cell membrane[62].

1.1.5 Proteolytic processing of APP

APP can undergo processing by enzymes termed secretases, which leads to the production of various proteolytic fragments[64,65]. Depending on the APP cleavage site, the protease activities are termed α-, β-, and γ-secretase. The proteolytic processing of APP can be divided in to a non-amyloidogenic and an amyloidogenic pathway (Figure 1.3). Both pathways coexist in healthy individuals[66]. The first step of the non-amyloidogenic pathway is α-cleavage, which occurs approximately in the middle of the Aβ region[67]. α-secretase activity is mainly found on the cell surface and releases a large N-terminal fragment of APP (APPsα) leaving a small C-terminal APP fragment in the plasma membrane (αAPP CTF or C83). αAPP CTF is further processed by γ-secretase, releasing a truncated Aβ peptide termed p3[68] to the extracellular space, and generates the APP intracellular domain (AICD)[69]. All known APP α-secretases are members of the A disintegrin metalloprotease (ADAM) family[70]. By increasing α-secretase activity in animal or cell culture models, Aβ generation and amyloid plaque formation can be reduced[71,72].

The amyloidogenic and non-amyloidogenic pathways are thought to compete with each other[66]. An increase of β- and γ-secretase activities leads to a shift towards the amyloidogenic pathway, resulting in a higher production and extracellular deposition of Aβ[73]. The cellular location where β- and γ-cleavage of APP take place is a matter of debate.

Both endocytic compartments and the *trans*-Golgi network have been described as sites of amyloidogenic processing[74,75]. Generation of Aβ is initiated by β-cleavage, which leads to the release of a large part of the ectodomain of APP (APPsβ) leaving an APP C-terminal fragment within the cell membrane (βAPP CTF or C99). βAPP CTF is then cleaved by γ-secretase, releasing extracellular/intraluminal Aβ and intracellular AICD[76].

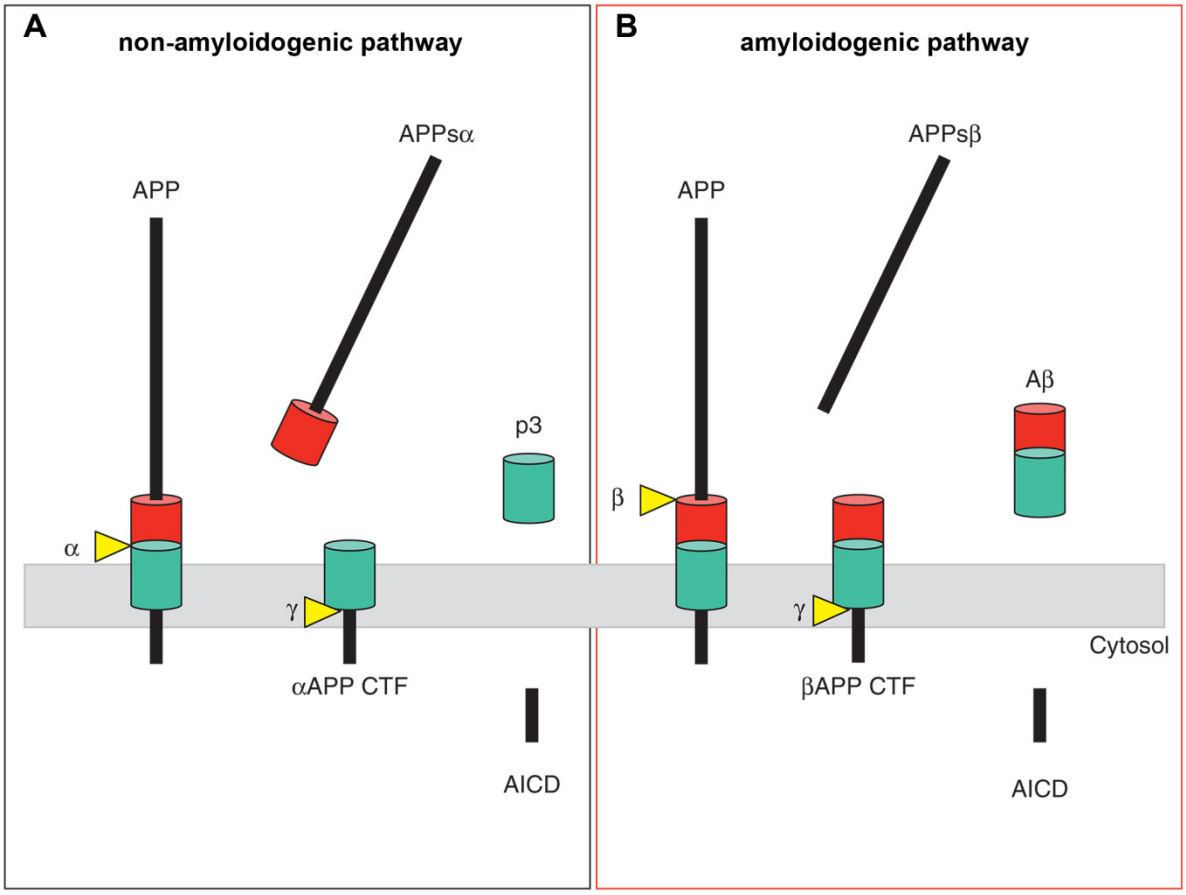

Figure 1.3: Proteolytic processing of APP.

(A) In the non-amyloidogenic pathway, APP is initially cleaved by α-secretase, which leads to the release of APPsα to the extracellular space. The membrane spanning αAPP CTF remains in the plasma membrane and is subsequently cleaved by γ-secretase releasing extracellular p3 and intracellular AICD. (B) The amyloidogenic pathway is initiated by β-secretase cleavage of APP, which produces extracellular APPsβ and the membrane spanning βAPP CTF. βAPP CTF is then processed by γ-secretase, leading to the release of extracellular Aβ and intracellular AICD (modified from Haas 2012)[66].

The enzyme responsible for β-secretase activity is b-site APP cleaving enzyme-1 (BACE1), a membrane bound aspartyl protease[77]. The active site of BACE1 is located in the lumen/extracellular space[78]. BACE1 is the only β-secretase with specificity for APP, since a knockout of BACE1 completely blocks β-cleavage of APP[79]. The final step in the production of Aβ is γ-cleavage. The γ-secretase protein complex belongs to the intramembrane-cleaving aspartyl proteases and is made up of four subunits: presenilin (PS), anterior pharynx-

defective 1 (APH-1), nicastrin, and presenilin enhancer 2 (PEN-2)[80]. APP cleavage by γ-secretase has been defined as regulated intermembrane proteolysis, because APP γ-cleavage is achieved through a series of sequential proteolytic events at the γ-, ε- and ζ-sites, starting from the C-terminal end of the substrate moving towards the N-terminal end (Figure 1.4)[81]. These cleavage events are not precise. Under physiological conditions the final γ-cleavage can occur between amino acid (aa) 37 and 43, with Aβ40 and Aβ42 as the main cleavage products[82].

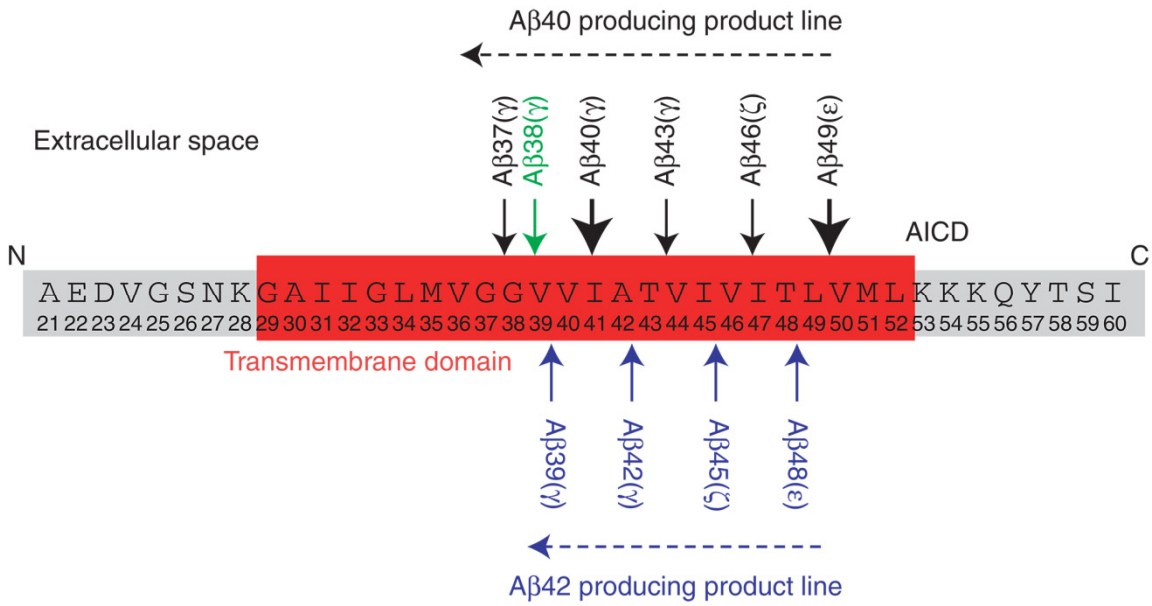

Figure 1.4: The APP cleavage events that lead to the production of different Aβ isoforms.

Sequential proteolytic cleavage events of APP between aa 37 and 50 at the γ-, ε- and ζ-sites lead to the production of Aβ isoforms of various sizes, ranging from 37 to 48 amino acids. The direction of the sequential cleavage is depicted by arrows. The upper sequence favors the production of $A\beta_{40}$, whereas the lower sequence favors the production of the more toxic $A\beta_{42}$. All γ-, ε- and ζ cleavage events occur inside the plasma membrane (figure taken from Haass 2012)[66].

This has important implications for the pathology of AD because Aβ42 is prone to aggregation and has also been described to be the most cytotoxic Aβ isoform[83].

1.1.6 Amyloid beta

It is undisputable that Aβ plays a central role in the pathology of AD[84]. Aβ is the major component of amyloid plaques, which consist of amyloid fibrils that are made up of cross-ß-sheet units of Aβ peptides[85]. Amyloid fibrils are the final product in the Aβ aggregation cascade (Figure 1.5).

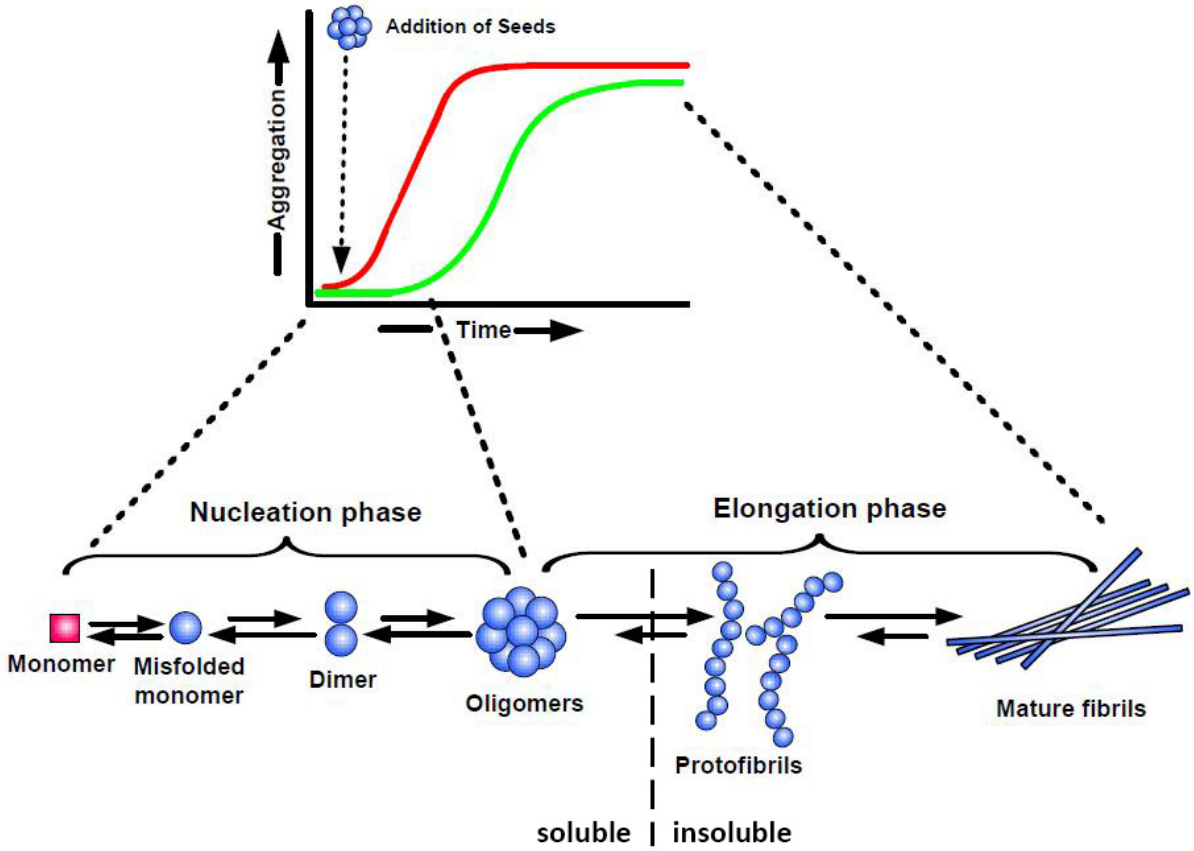

Figure 1.5: Aβ aggregation cascade.

The process of Aβ aggregation can be divided into two phases. During the nucleation phase, Aβ monomers are subject to conformational changes and misfolding. Misfolded Aβ monomers tend to associate to form multimers and eventually soluble oligomeric Aβ nuclei. During the elongation phase these nuclei assemble to insoluble protofibrils and grow by further incorporation of monomers to finally produce mature Aβ fibrils. The green curve is a representation of Aβ aggregation kinetics. The nucleation phase is thermodynamically unfavorable and proceeds slowly compared to the elongation phase, which proceeds far more quickly. The elongation phase is accelerated upon the addition of preformed seeds (Aβ nuclei) and is depicted by the red curve (modified from Kumar 2011)[86].

According to the amyloid-hypothesis, generation and extracellular deposition of Aβ leads to neurodegeneration and a condition termed "amyloidosis"[9,10]. Early studies correlated the number of amyloid plaques to appearance and severity of dementia[87]. Both theories have been widely disproven. Numerous clinicopathological studies have clarified that AD severity does not correlate with amyloid burden (reviewed in Serrano-Pozo 2011)[88]. Changes in Aβ

metabolism and amyloid plaques were found many years before the onset of clinical disease in some patients[20]. Furthermore, it has been shown that extracellular amyloid fibrils are not the main conveyor of cytotoxicity in AD, but rather diffusible assemblies of Aβ. These small, soluble, pre-fibrillar Aβ species are currently thought to be the most deleterious, causing synaptotoxicity and neuronal injury[11]. On a molecular level this toxicity might be explained by the exposure of hydrophobic surfaces on Aβ oligomers, which cause toxic alterations to cell membranes[89]. This data provides a reasonable explanation for the lack of correlation between amyloid plaque burden and AD severity. It also might explain the deposition of intracellular hyperphosphorylated tau due to damage to sensitive neurons[90].

The Aβ oligomers that have toxic properties are not yet clearly defined. In the early 1990s the conversion of non-toxic monomeric Aβ to toxic "high-molecular-weight species" was described *in vitro*[91]. Later studies applied atomic force microscopy, ultracentrifugation, and gel filtration to analyze Aβ preparations generated *in vitro* and defined them as "metastable Aβ protofibrils"[92,93]. Further analysis revealed that these protofibrils are smaller than amyloid fibrils, have a high β-sheet content and are likely en route to become amyloid fibrils[94]. Disturbance of neurotransmission and cell toxicity are thought to be caused by these and other oligomeric Aβ assemblies[95,96]. Soluble Aβ oligomeric species have been extracted from the brain tissue of AD patients and their presence correlates strongly with clinical symptoms[12,97,98]. However, amyloid plaques should not be considered as pathologically inert. A study in mouse has revealed synaptic and neuronal dysfunction in the vicinity of amyloid plaques. Aβ fibrils and toxic oligomers might coexist in a dynamic equilibrium leading to a constant turnover of toxic Aβ species in the vicinity of amyloid plaques[99].

1.2 The cellular prion protein (PrP^C)

The cellular prion protein (PrP^C) is attached to the outer leaflet of the plasma membrane via its glycophosphatidylinositol (GPI)-anchor (Figure 1.6) and has a molecular weight of about 35 kilo dalton (kDa). PrP^C has two glycosylation sites that lead to the characteristic three-band pattern upon Western blot detection. It is ubiquitously expressed with the highest expression levels in the nervous system[100]. Through different types of proteolytic processing PrP^C can be released from the cell membrane (reviewed in Altemeppen 2012)[101]. In its misfolded, β-sheet-rich conformation, PrP scrapie (PrP^{Sc}) has received much attention as the causative agent of prion diseases, such as bovine spongiform encephalopathy (BSE) and scrapie in animals, or Creutzfeldt-Jakob disease and Kuru in humans (reviewed in Aguzzi 2008)[100]. Although the functions of PrP^C are still poorly understood, PrP^C was recently identified as the receptor for toxic, β-sheet rich, oligomeric proteins, which has important implications for numerous neurodegenerative diseases such as AD, Chorea Huntington, Parkinson's disease and prion diseases[102,103].

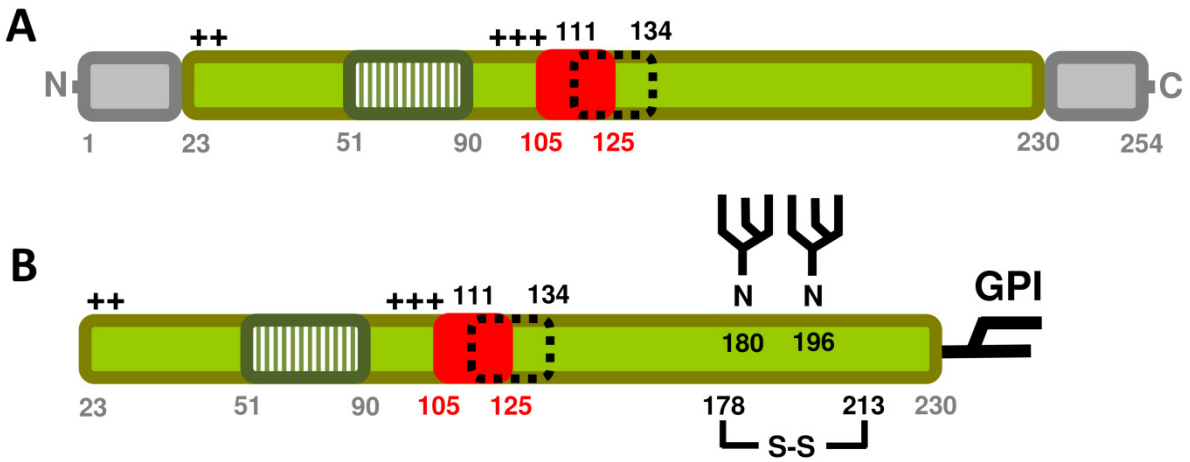

Figure 1.6: Schematic drawing of murine PrP^C.

(A) Before posttranslational modification PrP^C exists as a protein of 254 amino acids. The N-terminal (aa 1-23) and C-terminal (aa 230-254) signal peptides are removed by signal peptidases in the ER. (B) After removal of the C-terminal signal sequence a GPI-anchor is attached at aa 230. Mature PrP^C has an octameric repeat region at aa 51-90, a neurotoxic domain at aa 105-125, a hydrophobic core from aa 111-134, a disulfide bridge between aa 178 and 213 and two N-glycosylation sites at aa 180 and 196 (modified from Altmeppen 2012)[101].

1.2.1 Physiological functions of PrP^C

Over 20 years after its discovery[104] the physiological functions of PrP^C are still a matter of discussion. *Prnp* knockout mice are viable and display no major physiological or anatomical abnormalities[105]. Minor behavioral abnormalities have been reported[106] as well as changes

in olfactory function[107] and in myelination in the periphery[108]. PrP^C has been functionally implicated in processes involving cell-adhesion, such as neurite outgrowth[109], neuronal differentiation[110] and neuronal survival[111]. Furthermore, PrP^C might be required for normal synaptic development and function[112,113]. An involvement of PrP^C in excitotoxicity is also under debate. Excitotoxicity is a mechanism, by which aberrant activation of the NMDA receptor leads to an abnormal Ca^{2+} influx causing nerve cell damage and eventual death[114]. PrP^C is thought to have a protective role in excitotoxicity by inhibiting the NMDA receptor[115]. Another protective property has also been shown by overexpression of PrP^C in cell lines and primary neurons, which leads to protection from various apoptotic stimuli.

1.2.2 PrP^C and AD

PrP^C has been linked to AD in several ways (reviewed in Kellett 2009)[116]. Firstly, prion diseases show strong neuropathological similarities to AD[117]. PrP^C has been shown to colocalize with amyloid plaques[118] and to promote plaque formation, while levels of $A\beta_{40}$ and $A\beta_{42}$ as well as *APP* transcription were unchanged[119]. The *PRNP*-M129V polymorphism has been correlated with early onset AD[120] and enhanced amyloid plaque burden[121]. A direct influence of PrP^C on Aβ production has been proposed by Parkin *et al.* who showed that overexpression of PrP^C leads to inhibition of β-secretase cleavage of APP and therefore to a decrease in Aβ formation. On the contrary, PrP^C knockdown increases extracellular Aβ levels[122]. This line of evidence strongly suggests that PrP^C plays an important role in AD on several levels.

1.2.3 PrP^C as a receptor for oligomeric Aβ

In an unbiased screen for proteins that bind $A\beta_{42}$ oligomers, PrP^C was identified as a high affinity receptor, whereas monomers or fibrils did not interact with PrP^C. The unstructured N-terminus of PrP^C is required for the interaction and the Aβ binding site was mapped to aa 95-100 of murine PrP^{C102}. Chen *et al.* confirmed this binding site and identified a second one ranging from aa 23-27[123]. Furthermore, it was demonstrated that $A\beta_{42}$-induced synaptotoxicity depends on PrP^C and that suppression of LTP by $A\beta_{42}$ was absent in hippocampal slices of *Prnp*$^{0/0}$mice[102]. In another study the same group crossed *Prnp*$^{0/0}$ mice

with a strain carrying mutations in the genes encoding for APP and Presinilin-1 (APPswe/Psen1ΔE9), which is a model of AD. It was found that PrP^C is responsible for the cognitive deficits and reduced survival rate that is usually observed in APPswe/Psen1ΔE9 mice[103]. Subsequent studies demonstrated that PrP^C-specific antibodies are potent inhibitors of Aβ-mediated toxicity[124-126]. However, contradictory data has also started to emerge, suggesting that PrP^C does not play a role in Aβ-mediated learning and memory deficits[127,128], Aβ-induced inhibition of LTP[129] and several other synaptotoxic effects of Aβ oligomers[130]. One explanation for these contradictory reports could be the lack of definition for oligomeric Aβ. Preparation and handling may differ between laboratories, which may lead to different experimental outcomes. Furthermore, the use of different AD model systems might also hamper comparability of different studies. However, all studies agree on the fact that oligomeric Aβ binds to PrP^C (reviewed in Benilova 2010 and Biasini 2012)[131,132]. Toxic signaling via proto-oncogene tyrosine-protein kinase Fyn kinase due to this binding event is currently thought to be the cause for the demise of affected neurons[133,134]. Activation of the NMDA receptor and resulting excitotoxicity has also been linked to the interaction of membrane attached PrP^C with oligomeric Aβ and other β-sheet rich protein conformers (Figure 1.7)[135].

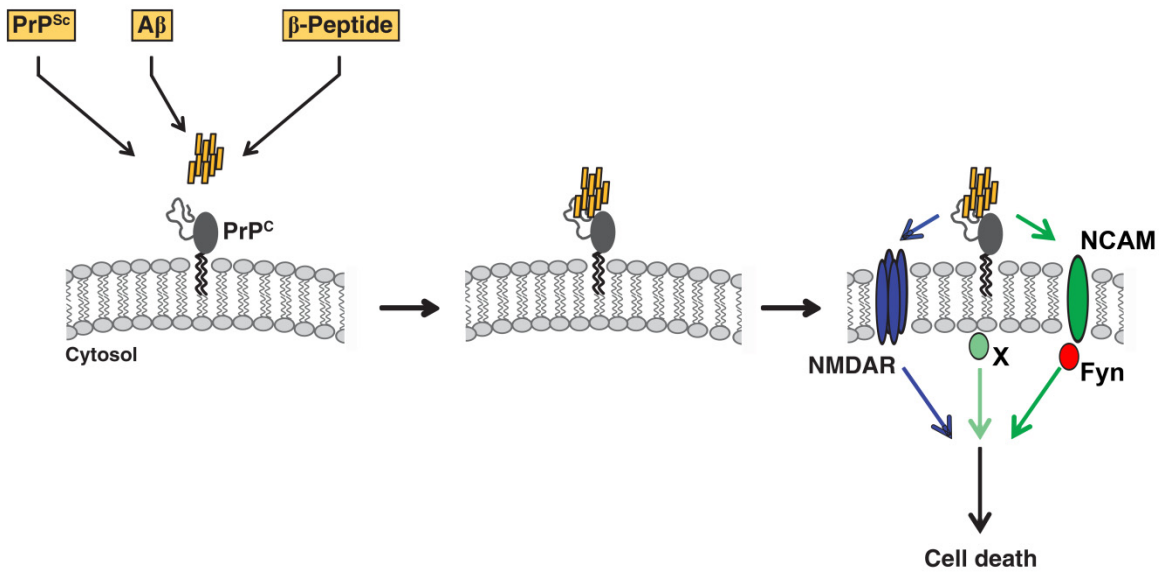

Figure 1.7: GPI-anchored PrP^C at the plasma membrane is a putative receptor for toxic β-sheet rich protein conformers.

Interaction of PrP^C at the plasma membrane with different β-sheet rich proteins has been shown. Among them are PrP^{Sc}, Aβ or designed β-peptides. Upon binding of β-sheet rich structures to PrP^C, a toxic signaling cascade is activated, which is likely to occur via activation of the NMDA receptor, activation of Fyn kinase via NCAM and/or other not yet identified adaptor proteins (modified from Resenberger 2011)[135]

1.3 Exosomes

Exosomes are small extracellular vesicles (EVs) of endosomal origin with a diameter of ~50-150 nm that are released by several cell types. Diverse functions have been assigned to exosomes, which can be attributed to their protein and ribonucleic acid (RNA) content as well as their lipid composition and lipid modifications. These factors may vary depending on the cell type these vesicles were isolated from[136]. Exosomes are distinct from other types of EVs, such as microvesicles (MVs) or apoptotic vesicles (AVs) in terms of lipid, protein and nucleic acid composition, as well as their origin, within mutivesicular endosomes (MVEs; reviewed in Théry 2009)[137].

1.3.1 Discovery

The pathway of exosome biogenesis was discovered in 1983. Harding *et al.* showed that during reticulocyte maturation the transferrin receptor is internalized by receptor mediated endocytosis into a trypsin-resistant compartment. They concluded that this compartment corresponds to MVEs and further observed that the content of MVEs gets released into the extracellular space by fusion of MVEs with the plasma membrane[138]. In 1985 Pan *et al.* described “simple vesicles of 100-200 nm”, which contained transferrin in their limiting membrane[139]. This was the first description of exosome-like vesicles of endosomal origin and the term exosome was introduced shortly after by Johnstone *et al.*[140]. Functional properties, similar to those of the plasma membrane, were described for reticulocyte exosomes. Furthermore, they introduced ultracentrifugation as a method for exosome purification, which is still the predominantly used method[136,140].

1.3.2 Biogenesis and secretion

The first step of exosome biogenesis is the invagination of the plasma membrane, which gives rise to an early endosome (Figure 1.8). The early endosome matures by inward budding of small vesicles into its lumen. The Endosomal Sorting Complex Required for Transport (ESCRT) machinery regulates the formation of intraluminal vesicles (ILVs) giving rise to MVEs[141]. The inactivation of ESCRT components leads to a decrease in MVE formation and exosome release in mammalian cells but MVEs are still generated[142]. Oligodendroglia

cells enhance the secretion of proteolipid protein (PLP) positive exosomes after ESCRT inhibition. This ESCRT independent exosome pathway depends on the sphingolipid ceramide and the enzyme sphingomyelinase, which is crucial for ceramide biosynthesis[143].

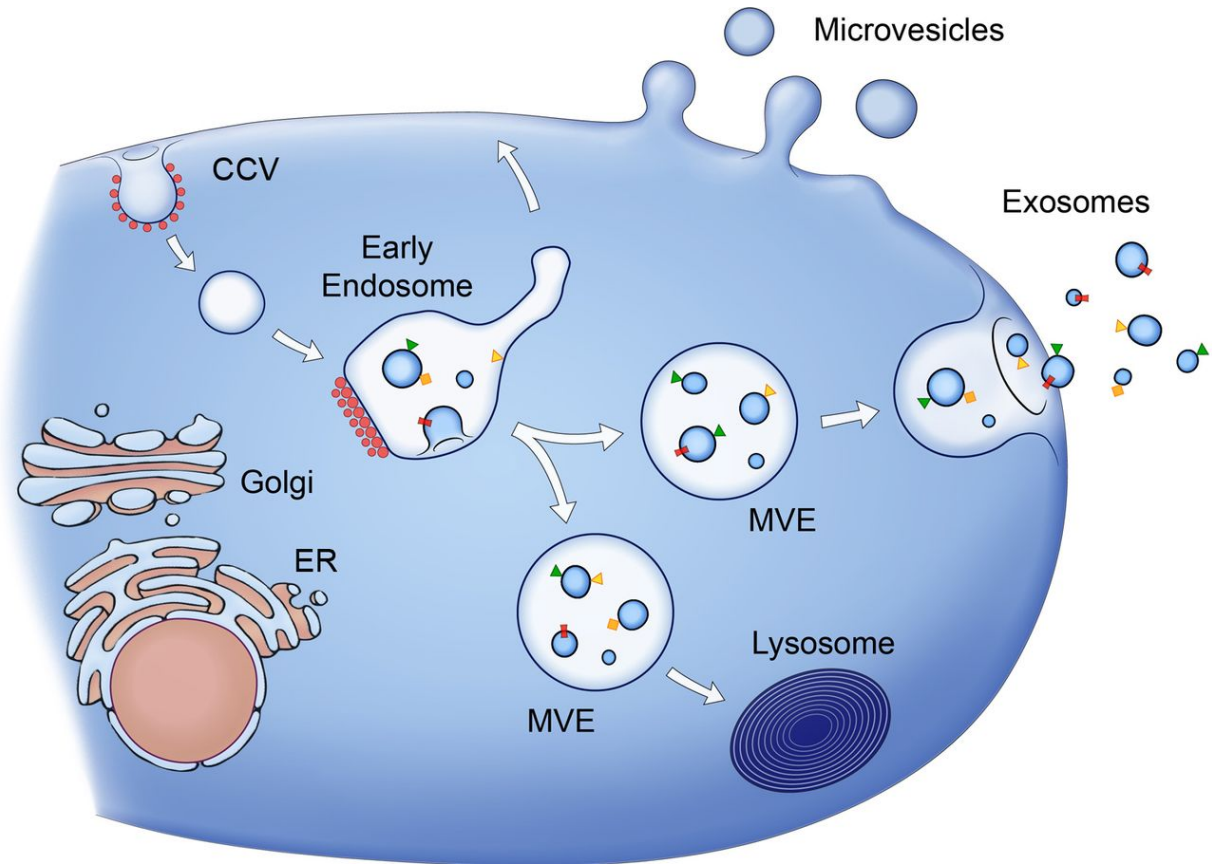

Figure 1.8: Exosome and microvesicle biogenesis.

An early endosome arises by invagination of the plasma membrane. Inward budding of the early endosome membrane leads to the production of intraluminal vesicles as the endosome matures to become a multivesicular endosome (MVE). MVEs are either degraded in the lysosomal system or fuse with the plasma membrane to release small (50-150nm) EVs, termed exosomes, into the extracellular space. Another type of EVs called micsovesicles (100-1000nm in size) bud directly from the plasma membrane (figure taken from Raposo 2013)[136].

Proteins of the tetraspanin family have been shown to select cargoes for the release via exosomes in a ceramide and ESCRT-independent manner[144-146] suggesting that other pathways of MVE biogenesis exist. Recent data has provided some evidence pointing to the existence of sub-populations of MVEs[147,148].

Soluble NSF-attachment protein receptor (SNARE) complexes have been linked to exosome secretion. They are involved in the fusion of intercellular compartments by controlling fusion of lipid bilayers[149]. SNARE complexes are required for the fusion of secretory lysosomes[150] with the plasma membrane but are not necessarily instrumental in fusion of MVEs to the

plasma membrane. Due to the fact that the membrane orientation switches twice during exosome biogenesis, (i) inward budding of the cell membrane and (ii) budding of vesicles into the endosomal lumen, exosomes have the same membrane topology as the cell membrane[137].

1.3.3 Composition

Exosomes are enriched in cholesterol, sphingomyelin, ceramide, and phospatidylserine[151]. All studies that have focused on the lipid composition of exosomes have found differences to the cell membrane as well as differences in exosomes isolated from different sources[143,152-156]. Similarities of exosomes with lipid rafts, distinct detergent resistant subdomains of the plasma membrane, were found in respect to lipid and protein composition. Sphingomyelin and cholesterol are abundant in both structures as well as GPI-anchored proteins (e.g. PrP^C and Flotillins)[157]. It has been demonstrated in mesenchymal stem cells that lipid rafts are endocytosed during MVE formation and eventually secreted via exosomes[158]. The selective incorporation of proteins into exosomes was proposed by Fang *et al.* who showed by protein modification that certain signals led to the exosomal release of these proteins[159]. A growing number of proteins have been found to be specifically associated with exosomes, some of which have been defined as exosomal marker proteins. Among these are endosome-associated proteins (e.g. Ras superfamily of monomeric G proteins (Rab GTPases), SNAREs, Annexins and Flotillin), proteins involved in MVB biogenesis (e.g. Alix and Tumor susceptibility gene 101 (Tsg101)) and - as already mentioned - lipid rafts proteins. Exosomes are free of serum proteins and proteins of intracellular compartments like the endoplasmic reticulum (ER), Golgi complex or mitochondria[160]. The overall protein composition of exosomes depends on their origin[161]. It often reflects the expression profile of the cell type they were derived from - at least in part - making these vesicles a valuable tool in cancer diagnostics[162]. RNAs are another intensively studied component of exosomes and messenger RNA (mRNA) as well as micro RNA (miRNA) were the first types of RNAs to be identified in exosomes. Further, it was shown that recipient cells translated exosomal mRNAs into proteins[163,164].

1.3.4 Functions and target cell interaction

Various cell types have been described to release exosomes via MVE-PM fusion, e.g. reticulocytes[139,165], B lymphocytes[166], dendritic cells[167], cytotoxic T cells[168], platelets[169], mast cells[170], neurons[171], oligodendrocytes[172], Schwann cells[173], and intestinal epithelial cells[174]. Exosome-like vesicles have also been isolated from a number of human bodily fluids including prostatic fluid[175], blood[176], urine[177], saliva[178], breast milk[179], amniotic fluid[180], ascites fluid[181], cerebrospinal fluid[182], and bile[183]. The target cell specificity of exosomes has been shown to be dependent on the configuration of tetraspanin complexes in exosomes[184], which in turn might have a modulating influence on exosomal adhesion molecules, like integrins[185]. Upon binding of exosomes to a recipient cell different scenarios are likely to occur: exosomes (i) stay associated to the plasma membrane, (ii) dissociate, (iii) are internalized and may fuse with endosomal compartments or be degraded in lysosomes, or (iv) fuse with the cell membrane to release their cargo in the cytoplasm (Figure 1.9)[136].

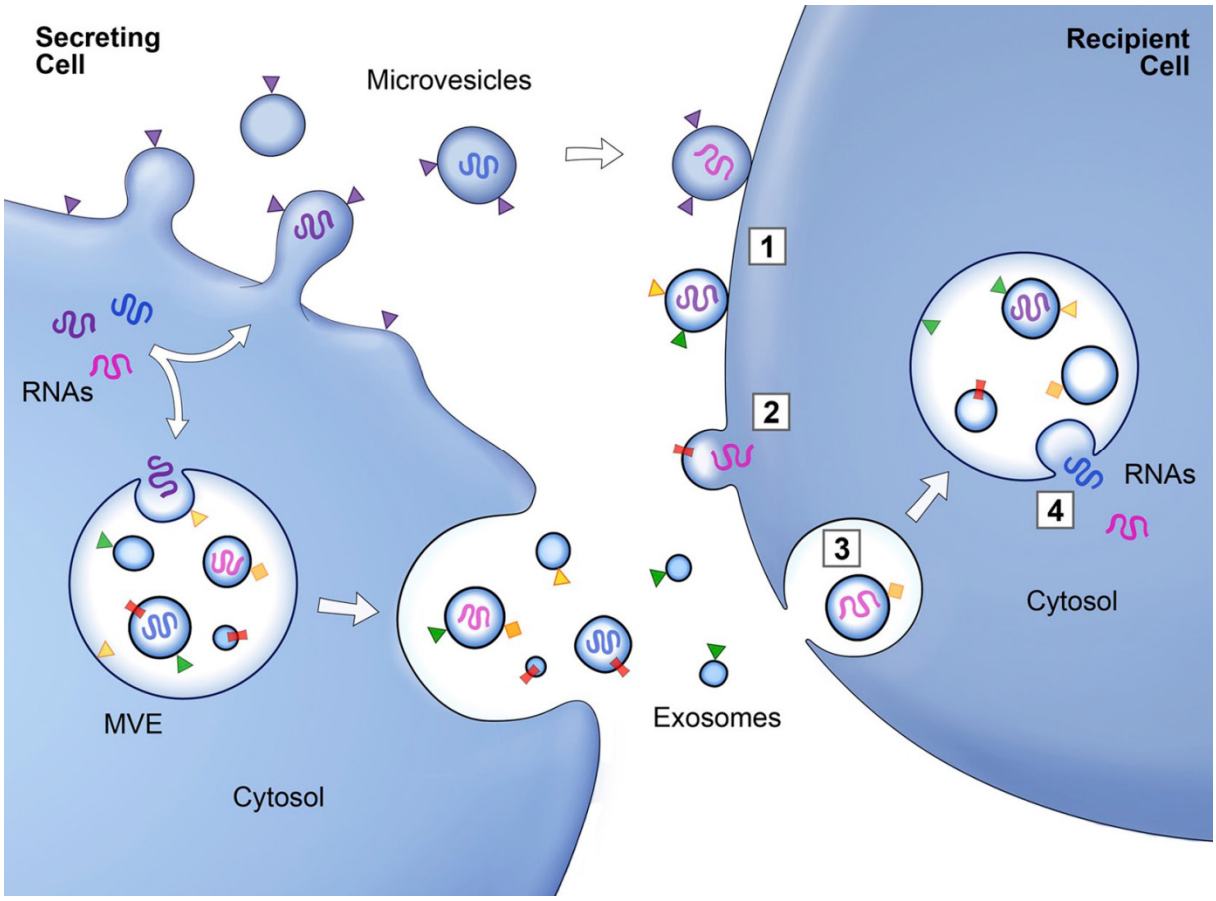

Figure 1.9: Vesicle secretion and target cell interaction.

Transmembrane proteins (rectangles), membrane-associated proteins (triangles), and RNAs are continuously and selectively sorted into intraluminal vesicles of MVEs or into MVs that bud from the cell membrane. Exosomes carrying cargo are released by fusion of MVEs with the plasma membrane. EVs dock to the plasma membrane of a target cell (1) and may fuse with the plasma membrane (2), be directly endocytosed (3) or dissociate. Fusion of endocytosed vesicles with the newly formed endocytotic compartment may occur (4). Both modes of vesicle entry, fusion and endocytosis, lead to delivery of exosome cargo into the membrane or cytosol of the target cell (figure taken from Raposo 2013)[136].

The first functional studies of exosomes from the early 1980s led to the conclusion that exosome secretion is a mechanism to get rid of cellular debris[186]. Since then, manifold functions have been assigned to exosomes. These include antigen presentation under inflammatory conditions[187] as well as antigen-presentation leading to anti-tumor immune responses[188]. Tumor derived vesicles have been shown to have immunosuppressive properties[189].

1.3.5 Exosomes in the nervous system

Only a few studies have focused on the function of exosomes in the healthy nervous system, whereas the majority have dealt with neurodegeneration and neurological disorders. Cell

types found in the brain, which have been shown to secrete EVs in vitro are neurons[171], neural stem cells[190], oligodendrocytes[172], astrocytes[191], Schwann cells, and microglia[192]. As a consequence exosomes can be found in the cerebral spinal fluid (CSF)[193]. Exosomes derived from glia cells promoted neurite outgrowth and neuronal survival by releasing synapsin and consequently establish the interaction between glia and neurons[194]. Another physiological function assigned to exosomes is the inhibition of myelin formation by exosome-like vesicles derived from oligodendrocytes. Furthermore, they inhibit the morphological differentiation of oligodendrocytes. The effect was diminished in conditioned neuronal media, which led the authors to the conclusion that neurons control myelin sheath formation by inhibiting the release of oligodendrocyte-derived exosomes[195].

1.3.6 PrP^{C} and PrP^{Sc} on exosomes

The initial discovery of vesicles containing PrP^{C} was made by Ecroyd *et al.* who described extracellular membrane bound vesicles that contained PrP^{C}[196]. The vesicles were purified from the male reproductive tract and referred to as epididymosomes, which are presumably exosomes due to the same purification method used to isolate them and the similarity of physical properties. PrP^{C} was also found on platelet derived exosomes from human blood of healthy individuals. PrP^{C} could be transiently expressed on the platelet surface by platelet activation and was subsequently released on both exosomes and MVs[197]. This was postulated as a mechanism for PrP^{Sc} spread via blood, which has been confirmed indirectly in an experimental prion disease sheep model by leucocyte depletion of blood and the application of prion reduction filters[198]. The observation that the highest concentration of PrP^{C} in neurons was found on the cell membrane and in MVEs[199] is coherent with its localization in exosomes. Whether PrP^{C} is released to the extracellular space in association to exosomes, or in a soluble form, depends on the cell type[200]. An exosomal release of PrP^{C} was observed in cultured cortical neurons[171] and PrP^{C} was enriched on exosomes isolated from bovine CSF[193].

The first evidence for a possible involvement of exosomes in neurodegenerative diseases was presented by Fevrier *et al.* who demonstrated that PrP^{Sc} is released via exosomes from prion infected cell lines. Furthermore, they were able to show that PrP^{C} is also released by exosomes from neuronal cell lines[201]. This also holds true for Neuro 2a (N2a) cells, which

were shown to release PrP^{Sc} in exosomes and to a lower extent in viral particles[202]. The infectivity of exosomes loaded with PrP^{Sc} was analyzed using exosomes derived from neuronal and non-neuronal cells. Both types of exosomes had the capacity to transmit prion infection between cell lines and to induce clinical prion disease in mice[182]. In a recent study it was demonstrated that the majority of extracellular prions are released via the exosomal pathway. The ratio of exosome associated PrP^{Sc} to free PrP^{Sc} strongly depended on the prion strain[203]. Since it is poorly understood how prions cross the blood brain barrier and spread in the brain, an organ with very little cell motility, exosomes are thought be fundamentally involved in prion disease pathogenesis. The conversion of PrP^{C} to PrP^{Sc} was suggested to occur in lipid rafts[204]. Exosomes are derived from the cell membrane and contain numerous lipid rafts proteins, which explains why PrP^{Sc} is found on exosomes. Furthermore, the hypothesis that insertion of PrP^{Sc} into lipid rafts is curial for prion infection[205] is explainable by prion transmission via exosomes. PrP^{Sc} might be inserted into lipid rafts upon exosome docking and fusion. Also worth mentioning is the observation that lipids assist in the formation of *de novo* prions through stabilization of intermediary isoforms[206,207].

1.3.7 Exosomes in AD

Rajendran *et al.* were the first to describe a connection between exosomes and AD. Using HeLa and N2a cells expressing the Swedish mutant of APP they demonstrated that β-cleavage of APP by BACE occurs in Rab5-positive endosomes. Rab4 overexpression accelerated the recycling of cargo from endosomes to the plasma membrane and reduced β-cleavage activity, which further strengthens that theory. Logically, a fraction of intracellular Aβ was found to be localized in MVEs and released in association with exosomes. Furthermore, by analysis of immunohistochemically stained brain sections of AD patients, the exosomal markers Alix and Flotillin were found to be colocalized with amyloid plaques. These results led to the conclusion that Aβ is released via exosomes in to the extracellular space, which promotes amyloid plaque formation[208]. In a similar study Chinese hamster ovary (CHO) cells transfected with APP expression constructs were used. The authors described the presences of Aβ as well as APP C-terminal fragments in exosomes, which belong to the non-amyloidogenic pathway. They also investigated the presence of APP secretases in exosomes and identified BACE, PS1, PS2, and ADAM10 to be present in the

vesicles, leading to the conclusion that exosomes might also be a site of APP processing[209]. The first mechanistic study focused on exosomes in AD was published in 2012 by Yuyama *et al.* By incubating Aβ with exosomes from N2a cells and primary neurons they were able to demonstrate that exosomes promote Aβ fibrillization, which leads to its subsequent uptake and clearance by microglia. Additionally, they presented experimental evidence that exosomes from neuronal cells reduce Aβ mediated cytotoxicity. Removal of exosomal glycosphingolipids (GSLs) by Endoglycoceramidase (EGCase) treatment nearly abolished the fibril-promoting effect of exosomes[210]. GSLs are known to facilitate fibril formation[211] and to associate with PrP^{C} when present on synthetic liposomes[212] making them a putative player in exosome driven Aβ aggregation. In 2014 Yuyama *et al.* published a follow up study where they presented evidence that GSLs are required for the association of Aβ with exosomes *in vitro* and *in vivo*. To investigate the involvement of exosomes in AD *in vivo* exosomes isolated from N2a cells were injected into the hippocampi of APP_{SweInd} transgenic mice. 3h post injection, hippocampal Aβ was detectable in these exosomes. Furthermore, an increase in hippocampal Aβ localization was observed. Continuous injections of exosomes for a time period of two weeks reduced Aβ pathology and synaptic dysfunction in the treated group[213]. In another *in vivo* study rats were subjected to injection of soluble Aβ, which is known to disrupt LTP in the brain. Disruption of LTP was nearly completely averted by prior injection of N2a exosomes. In accordance with Yuyama *et al.* Aβ degrading properties of exosomes could not be observed for N2a exosomes. By comparing exosomes isolated from wild type (WT) hippocampal cells (HW8-1) to hippocampal *Prnp* knock-out cells (Hpl3-4) the authors concluded that PrP^{C} is crucial for binding of Aβ to exosomes and for the observed protective effects of exosomes against Aβ[214]. These results may be interpreted with caution due to inconsistencies in experimental design, which will be dealt with in the discussion of this work. In summary, all of the described observations assign exosomes a rather protective function in molecular mechanisms of AD. On the contrary, MVs isolated from microglia cells convert Aβ fibrils into smaller soluble forms, which are neurotoxic and damaging to dendrites *in vitro*. Binding of MV-generated soluble Aβ to neurons could be competed by recombinant PrP^{C}[215].

1.4 Objective of this study

In recent years it has become clear that exosomes could play an important role in the pathogenesis of AD. The first substantiating evidence for this theory was presented by Rajendran *et al.* in 2006 who showed that Aβ is released via exosomes derived from neuronal cells and that exosomal markers co-localize with amyloid plaques in brains of AD patients[208]. Subsequent studies have concluded that exosomes bind Aβ in a GSL-dependent manner, promote Aβ fibrillization and their subsequent uptake and degradation of Aβ by microglia. Furthermore, application of exosomes in an AD mouse model lead to an extenuated course of disease[210,213]. Finally, exosomes were shown to protect rats from Aβ -induced LTP, which was attributed to PrP^C on these exosomes[214].

Since PrP^C is highly enriched on exosomes derived from ovine CSF[193] and neuronal cells (Figure 3.16-3.17) and Aβ-binding by PrP^C has been described in several studies[132], the aim of this study was to clarify if exosomal PrP^C modulates the effects of exosomes on mechanisms so far described in AD. To achieve this, a mouse neuroblastoma N2a PrP^C knockout cell line was generated, using transcription activator-like effector nucleases (TALENs). This and a human neuroblastoma cell line served as model systems to test whether exosomes bind Aβ in a PrP^C dependent fashion, if exosome induced Aβ aggregation is conferred by PrP^C and if the protection from Aβ-mediated neurotoxicity by exosomes is modulated by PrP^C. The data provided by this study give further mechanistic insights into the mode of action of exosomes in AD and may contribute to the development of an exosome based therapy for AD.

2 Material and methods

2.1 Material

2.1.1 Instruments

Instruments	
7500 Fast Real Time PCR system	Applied Biosystems
Analysis balance (MC1 Research RC210P)	Satorius
Attofluor® cell chamber	Life Technologies
Centrifuge (F45-24-11)	Eppendorf
Chemi Doc Gel imaging system	BioRad
Chemi Doc MP detection system	BioRad
Confocal microscope (TCS SP5)	Leica
FACS Aria II	BD Biosciences
FACS Canto II	BD Biosciences
Fine balance (CP3202S)	Satorius
Freezer (-80°C) (UF80-450S)	Colora Messtechnik GmbH
Hot plate stirrer (Ikamag RCT)	IKA
Incubator (Heraeus)	Thermo Scientific
Light microscope (DMD 108)	Zeiss
Magnetic stirrer (Variomag mono)	Thermo Electron Corporation
Marlin F-033B IRF camera	Allied Vision Technology
Microplate spectrophotometer (µQuant)	BioTek
Microscope (DMI 4000B)	Leica
Microscope (Eclipse TS 100)	Nikon
Microwave (R334-W)	Sharp
Mini Trans-Blot	BioRad
Mini-PROTEAN electrophoresis cell	BioRad
Mini-Sub Cell GT gel-electrophoresis chamber	BioRad
Nanodrop ND 1000	Wilmington
Nanosight LM10	Nanosight
Neubauer (improved)	Fuchs Rosenthal
pH meter (CG 840)	Schott
Pipetteboy	Integra Biosciences
Pipettes	Eppendorf
Platform rocker (STR6)	Stuart Scientific
Printer P93D	Mitsubishi
Rotator (Stuart SB3)	Bibby Scientific
Safire2 microplate reader	Tecan
Single-lens reflex camera (D5000)	Nikon
Spectrofluorometer (LS50)	Perkin-Elmer
Table-top centrifuge (5415R)	Eppendorf
Table-top centrifuge (5804R)	Eppendorf
Thermocycler MyCycler PCR	BioRad
ThermoMixer C	Eppendorf
Ultracentrifuge Optima L-100 XP (rotor: SW40Ti)	Beckman Coulter
Vortex MS minishaker	IKA, Germany
Water cath	P-D Industrie
Water purification system (Milli-RX20)	MilliPore, USA

2.1.2 Consumables

Consumables	
12 well-plates	Thermo Scientific
145cm^2 cell culture dish	Nunc
24 well-plates	Thermo Scientific
6 well-plates	Thermo Scientific
96 well-plates	Thermo Scientific
Amicon Ultra 100kDa cut-off filter	Merck
Costar 96 well-plates black flat bottom	Merck Millipore
Cover slips	Menzel
Cryo tubes	Sarstedt
Disposable pipettes (2ml, 5ml, 10ml, 25ml)	BD Biosciences
Microscopy slides	Roth,
Nitrocellulose membrane	BioRad
Novex® Bis-Tris Gele (4-12 %)	Life Technologies
Parafilm	SPI Supplies
PCR tubes	Rapidozym
PCR tube-stripes	Kisker Biotech
Pipette tips	Eppendorf
Reaction tubes (1.5ml, 2ml)	Eppendorf
Reaction tubes (15ml, 50ml)	Greiner Bio One
Sterile filter (0.22µm) for syringes	Roth
Syringes (10ml)	TERUMO
Syringes (1ml, 30ml)	Braun
Syringes (50ml)	BD Biosciences
T25 and T75 cell culture flasks	Sarstedt
Ultracentrifucation tubes (Polyallomer 14x95mm)	Beckman Coulter
Whatman paper	BioRad

2.1.3 Biological resources

Biological Ressources	
Alkaline Phosphatase	Fermentas
Dream *Taq* DNA Polymerase	Thermo Scientific
E. coli SURE 2 supercompetent cells	Stratagene
E. coli XL-10 Gold competent cells	Stratagene
Fast Digest restriction enzymes *Afl*II, *Apa*I, *BamH*I, *Bgl*II, *EcoR*I, *Hind*III, *Nhe*I, *Not*I	Fermentas
Golden Gate TALEN and TAL Effector Kit 1.0 and 2.0	Addgene
N2a mouse neuroblastoma cells	ATTC
pCDNA3.1(-)	Invitrogen
pCDNA3.1(+)-Zeo	Invitrogen
pDrive	Qiagen
pEGFP	Clontech
Pfu Ultra II Fusion DNA polymerase	Fermentas
pIRES	Clontech
Restriction Enzyme *Esp3*I	Fermentas
Restriction Enzymes *Afl*II, *Xba*I, *Bsa*I	New England Biolabs
SH-SY5Y human neuroblastoma cells	Nigel Hooper, University of Leeds, England
T4 DNA-Ligase	New England Biolabs

2.1.4 Antibodies

Primary antibodies:

Antibody	Target	Company	2nd Antibody
6E10	Aβ	DBS Emergo	α mouse
Actin	β-Actin	Sigma	α mouse
Flotillin	Flotillin	BD Pharmingen	α mouse
GM130	GM130	BD Pharmingen	α mouse
POM1	PrP^C	A. Aguzzi, Zürich, Switzerland	α mouse
POM2	PrP^C	A. Aguzzi, Zürich, Switzerland	α mouse

Secondary antibodies:

Antibody	Target	Company
Alexa Fluor® 555 Donkey	Mouse IgG	Life Technologies
Alexa Fluor® 488 Donkey	Mouse IgG	Life Technologies
Horseradish peroxidase-labeled anti-mouse	Mouse IgG	Promega

2.1.5 Chemical reagents and buffers

Chemical Reagents and Buffers	
0,05% Trypsin-EDTA	Gibco
1 kb DNA plus ladder	Life Technologies
10x Fast Digest Green Buffer	New England Biolabs
10x T4 DNA Ligase Buffer	Thermo Scientific
10xDream*Taq* Buffer	Thermo Scientific
2-propanol	Roth
2X SYBR® Green PCR Master Mix	Applied Biosystems
Human $A\beta_{40}$	Genic Bio
Human $A\beta_{42}$	Genic Bio
Acetic acid	Roth
Acrylamid solution (Rotiphorese 30%)	Roth
Agarose	Invitrogen
Ammoinum persulfate (APS)	BioRad
Ampicillin (Amp)	Sigma-Aldrich
ATP	Life Technologies
β-Mercaptoethanol	Thermo Scientific
Bovine serum albumin (BSA)	Roth
Bromophenol blue	Merck
Calcein	Life Technologies
DAPI Flouromount G	Southern Biotech
Dimethyl sulfoxide (DMSO)	Sigma-Aldrich
dNTP mix	Sigma-Aldrich
Donkey serum	Merck
Dulbecco's Modified Eagle Media (DMEM) High Glucose (4.5g/l)	gibco Life Technologies
Dulbecco's Modified Eagle Medium: Nutrient Mixture F-12 (DMEM-F12)	gibco Life Technologies
Dulbecco's phosphate buffered saline (PBS)	Gibco
EDTA (Ethylene diamine tetra-acetic acid)	Applichem
EDTA free protease inhibitor cocktail	Roche
Ethanol	J.T. Baker
Ethidium bromide	Roth
Exosome-depleted FBS	Atlas Biologicals
Fetal bovine serum (FBS)	PAA Laboratories
G418 (Gentamycin)	PAA
Glycerol	GE Healthcare
Hoechst 33342	Life Technologies
High performance liquid chromatography (HPLC) H_2O	Roth
Hydrochloric acid	Merck
Immersion oil (Immersol 518Fx)	Southern Biotech
Instant milk powder	GranoVita
IPTG (Isopropyl β-D-1-thiogalactopyranoside)	Fermentas
Magnesium chloride ($MgCl_2$)	Roth, Germany
Opti-MEM	gibco Life Technologies
PAGE Rule Prestained Protein Ladder (10-170kDa)	Fermentas
Paraformaldehyde (PFA)	Merck
Pierce ECL Western Blot Substrate	Thermo Scientific
Potassium chloride (KCl)	Roth, Germany
Propidium idodide	Life Technologies
Quick start bradford protein standard solution	BioRad

Sodium azide	Sigma-Aldrich
Sodium chloride (NaCl)	Sigma-Aldrich
Sodium deoxycholate	Sigma-Aldrich
Sodium dodecyl sulfate (SDS)	Bio-Rad
Spectinomycin (Spec)	Applichem
Super Signal West Femto Substrat	Thermo Scientific
Super Signal West Pico Substrat	Thermo Scientific
Tetracycline (Tet)	Sigma-Aldrich
Tetramethylethylenediamine (TEMED)	Roth
Thioflavin-T	Sigma-Aldrich
Tris-base	Sigma-Aldrich
Tris-HCl	Applichem
Tris-HCl	Sigma-Aldrich
Triton X100	Applichem
Tryptone	Applichem
Tween 20	Roth
Western blot stripping-buffer	Thermo Scientific
X-gal (5-bromo-4-chloro-3-indolyl-beta-D-galacto-pyranoside)	Fermentas
Xylene cyanol FF	Merck
Yeast extract	Applichem

2.1.6 Commercial kits

Commercial Kits	
GeneJet PCR purification Kit	Thermo Scientific
High Capacity cDNA Reverse Transcription Kit	Applied Biosystems
High Pure PCR Template Preparation Kit	Roche
NucleoSpin RNAII kit	Macherey Nagel
QIAGEN PCR Cloning Kit	QIAGEN
QIAprep® Midiprep Kit	QIAGEN
QIAprep® Miniprep Kit	QIAGEN

2.1.7 Software

Software	
Photoshop CS6	Adobe
LAS AF Lite	Leica
EndNote X4	THOMSON REUTERS
Office 2010	Microsoft
Prism 5	GraphPad
Quantity One	BioRad
NanoSight NTA 2.3 Build 0033	Malvern Instruments
pDRAW32	ACACLONE software
Inkscape	Free Software Foundation, Inc.
Image J	National Institute of Health, USA

2.1.8 Bioinformatic tools

Bioinformatic Tools	
Biology WorkBench 3.2	http://seqtool.sdsc.edu/CGI/BW.cgi
CCDS Database	http://www.ncbi.nlm.nih.gov/CCDS/CcdsBrowse.cgi
ClustalW2	http://www.ebi.ac.uk/Tools/clustalw2/
ExPASy translate tool	http://www.expasy.org/tools/dna.html
Invitrogen-Perfect Primer Design	http://tools.invitrogen.com/content.cfm?pageid=9716
NEBcutter V2.0	http://tools.neb.com/NEBcutter2/
Restriction Summary	http://www.ualberta.ca/~stothard/javascript/rest_summary.html
Reverse Complement	http://www.bioinformatics.org/sms/rev_comp.html
TAL Effector Nucleotide Targeter 2.0	https://tale-nt.cac.cornell.edu/

2.1.9 Oligonucleotides

Oligonucleotides (restriction site)	Primer Sequence (restriction site underlined)
EGFP-*EcoR*I-R1 (*EcoR*I)	AAAgaattcCTTGTACAGCTCGTCCATGC
EGFP-*NotI*-F1 (*Not*I)	AAAgcggccgcATGGTGAGCAAGGGCGAG
hsp70-F	GGTGAAGGTCGGTGTGAAC
hsp70-R	GGGGTCTCGCTCCTGGAA
LoxP-3‘ (*BamH*I, *Hind*III)	AAAggatccATAACTTCGTATAGCATACATTATACGAAGTTATaagcttGGG
LoxP-5’ (*Apa*I, *Not*I)	AAAgggcccATAACTTCGTATAGCATACATTATACGAAGTTATgcggccgcGGG
mPrP-3UTR-F1 (*Hind*III)	AAAaagcttGCCTCTGCAAAAAGCGG
mPrP-3UTR-R2 (*Afl*II, *Bgl*II)	AAAaagctt*AGATCT*ATTTATTCACTAGACCAAAACAAAGCC
mPrP-5’UTR-F1 (*Nhe*I, *Bgl*II)	AAAgctagc*AGATCT*ACTCAAACTCACCACGTGTGTG
mPrP-5’UTR-R1 (*Apa*I)	AAAgggcccGCCCAGTATTTAGGCTGAAGG
mPrP-KO-F1	ATGGCCTACTGGCATTTTG
mPrP-seq-R2	CCACTACTGCCCCAGCTG
mPrP-TAL-Scr-F2	AAAGCATTCATGCTGAACTCAA
mPrP-TAL-Scr-R3	AACAGCTCCTCGCCCTTG
pCR8_F1	TTGATGCCTGGCAGTTCCCT
pCR8_R1	CGAACCGAACAGGCTTATGT
Prnp-qPCR-F	AATGCTTACCGTGTGACCC
Prnp-qPCR-R	CATGCAGATTCAAAGACCAGC
SP6 reverse	CATACGATTTAGGTGACACTATAG
T7 forward	TAATACGACTCACTATAGGG
TAL_F1	TTGGCGTCGGCAAACAGTGG
TAL_R2	GGCGACGAGGTGGTCGTTGG
TAL_R3	GGCTCAGCTGGGCCACAATG
TAL_Seq_5-1	CATCGCGCAATGCACTGAC
Zeo-F1 (*Eco*RI)	AAAgaattcATGGCCAAGTTGACCAGTG
Zeo-R1 (*Bam*HI)	AAAggatccTCAGTCCTGCTCCTCGGC

2.1.10 Media and buffers

LB Medium (pH 7.0)

Pepton	10g
Yeast extract	5g
NaCl	5g
H_2O	add to 1l

LB Agar

Peptone	10g
Yeast extract	5g
NaCl	5g
Agar	12.5g
H_2O	add to 1l

NZY+ (pH 7.5)

NaCl	5g
$MgSO_4*7H_2O$	2g
Yeast extract	5g
NZ amine (casein hydrolysate)	10g
H_2O	add to 1l

Radioimmunoprecipitation assay (RIPA) buffer

Tris (pH 7-8)	50mM
NaCl	150mM
SDS	0.1%
Sodium deoxycholate	0.5%
Triton X 100	1%

1x TAE buffer, pH 8.0

Tris-HCl	40 mM
EDTA	1 mM
Acetic Acid	0.11%

6x agarose gel loading buffer

Bromphenol Blue	0.25%
Xylen Cyanol FF	0.25%
Glycerol	30%

2.2 Methods

2.2.1 Nucleic acid determination

The UV-Vis spectrophotometer NanoDrop 100 was utilised to measure deoxyribonucleic acid (DNA) concentration and purity. The extinction coefficient of 1-2 µl sample was measured and the purity was estimated by the ratio of absorbance at 260 nm (DNA) and 280 nm (Protein). The A260/A280 values between 1.8 and 2.0 indicated a pure DNA preparation.

2.2.2 Polymerase chain reaction (PCR)

Polymerase chain reactions (PCRs) for cloning purposes were set up as follows.

PCR setup	
10 ng	DNA template
0.5µl	forward primer (10 µM)
0.5µl	reverse primer (10 µM)
0.5µl	dNTPs (10 µM)
2.5µl	*Pfu* Ultra Buffer (10x)
0.2µl	*Pfu* Ultra II Enzyme
add to 25µl	HPLC-H_2O

EGFP

Template: pEGFP

PCR program	Temperature [°C]	Time	Cycles
Initial Denaturation	95	2’	
Denaturation	95	20’’	
Annealing	58	20’’	35
Elongation	72	20‘‘	
Final Elongation	72	2’	
Hold	4	∞	

Zeo

Template: pCDNA3.1(+)-Zeo

PCR program	Temperature [°C]	Time	Cycles
Initial Denaturation	95	2’	
Denaturation	95	20’’	
Annealing	62	20’’	35
Elongation	72	20‘‘	
Final Elongation	72	2’	
Hold	4	∞	

***Prnp*-5’-UTR**

Template: N2a-WT gDNA

PCR program	Temperature [°C]	Time	Cycles
Initial Denaturation	95	2’	
Denaturation	95	20’’	
Annealing	62	20’’	35
Elongation	72	20‘‘	
Final Elongation	72	2’	
Hold	4	∞	

Prnp-3'-UTR

Template: N2a-WT gDNA

PCR program	Temperature [°C]	Time	Cycles
Initial Denaturation	95	2'	
Denaturation	95	20''	
Annealing	53	20''	35
Elongation	72	20''	
Final Elongation	72	2'	
Hold	4	∞	

gDNA isolated from N2a cells was tested for genomic insertions by PCRs, which were set up as follows.

PCR genotyping setup	
1µl	gDNA (100ng/µl)
0.5µl	forward primer (10 µM)
0.5µl	reverse primer (10 µM)
0.5µl	dNTPs (10 µM)
2.5µl	Dream*Taq* Buffer (10x)
0.1µl	Dream*Taq* (5U/µl)
19.9µl	HPLC-H_2O

mPrP-KO-F1 / mPrP-Seq-R2

PCR program	Temperature [°C]	Time	Cycles
Initial Denaturation	95	5'	
Denaturation	95	45''	
Annealing	61	45''	35
Elongation	72	2'30''	
Final Elongation	72	5'	
Hold	4	∞	

mPrP-TAL-Scr-F2 / mPrP-TAL-Scr-R3

PCR program	Temperature [°C]	Time	Cycles
Initial Denaturation	95	5’	
Denaturation	95	45’’	
Annealing	60	45’’	35
Elongation	72	1‘	
Final Elongation	72	5’	
Hold	4	∞	

2.2.3 Agarose gel electrophoresis

Agarose powder (0.4 g) was added to 50 ml of 1x TAE buffer and boiled in a microwave until dissolved and the solution was poured into a gel electrophoresis chamber. The DNA sample was supplemented with DNA loading dye (6x) and separated at 80-120 V. Images were generated using the Chemi Doc Gel Imaging System after 20min incubation in ethidium bromide (0,5µg/ml in TAE buffer).

2.2.4 Vector and insert preparation

Plasmids were isolated from overnight (O/N) culture of *E. coli* containing the appropriate plasmid under antibiotic selection using QIAprep® Miniprep Kit. For cloning, 500 ng of plasmid were digested with appropriate restriction enzymes, loaded on a gel and the linear fragment was purified using GeneJet PCR purification Kit. The vectors were dephosphorylated with Alkaline Phosphatase for 1 h at 37 °C followed by 20 min at 65 °C for non-directional cloning. The PCR reaction (25 µl) was separated on a 0.8% agarose gel and the fragment of right size was extracted from the gel using InnuPrep Double Pure Kit (Analytik Jena, Germany). After digestion with restriction enzymes, the DNA was purified again for ligation.

2.2.5 Ligation and transformation

Ligation reactions were set up using a 1:3 molar ratio of digested plasmid to insert, i.e. 10 fmol of plasmid and 30 fmol of insert. The reactions containing T4 DNA ligase were incubated for 2 h at room temperature. 50 µl of competent *E. coli* cells were added to the ligation mix and incubated for 30 min on ice. The reactions were heat shocked at 42 °C for 45 s in a water bath followed by 1 min incubation on ice. 450 µl of NZY+ medium were added, and the transformation reactions were incubated for 1 h at 37 °C on a shaker Following a quick centrifugation, the cells were resuspended in 100 µl NZY+ medium and plated on LB agar containing the appropriate antibiotic. The plates were incubated for 16 h at 37 °C.

2.2.6 Verification of clones by colony PCR

Transformed *E. coli* colonies were picked and resuspended in 20µl of high performance liquid chromatography (HPLC) H_2O. 5µl of this bacterial suspension were used for one PCR reaction. The reactions (25µl) were set up as follows.

Colony PCR setup	
5µl	Bacterial suspension
0.5µl	forward primer (10 µM)
0.5µl	reverse primer (10 µM)
0.5µl	dNTPs (10 µM)
2.5µl	Dream*Taq* Buffer (10x)
0.1µl	Dream*Taq* (5U/µl)
15.9µl	HPLC-H_2O

Insert-specific primers were used for colony PCR using the following PCR program:

PCR program	Temperature [°C]	Time	Cycles
Initial Denaturation	95	5’	
Denaturation	95	45’’	
Annealing	*	45’’	30
Elongation	72	*	
Final Elongation	72	5’	
Hold	4	∞	

* Annealing temperature and elongation time depend on primer combination and on fragment size, respectively. 1 kb of DNA can be amplified in 1 min by the *Taq* Polymerase.

Positive clones were cultured O/N in LB media containing the appropriate antibiotic and plasmid DNA was isolated using QIAprep® Miniprep Kit. Clones were verified by restriction digest and, if necessary by PCR. Freezer stocks of positive clones were made in 25% glycerol and stored at -80 °C. Constructs were sequenced by Seqlab (Sequence Laboratories Göttingen GmbH, Germany) to check for mutational errors, reading frame and orientation of inserts.

2.2.7 Construction of a *Prnp* knockout cassette

To knockout the murine *Prnp* gene via homologous recombination, a selection cassette was fabricated containing 1kb of the 5'and 3'-untranslated regions (UTRs) flanking the *Prnp* start codon and a complementary DNA (cDNA) coding for an EGFP-Zeocin (EGFP-Zeo) fusion protein flanked by LoxP sites. The oligonucleotides LoxP-5', flanked by *Apa*I and *Not*I restriction sites, and LoxP-3', flanked by *BamH*I and *Not*I restriction sites, were synthesized by Sigma Aldrich. Both LoxP sites were cloned into pCDNA3.1(-) resulting in pCDNA3.1(-)-LoxP-5'-LoxP-3'. EGFP lacking a stop codon was amplified using primer combination EGFP-*Not*I-F1 and EGFP-*EcoR*I-R1 and cloned into pCDNA3.1(-)-LoxP-5'-LoxP-3' using *Not*I and *EcoR*I yielding pCDNA3.1(-)-LoxP-EGFP-LoxP. Zeo was amplified from pCDNA3.1(+)-Zeo with the primer pair Zeo-F1 and Zeo-R1 and inserted into pCDNA3.1(-)-LoxP-EGFP-LoxP using *EcoR*I and *BamH*I. *Prnp*-3'-UTR was amplified from N2a-WT gDNA with the primer pair mPrP-3'UTR-F1 and mPrP-3'UTR-R1 and cloned into pCDNA3.1(-)-LoxP-EGFP-Zeo-LoxP using *Hind*III and *Afl*II resulting in pCDNA3.1(-)-LoxP-EGFP-Zeo-LoxP-*Prnp*-3'-UTR. *Prnp*-5'-UTR was amplified from N2a-WT gDNA with the primer pair mPrP-5'UTR-F1 and mPrP-5'UTR-R1 and cloned into pCDNA3.1(-)-LoxP-EGFP-Zeo-LoxP-*Prnp*-3'-UTR using *Nhe*I and *Apa*I yielding pCDNA3.1(-)-*Prnp*-5'-UTR-LoxP-EGFP-Zeo-LoxP-*Prnp*-3'-UTR. mPrP-5'UTR-F1 and mPrP-3'UTR-R2 both contain and additional *Bgl*II restriction sites for sub cloning of the *Prnp* knockout cassette (mPrP-KO-Cas). pCDNA3.1(-)-*Prnp*-5'-UTR-LoxP-EGFP-Zeo-LoxP-*Prnp*-3'-UTR was digested with *Bgl*II, which led to excision of the CMV promoter of the pCDNA3.1(-) vector and the whole mPrP-KO-Cas. mPrP-KO-Cas was reinserted into the vector backbone yielding pCDNA3.1(-)-*Prnp*-5'-UTR-LoxP-EGFP-Zeo-LoxP-*Prnp*-3'-UTR-w/o-Promoter (pCDNA3.1(-)mPrP-KO-Cas, Figure 2.1).

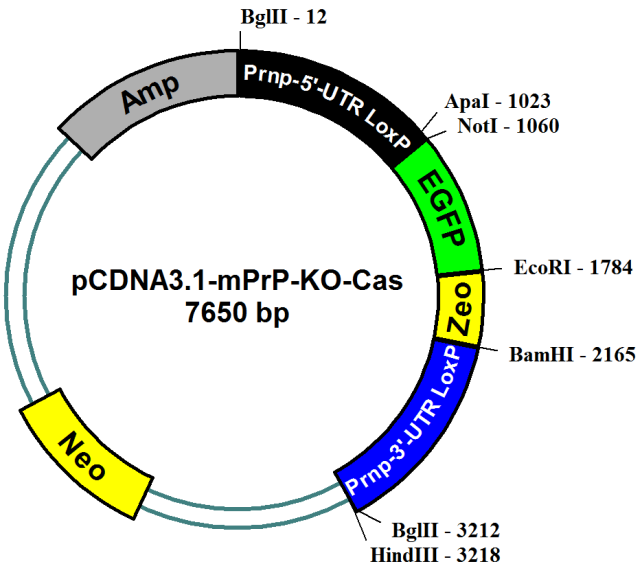

Figure 2.1: pCDNA3.1(-)-mPrP-KO-Cas.

The vector was assembled by multiple cloning steps to facilitate TALEN aided knockout of the *Prnp* gene. (Neo: Neomycine resistance gene; Zeo: Zeocin resistance gene; Amp: bacterial Ampicillin resistance gene; EGFP: Enhanced green fluorescent protein; UTR: untranslated region.)

2.2.8 TALEN design, construction and expression

TAL Effector Nucleotide Targeter 2.0[216] was used to screen the start codon region of the murine *Prnp* gene for putative TALEN binding sites with the following restrictions: (i) a repeat array length of 15-20 repeat variable di-residue domains and (ii) a spacer length of 15–24 nucleotides. Three different TALEN pairs, mPrP-TALEN01, mPrP-TALEN03 and mPrP-TALEN04, were assembled using the Golden Gate TALEN and TAL Effector Kit 1.0 and 2.0[217]. The repeat-variable di-residue (RVD) sequences of the TALENs are summarized in Table 2.1.

Table 2.1: RVD sequences of TALENs used for *Prnp* knockout.

TALEN	RVD Sequence
mPrP-TALEN01-5'	NN NI NG NI HD HD NG NG NN NG NG HD HD NG HD
mPrP-TALEN01-3'	NI NN HD HD NI NI NN NN NG NG HD NN HD HD NI NG NN NI
mPrP-TALEN03-5'	HD NI NG NG NG NG NN HD NI NH NI NG HD NI NN
mPrP-TALEN03-3'	HD NI HD NI NI NI NN NI NH NN NH HD HD NI NH HD NI NN HD HD
mPrP-TALEN04-5'	NG NG NG NN HD NI NH NI NG HD NI NH NG HD NI NG HD NI NG
mPrP-TALEN04-3'	HD NI HD NI NI NI NH NI NN NH NH HD HD NI NH HD NI NH HD HD

The workflow for the assembly of a vector containing a fully functional TALEN is depicted in Figure 2.2.

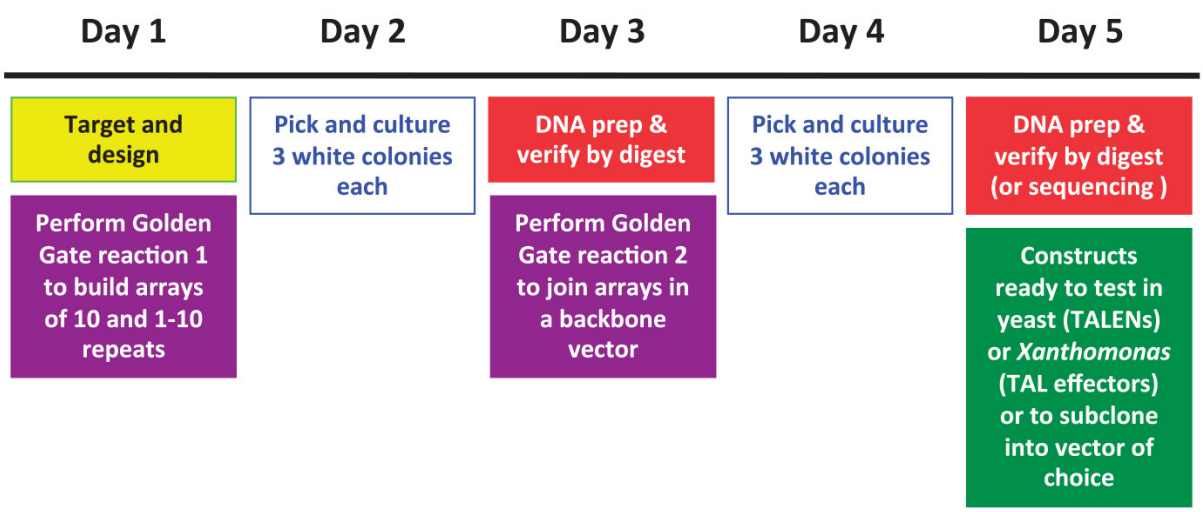

Figure 2.2: Design and assembly of TALENs with the Golden Gate TALEN and TAL Effector Kit.
A TALEN vector can be assembled in five days by multiple cloning steps (figure taken from Cermak 2011)[217].

After TALEN design the first 10 RVDs are assembled in one cloning reaction (Table 2.2).

Table 2.2: Golden gate reaction #1.

150ng of each module vector + 150ng of pFUS vector.
1µl BsaI
1µl T4 DNA ligase
2µl 10X T4 DNA ligase buffer
2µL 10X Bovine Serum Albumen (final concentration of 0.1mg/ml)
H_2O up to 20µl total reaction volume

Vector combinations for golden gate reactions #1a of mPrP-TALEN01, mPrP-TALEN03 and mPrP-TALEN04 are listed in Table 2.3. Destination vector in each reaction is pFUS-A.

Table 2.3: Golden gate reactions #1a for mPrP-TALEN pairs.

TALEN01-5'	TALEN01-3'	TALEN03-5'	TALEN03-3'	TALEN04-5'	TALEN04-3'
pNN1	pNI1	pHD1	pHD1	pNG1	pHD1
pNI2	pNN2	pNI2	pNI2	pNG2	pNI2
pNG3	pHD3	pNG3	pHD3	pNG3	pHD3
pNI4	pHD4	pNG4	pNI4	pNN4	pNI4
pHD5	pNI5	pNG5	pNI5	pHD5	pNI5
pHD6	pNI6	pNG6	pNI6	pNI6	pNI6
pNG7	pNN7	pNN7	pNN7	pNH7	pNN7
pNG8	pNN8	pHD8	pNI8	pNI8	pNI8
pNN9	pNG9	pNI9	pNH9	pNG9	pNH9
pNG10	pNG10	pNH10	pNN10	pHD10	pNN10
pFUS-A	pFUS-A	pFUS-A	pFUS-A	pFUS-A	pFUS-A

Golden gate reactions #1b were set up with pFUS-B destination vectors. The destination vector varies depending on RVD number of each respective TALEN (Table 2.4).

Table 2.4: Golden gate reactions #1b for mPrP-TALEN pairs.

TALEN01-5′	TALEN01-3′	TALEN03-5′	TALEN03-3′	TALEN04-5′	TALEN04-3′
pNG1	pHD1	pNI1	pNH1	pNI1	pNH1
pHD2	pNN2	pNG2	pHD2	pNH2	pHD2
pHD3	pHD3	pHD3	pHD3	pNG3	pHD3
pNG4	pHD4	pNI4	pNI4	pHD4	pNI4
pFUS-B4	pNI5	pFUS-B4	pNH5	pNI5	pNH5
	pNG6		pHD6	pNG6	pHD6
	pNN7		pNI7	pHD7	pNI7
	pFUS-B7		pNN8	pNI8	pNN8
			pHD9	pFUS-B8	pHD9
			pFUS-B9		pFUS-B9

Golden gate reactions #1 were incubated in a thermo cylcler (Table 2.5).

Table 2.5: Incubation program of golden gate reaction #1.

Temperature [°C]	Time	Cycles
37 16	5' 10'	 10
50	5'	1
80	5'	1

To destroy unligated linear dsDNA fragments all golden gate reactions #1 were subjected to Plasmid-Safe nuclease treatment. 1µl 10mM ATP and 1µl Plasmid-Safe nuclease was added to the reactions and incubated at 37°C for 1h. Chemically competent *E. coli* cells were transformed with 5µl of each golden gate reaction #1 respectively and plated on LB agar plates containing spectinomycin, X-Gal and IPTG. Plates were incubated O/N at 37°C and white colonies were picked for colony PCR analysis using primers pCR8_F1 and pCR8_R1 (Table 2.6).

Table 2.6: Program for colony PCR after transformation of golden gate reaction #1.

colony PCR golden gate reaction #1			
PCR program	**Temperature [°C]**	**Time**	**Cycles**
Initial Denaturation	95	5'	1
Denaturation	95	30''	
Annealing	55	30''	35
Elongation	72	1'45''	
Final Elongation	72	5'	1
Hold	1	∞	

Positive clones were cultured O/N and plasmids were isolated by mini prep. Golden gate reaction #2 (Table 2.7) was set up using pFUS-A and pFUS-B vectors of each respective TALEN together with one of five pLR vectors depending on the last RVD of the TALEN (Table 2.8) and the destination vector pTAL3.

Table 2.7: Golden gate reaction #2.

150ng of each pFUS vector
150ng of respective pLR vector
75ng of destination vector pTAL3
1µl Esp3I restriction enzyme
1µl T4 Ligase
2µl 10X T4 DNA ligase buffer (the buffer for the Esp3I enzyme)
H_2O up to 20µl

Table 2.8: pLR vectors used for TALEN assembly.

TALEN	pLR-vector
mPrP-TALEN01-5’	pLR-HD
mPrP-TALEN01-3’	pLR-NI
mPrP-TALEN03-5’	pLR-NN
mPrP-TALEN03-3’	pLR-HD
mPrP-TALEN04-5’	pLR-NG
mPrP-TALEN04-3’	pLR-HD

The incubation program for golden gate reaction #2 is shown in Table 2.9.

Table 2.9: Incubation program of golden gate reaction #1.

Temperature [°C]	Time
37	10'
16	10'
37	15'
80	5'

5µl of each reaction were used for transformation of chemically competent bacteria. Bacteria were grown on LB agar plates containing Amp, X-Gal and IPTG. White colonies were screened by colony PCR using primers TAL_F1 and TAL_R2 (Table 2.10) and cultured O/N.

Table 2.10: Program for colony PCR after golden gate reaction #2.

colony PCR golden gate reaction #2			
PCR program	**Temperature [°C]**	**Time**	**Cycles**
Initial Denaturation	95	5'	1
Denaturation	95	30''	
Annealing	55	30''	35
Elongation	72	3'	
Final Elongation	72	5'	1
Hold	1	∞	

Miniprep of O/N cultures resulted in the acquisition of the following plasmids: pTAL3-mPrP-TALEN01-5', pTAL3-mPrP-TALEN01-3', pTAL3-mPrP-TALEN03-5', pTAL3-mPrP-TALEN03-3', pTAL3-mPrP-TALEN04-5', and pTAL3-mPrP-TALEN04-3'. To ensure correct TALEN assembly all vectors were analyzed by sequencing with primers SeqTALEN 5-1 and TAL_R2. For expression in mammalian cells the TALEN arrays were subcloned into pCDNA3.1(-) vector using restriction enzymes *Afl*II and *Xho*I. Additionally, mPrP-KO-Cas was cloned into pIRES using *Bgl*II and mPrP-TALEN03-5' was subsequently inserted using *Xho*I and *Mlu*I resulting in pIRES-mPrP-TALEN03-5'-mPrP-KO-Cas. All final TALEN vectors that were assembled in this study are depicted in Figure 2.3.

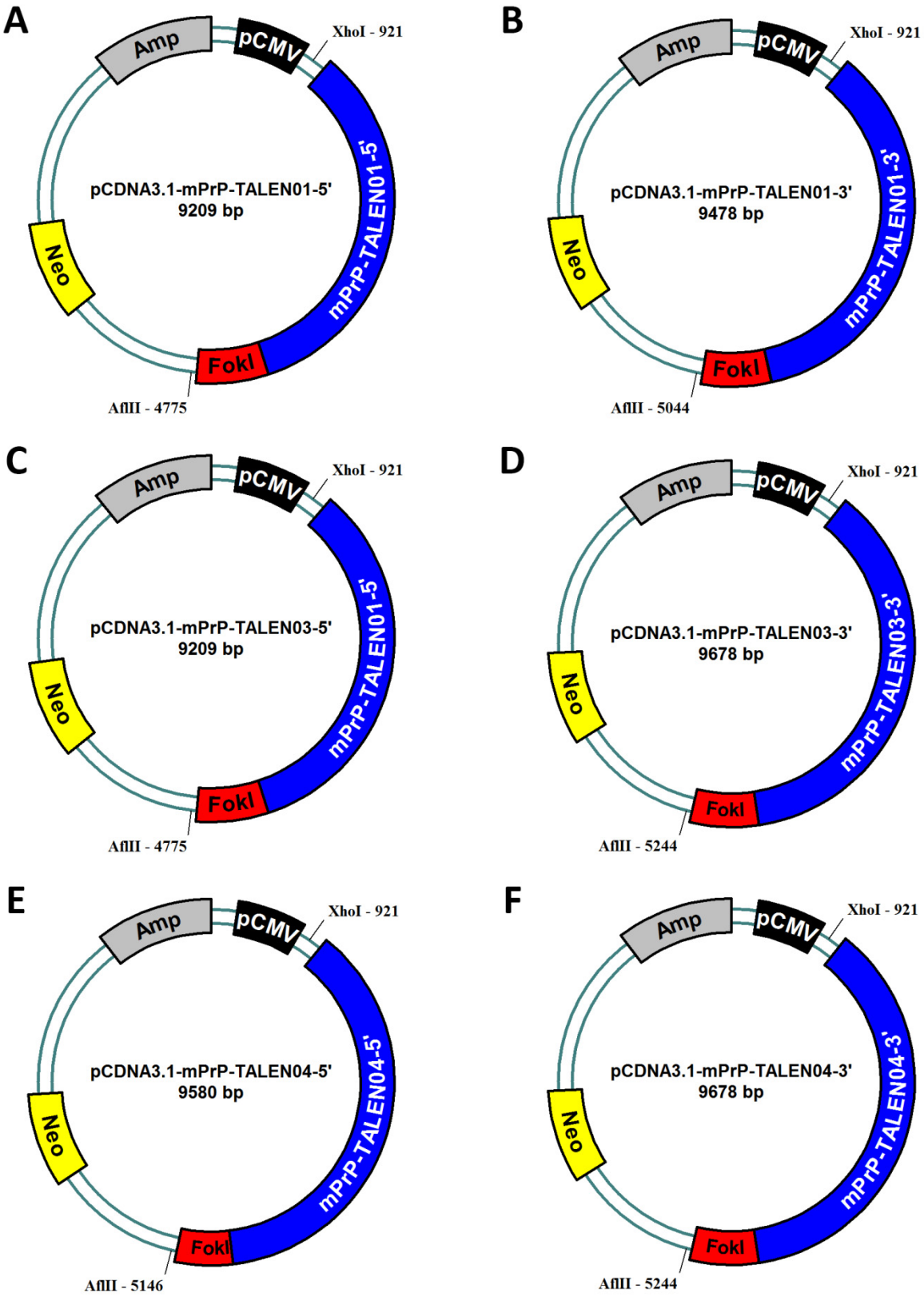
A
Amp
pCMV
XhoI - 921
pCDNA3.1-mPrP-TALEN01-5'
9209 bp
mPrP-TALEN01-5'
Neo
FokI
AflII - 4775
B
Amp
pCMV
XhoI - 921
pCDNA3.1-mPrP-TALEN01-3'
9478 bp
mPrP-TALEN01-3'
Neo
FokI
AflII - 5044
C
Amp
pCMV
XhoI - 921
pCDNA3.1-mPrP-TALEN03-5'
9209 bp
mPrP-TALEN01-5'
Neo
FokI
AflII - 4775
D
Amp
pCMV
XhoI - 921
pCDNA3.1-mPrP-TALEN03-3'
9678 bp
mPrP-TALEN03-3'
Neo
FokI
AflII - 5244
E
Amp
pCMV
XhoI - 921
pCDNA3.1-mPrP-TALEN04-5'
9580 bp
mPrP-TALEN04-5'
Neo
FokI
AflII - 5146
F
Amp
pCMV
XhoI - 921
pCDNA3.1-mPrP-TALEN04-3'
9678 bp
mPrP-TALEN04-3'
Neo
FokI
AflII - 5244

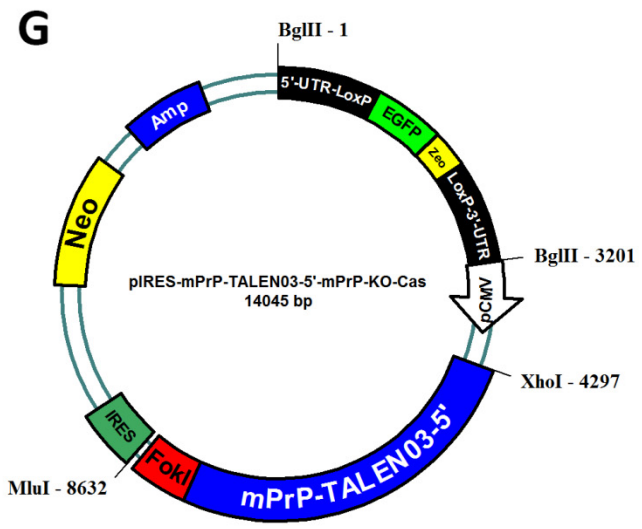

Figure 2.3: TALEN vectors.

(A) pCDNA3.1-mPrP-TALEN01-5', (B) pCDNA3.1-mPrP-TALEN01-3', (C) pCDNA3.1-mPrP-TALEN03-5', (D) pCDNA3.1-mPrP-TALEN03-3', (E) pCDNA3.1-mPrP-TALEN04-5', (F) pCDNA3.1-mPrP-TALEN04-3', (G) pIRES-mPrP-TALEN03-5'-mPrP-KO-Cas. (Neo: Neomycine resistance gene; Zeo: Zeocin resistance gene; *Fok*I: restriction endonuclease; Amp: bacterial Ampicillin resistance gene; IRES: internal ribosome entry site; UTR: untranslated region.)

2.2.9 Cell culture

N2a cells were cultured in Dulbecco's modified Eagle medium (DMEM) supplemented with 10% fetal bovine serum (FBS). SH-SY5Y human neuroblastoma cells, which do not express detectable levels of endogenous PrP^C, stably transfected with either empty pIRESneo vector (SH-SY5Y-PrP(-)) or with pIRESneo vector containing murine PrP^C (SH-SY5Y-PrP(+)) were cultured in Dulbecco's modified Eagle's F12 medium (DMEM-F12) supplemented with 10% FBS[218]. All cell cultures were maintained in an environment of 5% CO_2/95% O_2 at 37°C.

2.2.10 Transfection of N2a cells

N2a cells were seeded in 6-well plates to a confluence of 60-80% after O/N incubation. The desired amount of plasmid DNA was mixed with Opti-MEM to a final volume of 200µl and the desired amount of Lipofectamine 2000 was mixed with Opti-MEM to a final volume of 200µl. Both solutions were incubated separately at room temperature for 5min, mixed and gently inverted five times. The mixture was incubated at room temperature for 20 min. Cells were washed two times with phosphate buffered saline (PBS) and 1.5ml Opti-MEM was added to the well. The DNA/Lipofectamine 2000/Opti-MEM mixture was applied to the cells

and the plate was gently agitated. After 4-8h the medium was aspirated and exchanged for DMEM supplemented with 5% FBS. G418 (gentamycin) was added after O/N incubation to select for successfully transfected cells.

2.2.11 qPCR

RNA was extracted from N2a-WT cells and three putative PrP^C knockout clones, derived from N2a-WT cells after transfection with TALEN plasmids and subsequent selection, using the NucleoSpin RNAII kit. RNA concentration was determined using the NanoDrop system. First-strand cDNA was synthesized using 1 µg of total DNase-treated RNA in a 20µl reverse transcriptase reaction mixture according to the product's manual (High Capacity cDNA Reverse Transcription Kit). Real-Time PCR reactions were performed in a volume of 10 µl consisting of 10ng of cDNA preparation, 2X SYBR® Green PCR Master Mix, and 0.2 µM of each primer. The primer pairs *Prnp*-qPCR-F and *Prnp*-qPCR-R were used for the detection of the murine *Prnp* gene. The 7500 Fast Real-Time PCR System was used to quantify gene expression. To calculate the fluorescence threshold value the 7500 system SDS-software was used. The gene encoding the 70 kilo dalton heat shock protein (*hsp70*; primers: hsp70-F, hsp70-R) was used as a reference to compare the relative expression level of target genes.

2.2.12 Exosome isolation

Exosomes were isolated from the supernatants of N2a and SH-SY5Y cells after 48h of incubation using exosome-depleted FBS. Supernatants were centrifuged at 1,000 x g for 10min, 7,500 x g for 15min, passed through a 0.22µm filter and finally centrifuged at 100,000 x g for 1h in a Optima L-100 XP Ultracentrifuge using a Sw40Ti rotor[176,219,220]. The exosome pellets were resuspended in PBS containing EDTA free protease inhibitor cocktail, quantified by NTA and used for further experiments[221].

2.2.13 Nanoparticle tracking analysis

Exosomes were quantified and characterized using a NanoSight LM10 (Malvern Instruments, NanoSight NTA 2.3 Build 0033) equipped with a 638nm laser and a Marlin F-033B IRF camera. Samples were diluted to a concentration of $8x10^8$-$2x10^9$ particles/ml and videos

were obtained at a camera intensity of 16. Five videos of 30s length respectively were used to calculate average exosome size and particle concentration using the batch processing function of the NanoSight NTA 2.3 software.

2.2.14 Western blotting

Cell lysates were prepared as follows. Cells were washed with PBS, trypsinized for 2min, resuspended in twice the amount of DMEM+FBS, centrifuged at 200 x g for 5min, washed twice with PBS, lysed in an appropriate amount of radioimmunoprecipitation assay buffer (RIPA) buffer (50mM Tris pH 7-8, 150mM NaCl, 0.1% sodium dodecyl sulfate (SDS), 0.5% sodium deoxycholate, 1% Triton X 100) containing protease inhibitor cocktail, incubated on ice for 10min, centrifuged at 15,000 x g for 10min and the protein concentrations of supernatants were determined by Bradford assay in a microplate spectrophotometer. The desired amount of total protein or exosomes was mixed with 5x sample buffer (0.5M Tris-HCl, pH 6.8. 15% SDS. 50% glycerol. 25% β-mercaptoethanol. 0.01% bromophenol blue), incubated at 95°C for 5min and loaded on a gel. For the characterization of cell lines and exosomes self-cast 10% Bis/Tris SDS gels were used. Gels were run in 1x SDS page running buffer and proteins were separated at 100-120V for 90min. To analyze Aβ NuPAGE® Novex® 4-12% Bis-Tris protein gels were used and gels were run using 1x 2-ethanesulfonic acid (MES)/SDS buffer at 200V for 35min. Proteins were transferred to nitrocellulose membranes in 1x blotting buffer with an electric current of 400mA. Proteins were detected using mouse monoclonal antibodies against PrP^C (POM1, POM2, 1:2,500), β-actin (1:5,000), Aβ (6E10, 1:2,000), Flotillin (1:1,000), GM130 (1:500), and horseradish peroxidase-labeled anti-mouse secondary antibody (1:5,000).

2.2.15 $A\beta_{42}$ preparation

2mM stock solutions of $A\beta_{42}$ were prepared by dissolving the peptide in dimethylsulfoxide (DMSO) and aliquots were directly used or frozen at -80°C (Figure 2.4). Aliquots were thawed immediately before the experiments.

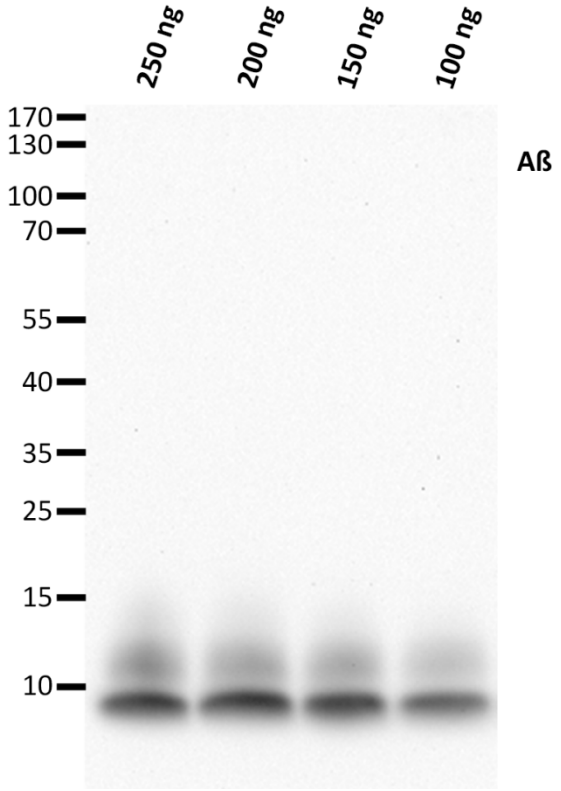

Figure 2.4: Western blot analysis of freshly dissolved synthetic Aβ_{42} in DMSO.
Different concentrations of freshly dissolved Aβ_{42} were analyzed by Western blotting (molecular weight in kDa).

2.2.16 Aging of Aβ

Aβ was aged O/N in PBS at a final concentration of 2mM at room temperature to achieve aggregation of the peptide.

2.2.17 Aβ pull-down by exosomes

Exosomes were incubated in a Stuart SB3 rotator at room temperature with 110nM synthetic human Aβ_{42} with a final concentration of 7.5×10^9 particles/ml for N2a exosomes and 1.9×10^9 particles/ml for SH-SY5Y exosomes in a total volume of 1ml PBS containing protease inhibitor cocktail. After 14h rotation at 20 x rpm in the rotator, samples were centrifuged at 100,000 x g for 1h and the exosome pellets were resuspended in RIPA buffer for Western blot analysis.

2.2.18 Thioflavin T assay

Measurements of $A\beta_{42}$ aggregation states were adapted from published protocols[215,222] using a Safire[2] microplate reader. N2a exosomes ($3.8x10^9$ particles/ml) and SH-SY5Y exosomes ($9.5x10^8$ particles/ml) were incubated with 2µM $A\beta_{42}$ and 10µM Thioflavin T (ThT) in a final volume of 170µl at 37°C under mild agitation. ThT was excited at a wavelength of 450±5nm and emission was detected at a wavelength of 482±10nm. $A\beta_{40}$ aggregation states were measured using a Perkin-Elmer LS50 spectrofluorometer ThT at a final $A\beta_{40}$ concentration of 5µM. SH-SY5Y exosomes ($2.4x10^9$ particles/ml) were incubated with 5µM $A\beta_{40}$ at 37°C in a water bath and fluorescence emission spectra were recorded between 465 and 565nm with 5nm slits, using an excitation wavelength of 450nm.

2.2.19 Confocal immunofluorescence microscopy

N2a cells were seeded on glass cover slips at a density of $3x10^5$ cells per well in a 12-well plate and grown O/N. Cells were washed three times with PBS, fixed with 4% paraformaldehyde (PFA), washed three times with PBS, blocked with PBS containing 2% donkey serum for 1h, incubated with POM1 antibody (1:200 in blocking buffer) for 2h, washed three times, incubated with Alexa Fluor® 488 (Excitation: 495nm, Emission: 519nm) or Alexa Fluor® 555 (Excitation: 555nm, Emission: 565nm) Donkey Anti-Mouse IgG (1:400 in blocking buffer) for 1h, washed three times and mounted with DAPI Fluoromount-G (Excitation: 350nm, Emission: 470nm). The fixed samples were analyzed with a Leica TCS SP5 (Leica Microsystems) confocal microscope.

2.2.20 Fluorescence-activated cell sorting

N2a cells were washed with warm PBS and 2ml trypsin were subsequently added. Cells were incubated for 2min at 37°C, resuspended in 2ml DMEM containing 10% FBS and centrifuged at 200 x g for 5min. Afterwards cells were washed two times with PBS and finally diluted to a concentration of 10^4 cells/µl in a final volume of 100µl. 1µl POM1 or POM2 antibody was added to the suspension and incubated on ice under mild agitation for 20min. Cells were washed two time with PBS and 1µl Alexa488 conjugated secondary antibody was added. Suspension was incubated on ice under mild agitation for 20min. Cells were washed two

times with PBS, passed through a 30µm filter and resuspended in a final volume of 1ml PBS. Unstained cells were isolated using a BD FACS Aria II with a FITC filter.

2.2.21 Cell viability assay based on flow cytometry

N2a-WT cells were seeded at a density of $3x10^5$ cells per well in a 12-well plate and grown O/N. Exosomes were mixed with $A\beta_{42}$ in 500µl of DMEM containing FBS to a final exosome concentration of $9.5x10^9$ particles/ml and a final $A\beta_{42}$ concentration of 5µM. The freshly prepared mixtures were applied to N2a-WT cells and incubated at 37°C for 24h. Cells were detached by trypsinization and washed three times with PBS in a table top centrifuge at 300 x g for 5min. Cell death was determined by adding propidium idodide (Excitation: 535nm, Emission: 617nm) to a 500µl cell suspension in PBS at a final concentration of 1 µg/ml. After incubation for 1min at room temperature cells were analyzed by flow cytometry in a FACSCanto II™ using the PE-Texas Red® filter.

2.2.22 Cell viability assay based on life cell imaging

SH-SY5Y-PrP(+) cells were seeded on coverslips and grown O/N to a final confluence of 80%. Aggregated $A\beta_{42}$ was incubated with SH-SY5Y exosomes ($2.4x10^9$ particles/ml) O/N in medium in a final volume of 400µl. The preincubated mixtures were added to SH-SY5Y-PrP(+) cells for 24h and subsequently mounted in an Attofluor® Cell Chamber. Cell viability was analyzed by simultaneous staining with calcein-AM (0.5mg/ml; Excitation: 495nm, Emission: 515nm), propidium iodide (1mg/ml) and Hoechst (8.1 mM; Excitation: 352nm, Emission: 461nm). Cells were incubated for 20min with the reagents in 500µl medium, washed 2 times with PBS and pictures were acquired with a Leica DMI 4000B microscope.

3 Results

Spread and aggregation of Aβ in the brain plays a key role in the development of AD. Exosomes, small extracellular vesicles of endosomal origin, might be involved in this process. The aim of this study was to determine if PrP^C on exosomes is involved in the association of Aβ to exosomes and whether exosomal PrP^C influences Aβ aggregation kinetics and toxicity.

3.1 Generation of a *Prnp* knockout cell line

Unfortunately, at the beginning of this study no reliable neuronal PrP^C knockout cell line was available. The options at that time were limited to hippocampal cell lines isolated from *Prnp*$^{0/0}$ mice (Hpl3-4)[223], Hpl3-4 cells transfected with PrP^{C224}, PK1 mouse neuroblastoma cells where *Prnp* expression was silenced by RNA interference (RNAi)[225], SH-SY5Y human neuroblastoma cells (SH-SY5Y-PrP(-)), which do not express detectable levels of endogenous PrP^C and (SH-SY5Y-PrP(+)) cells stably transfected with murine PrP^{C218}. For this study a neuronal wild type cell line with a corresponding *Prnp* knockout cell line derived from the wild type cell line was required. Since none of the systems mentioned above fulfils these requirements, we decided to generate a mouse N2a neuroblastoma *Prnp* knockout cell line was generated using TALENs. TALENs are pairs of site-specific DNA endonuclease that are composed of a transcription activator-like (TAL) effector fused to the catalytic domain of the *Fok*I nuclease[226]. The TAL effector domain was adapted from the plant pathogen *Xanthomonas*, where it enters the nucleus and binds to specific sequences in order to modulate host gene expression[227]. TAL-specificity is imparted by a central domain of 12-27 short aa repeats, with a length of 33-35 amino acids[228]. Each repeat contains a polymorphic pair of amino acids at positions 12 and 13, which is termed repeat-variable di-residue (RVD). RVDs determine DNA target specificity, since each naturally occurring RVD binds preferentially to one of the four bases[229,230] (Figure 3.1).

Affinity	low	high	high	low	intermediate
RVD:	NI	HD	NN	NG	NH
Base:	A	C	G/A	T	G

Figure 3.1: TALEN RVDs.

RVDs determine which DNA base the respective repeat in a TALEN array binds. Peptide pair NI binds adenine with low affinity, HD binds cytosine with high affinity, NN binds both guanine and adenine with high affinity, NG bind thymine with low affinity, and NH bind guanine with medium affinity.

The *Fok*I nuclease creates DNA double-strand breaks (DSBs) and is only active in its dimeric form[226]. Hence, TALENs are always deployed in pairs, designed to bind the 5' strand in front and the 3' strand behind the genomic target region (Figure 3.2).

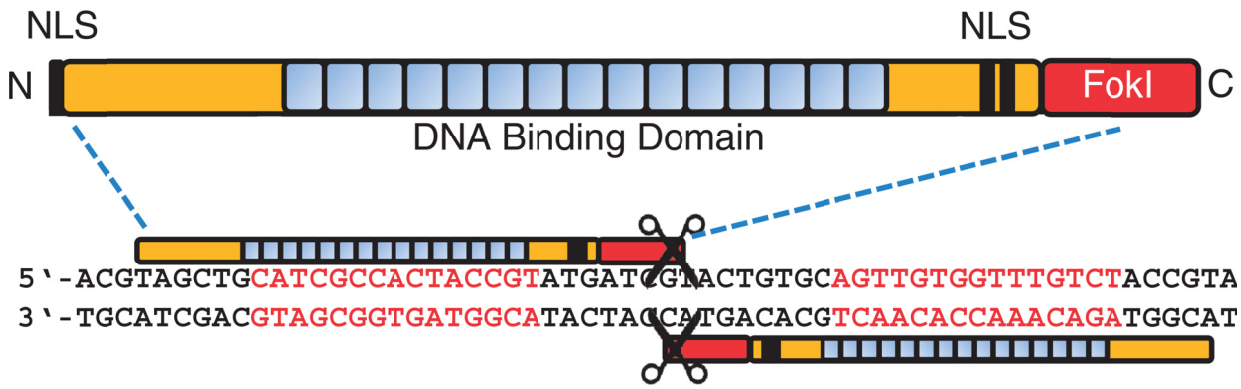

Figure 3.2: The TALEN principle.

Schematic representation of a TALEN induced DNA DSB. Specific DNA binding domains in each TALEN determine the nucleotide sequence where the TALENs bind. Dimerize the *Fok*I nuclease monomers upon 5' and 3' TALEN binding, a DNA DSB is introduced into the DNA by its endonuclease activity. This DSB mostly occurs within the spacer region between the TALEN binding sites (NLS: nuclear localization signal, N: N-terminal, C: C-terminal; modified from Cermak 2011)[217].

Once a DNA DSB has been induced, mammalian cells repair the damage either by non-homologous end joining (NHEJ)[231] or homologous recombination[232]. DNA repair by NHEJ may lead to incorporation of additional nucleotides, and therefore might lead to a frame shift, or loss of nucleotides, hence a deletion. To generate a *Prnp* knockout cell line, a TALEN approach was employed with the intent to induce a DNA DSB in the start codon region of *Prnp* to produce a frame shift or deletions in the *Prnp* gene. For that purpose mPrP-TALEN01 was designed and assembled with the Golden Gate TALEN and TAL Effector Kit 1.0 (Figure 3.6) and finally expressed in N2a-WT cells using the pCDNA3.1(-) vector. Cells were transfected with 2µg of each TALEN vector and selected using 500µg/ml G-418 for two days. Seven days post transfection cells were labeled using anti-PrP^C POM1 or POM2 primary antibodies and Alexa488 labeled secondary antibody in order to stain cell surface PrP^C. PrP^C

negative cells were isolated by fluorescence-activated cell sorting (FACS; Table 3.1; Appendix 1) and clones were cultured in 96-well plates.

Table 3.1: FACS sorting of N2a cells after transfection of mPrP-TALEN01.

Cells were labeled using anti-PrP^C POM1 or POM2 primary antibodies and Alexa488 labeled secondary antibody 7 days post transfection and Alexa488 negative cells were isolated. (TAL1: mPrP-TALEN01 transfection 1, TAL2: mPrP-TALEN01 transfection 2)

Cells	Antibody	% Alexa488 negative
TAL1	POM1	0.3
TAL1	POM2	0.2
TAL2	POM1	0.8

Clones isolated by FACS sorting were screened by immunofluorescence staining (Figure 3.3) and clones that showed low PrP^C signal were expanded and analyzed by Western blotting (Figure 3.4). Although some clones appeared to be PrP^C negative in immunofluorescence analysis, Western blotting revealed that all clones still expressed PrP^C.

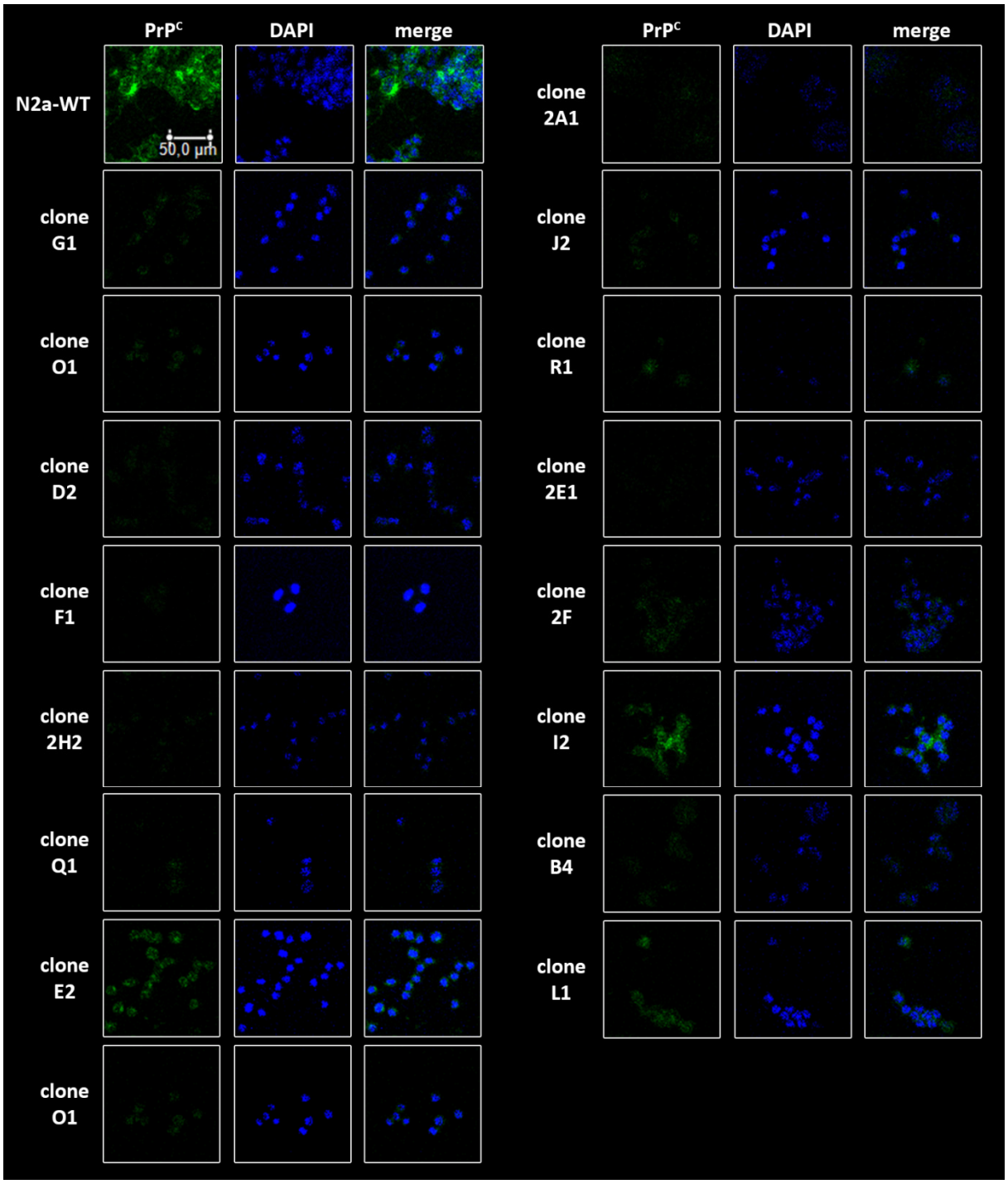

Figure 3.3: Confocal immunofluorescence microscopy for PrP^C in non-permeabilized N2a-WT cells and N2a cells transfected with mPrP-TALEN01 after FACS.

Cells were stained with anti PrP^C antibody POM1 and Alexa488 labeled secondary antibody (scale bar=50µm).

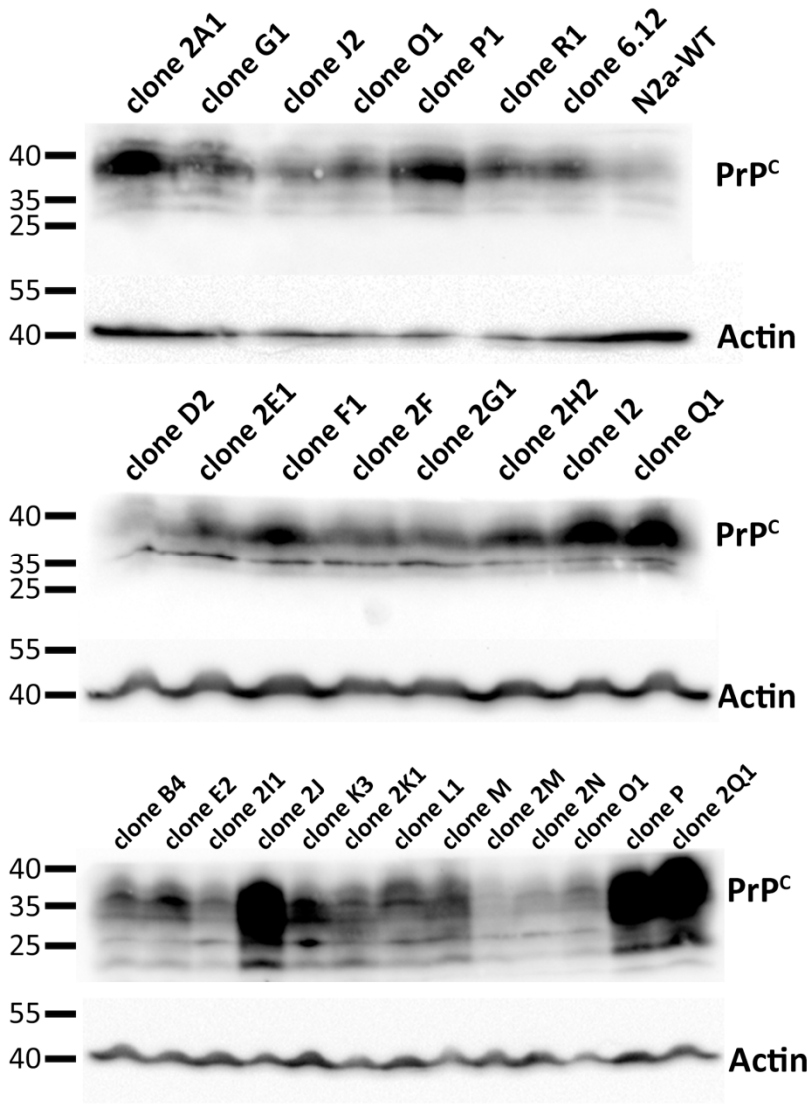

Figure 3.4: Western blot of putative *Prnp* knockout clones after TALEN transfection and flow cytometric sorting.

PrP^C was still detectable in all clones that were analyzed (molecular weight in kDa).

To achieve an efficient *Prnp* knockout, improvement of TALEN specificity was intended and two selection markers were employed in the second knockout strategy. Two additional TALEN pairs (mPrP-TALEN03 and mPrP-TALEN04) were designed and assembled using the Golden Gate TALEN and TAL Effector Kit 2.0 (Figure 3.6), which includes the newly introduced RVD NH (Figure 3.1). Furthermore, a LoxP-EGFP-Zeo-LoxP insertion cassette flanked by 1kb homologous DNA regions 5’ and 3’ of the *Prnp* start codon (mPrP-KO-Cas) was created with the intent to exploit homologous recombination for specific replacement of the *Prnp* start codon with mPrP-KO-Cas (Figure 3.5).

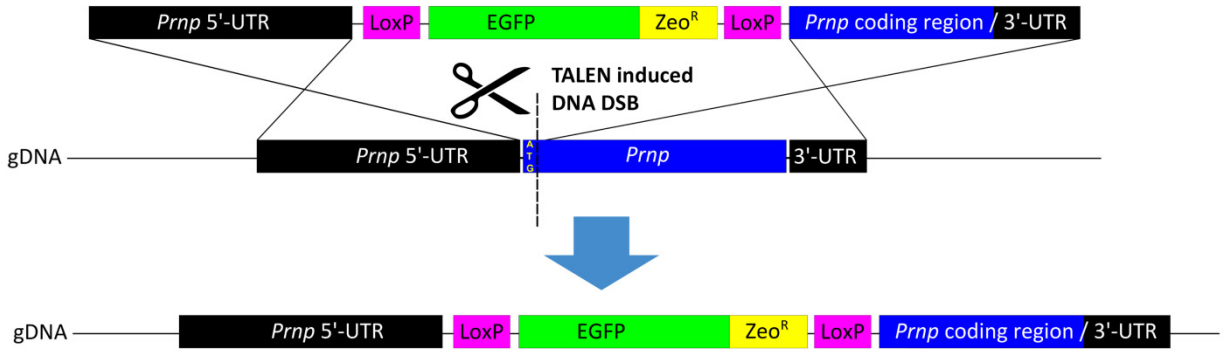

Figure 3.5: *Prnp* knockout strategy.

Scheme of the knockout strategy. A TALEN pair induces a DSB in the *Prnp* gene, which leads to insertion of a LoxP flanked EGFP-Zeo selection cassette, replacing the start codon.

Three different TALEN pairs (Figure 3.6) were designed and tested using different combinations of plasmids, DNA amounts and volumes of Lipofectamine. The results are summarized in Table 3.2.

mPrP-TALEN01

5′-TALEN

NN NI NG NI HD HD NG NG NN NG NG HD HD NG HD

3′-TALEN

NI NN HD HD NI NI NN NN NG NG HD NN HD HD NI NG NN NI

gDNA

5′-binding site

T GATACCTTGTTCCTC attttgcagatcagtca TCATGGCGAACCTTGGCT A

3′-binding site

mPrP-TALEN03

5′-TALEN

HD NI NG NG NG NG NN HD NI NH NI NG HD NI NN

3′-TALEN

HD NI HD NI NI NI NN NI NH NN NH HD HD NI NH HD NI NN HD HD

gDNA

5′-binding site

T CATTTTGCAGATCAG tcatcatggcgaaccttggctact GGCTGCTGGCCCTCTTTGTG A

3′-binding site

mPrP-TALEN04

5′-TALEN

NG NG NG NN HD NI NH NI NG HD NI NH NG HD NI NG HD NI NG

3′-TALEN

HD NI HD NI NI NI NN NI NH NN NH HD HD NI NH HD NI NN HD HD

gDNA

5′-binding site

T TTTGCAGATCAGTCATCAT ggcgaaccttggctact GGCTGCTGGCCCTCTTTGTG A

3′-binding site

Figure 3.6: TALEN pairs that were assembled for *Prnp* knockout.

mPrP-TALEN01 was designed to induce a DNA DSB in front of the start codon of the *Prnp* gene. Upon binding of mPrP-TALEN-03 the *Prnp* start codon (highlighted in yellow) is located in the first half of the space region. The 5' TALEN of mPrP-TALEN04 overlaps with the adenine and thymine of the *Prnp* start codon.

Table 3.2: Transfection outcome of different TALEN combinations targeting the *Prnp* gene in N2a cells.
Only cotransfection of mPrP-TALEN01 with mPrP-KO-Cas yielded EGFP positive clones.

Vector Insert(s)	µg DNA	µl Lipofectamine	EGFP expression
TAL01-5'	1.0		
TAL01-3'	1.0	20.0	-
mPrP-KO-Cas	2.0		
TAL01-5'	1.5		
TAL01-3'	1.5	30.0	+
mPrP-KO-Cas	3.0		
TAL03-5'	1.0		
TAL03-3'	1.0	20.0	-
mPrP-KO-Cas	2.0		
TAL03-5'	1.3		
TAL03-3'	1.3	20.0	-
mPrP-KO-Cas	1.3		
TAL03-5'	1.5		
TAL03-3'	1.5	30.0	-
mPrP-KO-Cas	3.0		
TAL04-5'	1.0		
TAL04-3'	1.0	20.0	-
mPrP-KO-Cas	2.0		
TAL04-5'	1.3		
TAL04-3'	1.3	20.0	-
mPrP-KO-Cas	1.3		
TAL04-5'	1.5		
TAL04-3'	1.5	30.0	-
mPr-PKO-Cas	3.0		
TAL03-5' + mPrP-KO-Cas	1.5		
TAL03-3'	1.0	20.0	-
mPrP-KO-Cas	1.5		
TAL03-5' + mPrP-KO-Cas	2.0		
TAL03-3'	2.0	20.0	-
TAL03-5' + mPrP-KO-Cas	4.0		
TAL03-3'	2.0	30.0	-

The only TALEN pair able to induce EGFP expression, and thus, a homologous recombination event at the *Prnp* locus, was mPrP-TALEN01 (Figure 3.7).

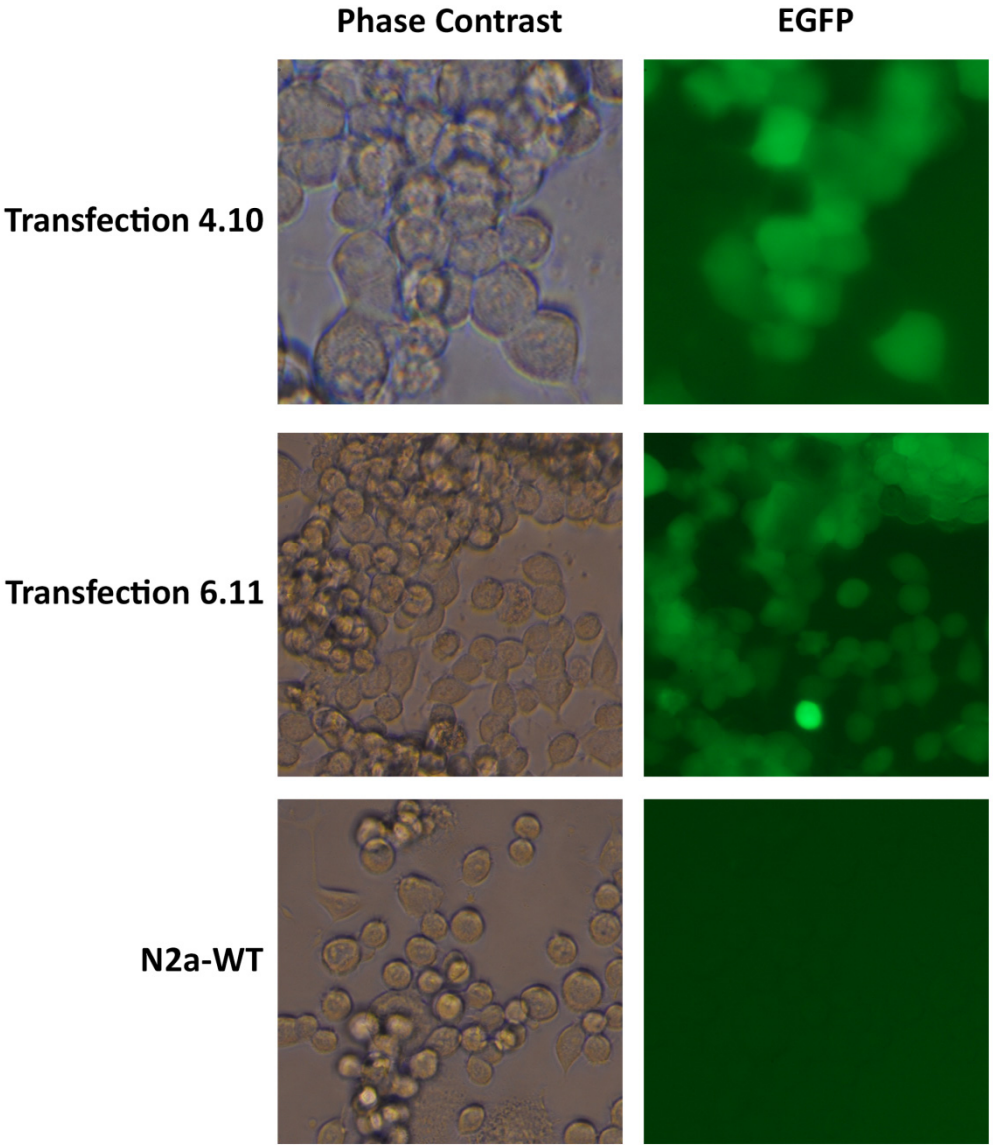

Figure 3.7: Exemplary EGFP positive colonies after cotransfection of N2a cells with mPrP-TALEN01 and mPrP-KO-Cas.

Transfection 4.10 and 6.11 yielded EGFP positive clones (scale bar not available because pictures were taken with a conventional single-lens reflex camera).

Furthermore, an unusually high amount of total DNA of 6µg and 30µl Lipofectamine were needed to achieve the desired result. Multiple EGFP-expressing colonies were isolated, expanded and cloned two times in 96 well plates by dilution plating, to assure purity of the obtained clones. EGFP positive cell cultures were not resistant to Zeocin and exhibited a noticeable lower adherence to the polystyrene surface of the culture flasks. Hence, the three

most adherent clones were selected for further analysis. Western blot analysis showed no detectable PrP^C in clones C2, D4 and E4 (Figure 3.8).

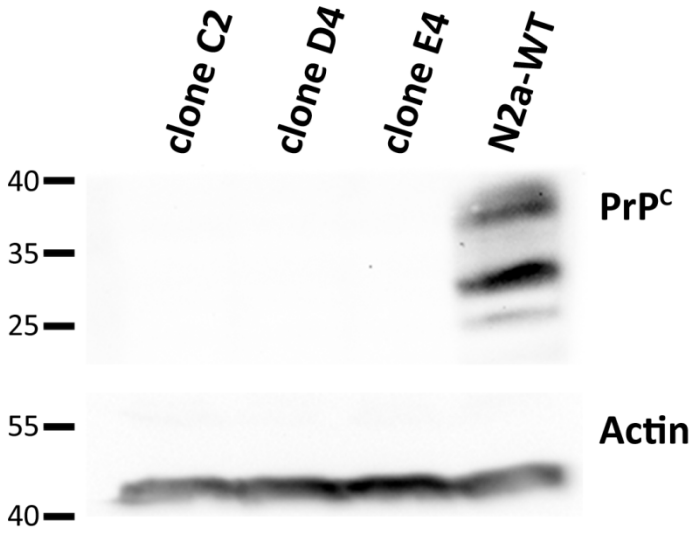

Figure 3.8: Western blot analysis of N2a-WT cells and three N2a *Prnp* knockout clones.

Western blot analysis of the parental N2a-WT cells and three selected *Prnp* knockout clones shows absence of PrP^C (molecular weight in kDa, n=4).

As analyzed by quantitative PCR (qPCR), *Prnp* mRNA could neither be detected in these clones (Figure 3.9).

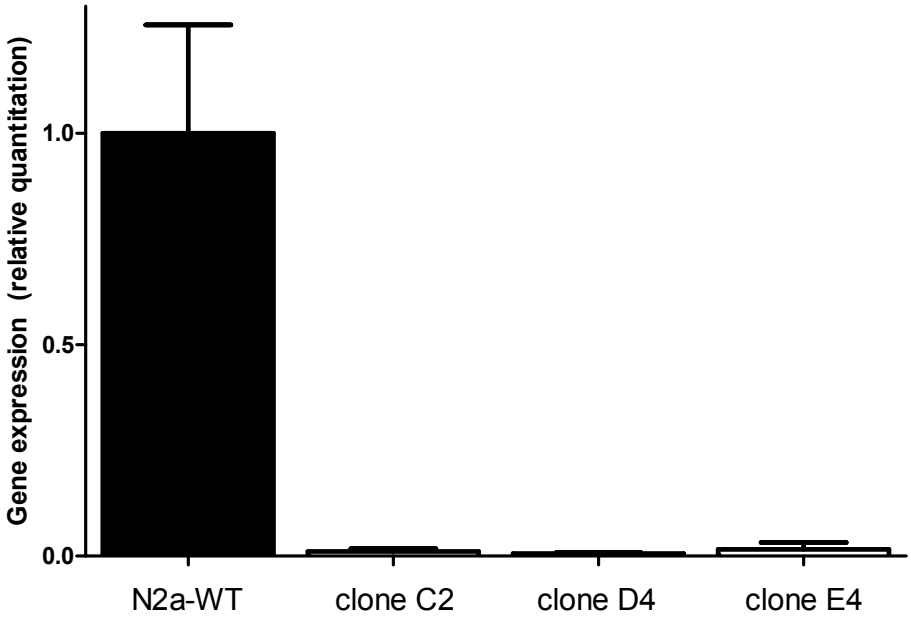

Figure 3.9: qPCR of N2a-WT cells and three N2a *Prnp* knockout clones.

qPCR of the parental N2a-WT cells and three selected *Prnp* knockout clones shows absence of *Prnp* mRNA (N2a-WT: 1.0±0.233; clone C2: 0.011±0.005; clone D4: 0.006±0.002; clone E4: 0.016±0.012; n=3).

Clone D4 was chosen for further experiments and will now be referred to as N2a-PrP$^{0/0}$. An immunofluorescence staining of N2a-PrP$^{0/0}$ cells confirmed EGFP expression and the absence of PrP^{C} in contrast to the original N2a cells, expressing PrP^{C} (Figure 3.10). The parental N2a cell line is therefore designated N2a-WT.

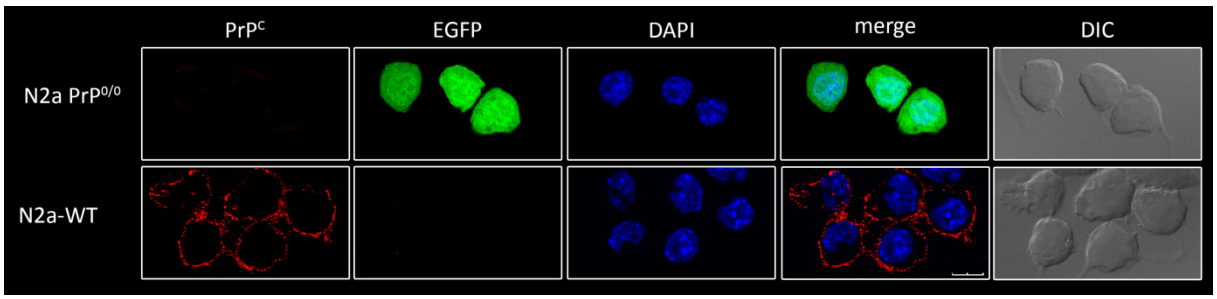

Figure 3.10: Confocal immunofluorescence microscopy for PrP^{C} in non-permeabilized N2a-PrP$^{0/0}$ and N2a-WT cells.

N2a-PrP$^{0/0}$ cells are positive for EGFP expression and PrP^{C} is absent. N2a-WT cells show no EGFP expression and are positive for PrP^{C} staining. PrP^{C} was stained using anti-PrP^{C} POM1 primary antibody and Alexa-555 labeled secondary antibody (DAPI: 4',6-diamidino-2-phenylindole, DIC: differential interference contrast, scale bar=10µm).

To decipher the recombination events that have taken place at the *Prnp* locus of the N2a-PrP$^{0/0}$ cells a PCR was performed using gDNA and the primers mPrP-TAL-scr-F2 and mPrP-TAL-scr-R3. In case of mPrP-KO-Cas integration in the start codon region of *Prnp*, a 1.1 kb amplicon should be detectable (Figure 3.11).

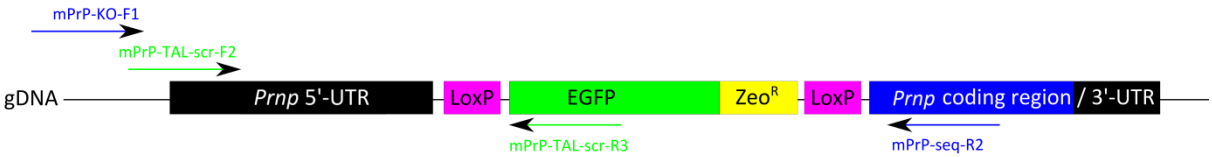

Figure 3.11: Scheme of PCR screening for correct insertion of the *Prnp* knockout cassette.

Primer combination mPrP-KO-F1 mPRP-seq-R2 should yield a PCR product of 1.8kb in case of the *Prnp* WT locus and a 2.9kb PCR fragment should be detectable if the desired integration of LoxP-EGFP-Zeo-LoxP in the *Prnp* locus has taken place. Primer combination mPrP-TAL-scr-F2 and mPrP-TAL-scr-R3 should only amplify a 1.1kb PCR product if LoxP-EGFP-Zeo-LoxP is inserted at the expected site in the genome.

Absence of a PCR product (Figure 3.12) indicated that the desired integration event has not taken place. With the primer combination mPrP-KO-F1 and mPrP-seq-R2 a PCR product of 1.8kb is amplified for the wild type *Prnp* locus. If insertion of LoxP-EGFP-Zeo-LoxP takes place at the expected site in the genome, an amplicon of 2.9 kb should be detectable (Figure 3.11). As shown in Figure 3.12 all three clones showed a weak signal at 1.8kb and a very strong band of about 1kb in size.

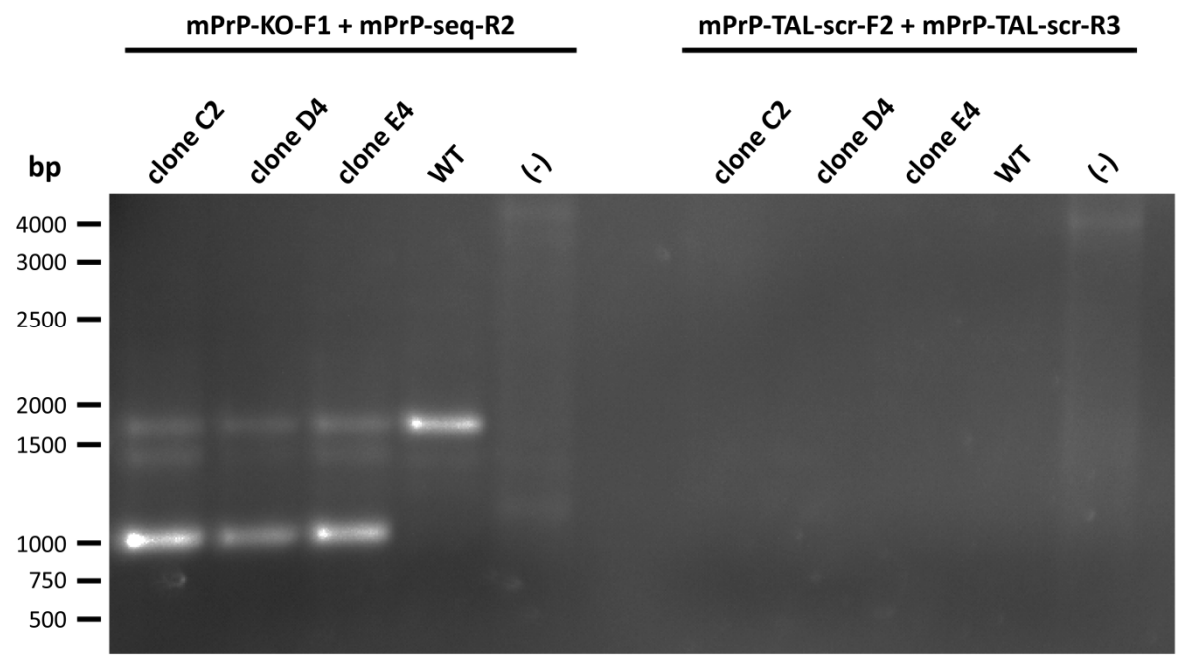

Figure 3.12: PCR screening of gDNA isolated from N2a cells.

Primer combination mPrP-KO-F1 and mPrP-seq-R2 should yield a 1.8kb PCR product if the *Prnp* is present and a 2.9kb fragment if integration of LoxP-EGFP-Zeo-LoxP has taken place. A PCR product of 1.8kb was detectable in all putative *Prnp* knockout clones and the wildtype DNA. Detectable only in probable *Prnp* knockout clones was a 1kb PCR product. Primer combination mPrP-TAL-scr-F2 and mPrP-TAL-scr-R3 should not yield a PCR product in case of the *Prnp* wildtype locus and case of knockout cassette integration a 1.1kb PCR product should be detectable. No PCR fragments could be amplified using this primer combination.

Sequencing of this PCR product and alignment to the *Prnp* locus revealed (Appendix 2), that a 793bp deletion has taken place, which includes the adenine and thymine of the *Prnp* start codon (Figure 3.13).

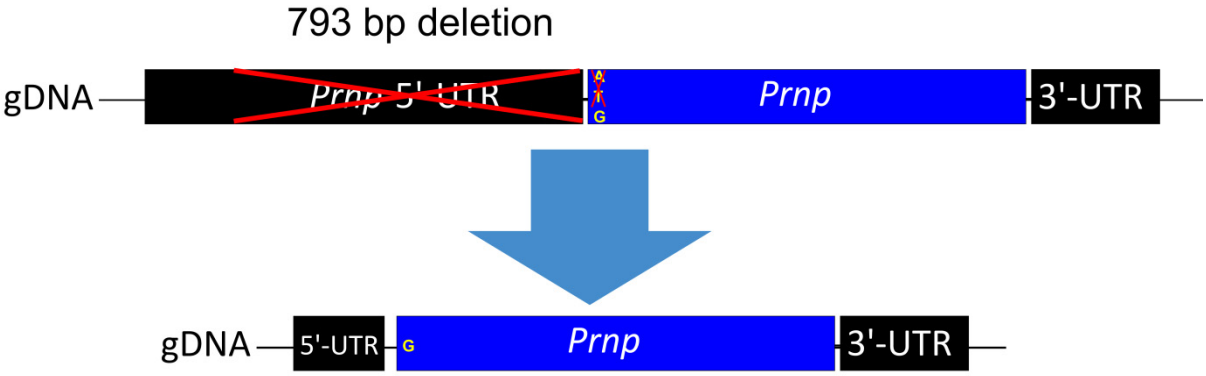

Figure 3.13: Schematic representation of the deletion event that has taken place on at least one chromosome of N2a *Prnp* knockout clones.

Sequencing of gDNA isolated from putative N2a *Prnp* knockout clones revealed a 793 bp deletion including the first two bases of the *Prnp* start codon.

Sequencing of the 1.8kb band showed that the *Prnp* locus was still intact (Appendix 3). Assuming that N2a cells do not contain extra copies of chromosomes, as described for HeLa cells[233], the PCR results suggest that on one chromosome a deletion event of 793bp has taken place, which led to inactivation of the *Prnp* gene. Since the analyzed part of the *Prnp* locus, comprising bases -1500 to +400, is still intact but *Prnp* mRNA as well as PrP^C expression are both absent, integration of mPrP-KO-Cas in the regulatory region of *Prnp* on one chromosome is very likely. The fact that the *Prnp* gene was disrupted on one chromosome and the assumption that the *Prnp* gene on the other chromosome cannot be transcribed due to integration of mPrP-KO-Cas in the promoter region, lead to the conclusion that the *Prnp* gene is knocked out in N2a-$PrP^{0/0}$ cells.

3.2 Characterization of exosomes isolated from N2a and SH-SY5Y cells

With the newly generated neuronal *Prnp* knockout cell model it is now possible to study PrP^C dependent effects in exosome biology *in vitro*. In order to generate reliable data and to exclude species specific effects, the human neuroblastoma cell line, SH-SY5Y, was additionally used in this study. Exosomes were isolated from cell culture supernatants after 48h of incubation and immediately analyzed by nanoparticle tracking analysis (NTA). NTA is a method for particle quantification and size determination based on single particle analysis. Particle size is determined by its Brownian motion and is not influenced by particle density or refractive index. The mode of exosomes isolated from cell lines used in this study were: N2a-$PrP^{0/0}$: 131.8 nm ± 1.9, n=13; N2a-WT: 131.3 nm ± 2.5, n=13; SH-SY5Y-PrP(-): 120.0 nm ± 1.3, n=10; SH-SY5Y-PrP(+): 119.6 nm ± 1.6, n=12 (Figure 3.14).

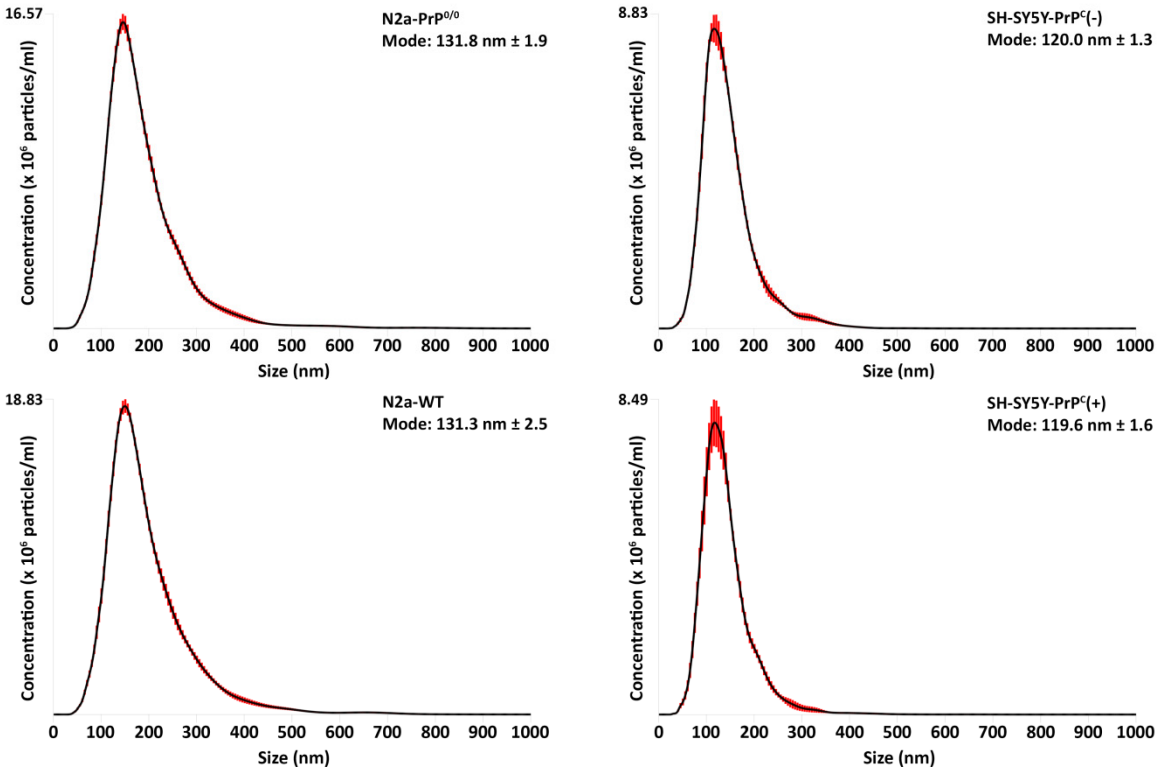

Figure 3.14: NTA characterization of exosomes isolated from N2a and SH-SY5Y cell lines.

Determination of exosome size distribution by NTA: N2a-PrP$^{0/0}$: 131.8 nm ± 1.9 n=13; N2a-WT: 131.3 nm ± 2.5 n=13; SH-SY5Y-PrP(-): 120.0 nm ± 1.3 n=10; SH-SY5Y-PrP(+): 119.6 nm ± 1.6 n=12.

PrP^{C} expression had no influence on the overall distribution of exosome size but significant differences were observed comparing N2a to SH-SY5Y exosomes, since the latter were significantly smaller (Figure 3.15; N2a-WT vs SH-SY5Y-PrP(+), unpaired t-test, p=0.0015; N2a-WT vs SH-SY5Y-PrP(-), unpaired t-test, p=0.0009; N2a-WT vs N2a-PrP$^{0/0}$, unpaired t-test, p=0.8853; N2a-PrP$^{0/0}$ vs SH-SY5Y-PrP(+), unpaired t-test, p<0.0001; N2a-PrP$^{0/0}$ vs SH-SY5Y-PrP(-), unpaired t-test, p<0.0001; SH-SY5Y-PrP(+) vs SH-SY5Y-PrP(-), unpaired t-test, p=0.8478).

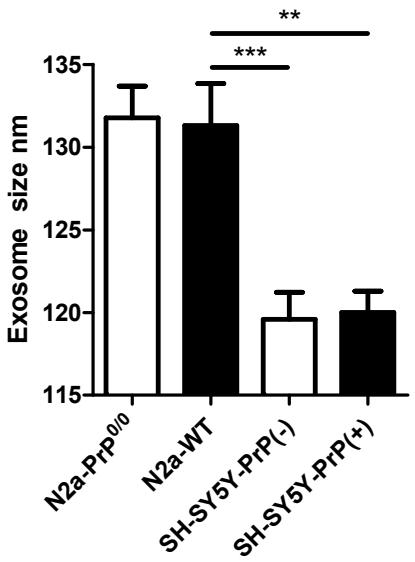

Figure 3.15: Comparison of exosome sizes obtained by NTA.

Comparison of vesicle sizes of shows that SH-SY5Y exosomes are significantly smaller than exosomes isolated from N2a cells (N2a-WT vs SH-SY5Y-PrP(+), **p=0.0015; N2a-WT vs SH-SY5Y-PrP(-), ***p=0.0009; N2a-WT vs N2a-PrP$^{0/0}$, p=0.8853; N2a-PrP$^{0/0}$ vs SH-SY5Y-PrP(+), ***p<0.0001; N2a-PrP$^{0/0}$ vs SH-SY5Y-PrP(-), ***p< 0.0001; SH-SY5Y-PrP(+) vs SH-SY5Y-PrP(-), p=0.8478).

For Western blot analysis exosome amounts were adjusted to 6.6 x 10^9 particles in case of N2a and to 1.9 x 10^9 particles for SH-SY5Y exosomes (Figure 3.16). The exosomal preparations were considered pure due to absence of the cis-Golgi matrix protein GM130 and presence of the exosome/lipid-raft marker Flotillin. PrP^C could not be detected on exosomes derived from N2a-PrP$^{0/0}$ and SH-SY5Y-PrP(-) cells but was present on exosomes that originated from N2a-WT as well as SH-SY5Y-PrP(+) cells.

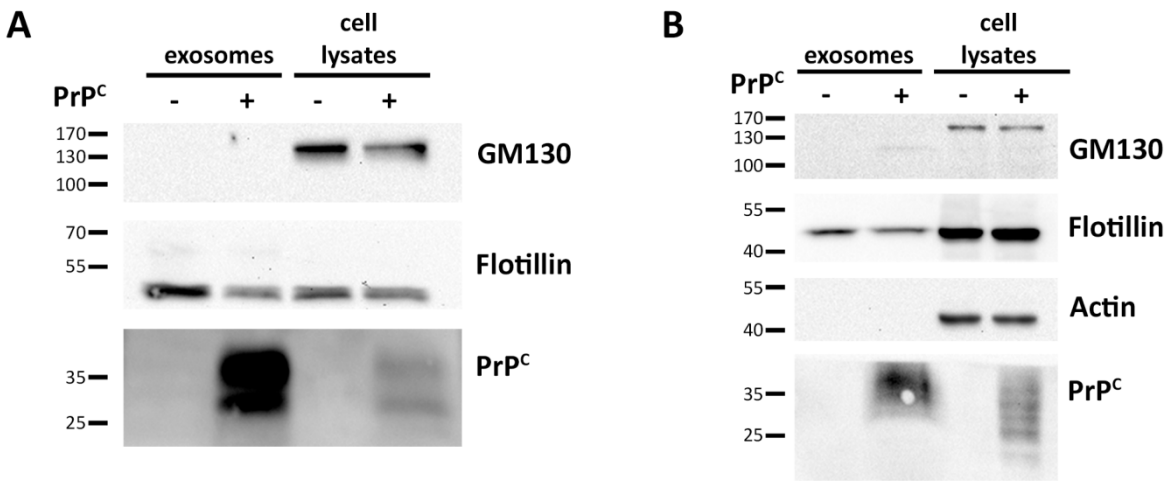

Figure 3.16: Western blot characterization of exosomes isolated from N2a and SH-SY5Y cell lines.
(A) Western blot analysis of exosomes isolated from N2a-PrP$^{0/0}$ and N2a-WT (6.6x10^{9} particles) cells shows absence of GM130 and presence of Flotillin. PrP^{C} could not be detected in N2a-PrP$^{0/0}$ exosomes (n=4). (B) Western blot analysis of exosomes isolated from SH-SY5Y-PrP(-) and SH-SY5Y-PrP(+) (1.9x10^{9} particles) cells shows absence of GM130 and presence of Flotillin. PrP^{C} could not be detected in SH-SY5Y-PrP(-) exosomes (molecular weight in kDa, n=3)

A tenfold enrichment of PrP^{C} on N2a-WT and SH-SY5Y-PrP(+) exosomes compared to cell lysates (15 µg protein/well) was observed when normalized to Flotillin expression (Figure 3.17; N2a-WT exosomes vs N2a-WT cell lysates, unpaired t-test, $p<0.0001$, n=4; SH-SY5Y-PrP(+) exosomes vs SH-SY5Y-PrP(+) cell lysates, unpaired t-test, p=0,0011, n=3).

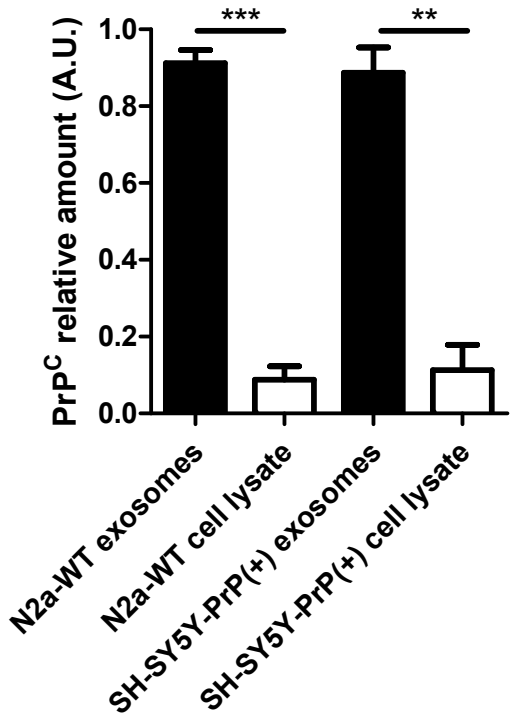

Figure 3.17: PrP^C is highly enriched on exosomes from neuronal cell lines.

Relative amounts of PrP^C on exosomes is 10-fold higher compared to cell lysates when normalized to Flotillin (N2a-WT exosomes vs N2a-WT cell lysates, unpaired t-test, ***p<0.0001, n=4; SH-SY5Y-PrP(+) exosomes vs SH-SY5Y-PrP(+) cell lysates, unpaired t-test, **p=0,0011, n=3).

3.3 $A\beta_{42}$ binding to exosomes in a PrP^C-dependent manner

To investigate if exosomes bind $A\beta_{42}$ and if binding occurs via PrP^C on the outer leaflet of exosomes, N2a-WT, N2a-$PrP^{0/0}$, SH-SY5Y-PrP(+) and SH-SY5Y-PrP(-) exosomes were incubated O/N with $A\beta_{42}$. Exosome bound $A\beta_{42}$ was pulled down by ultracentrifugation and the obtained pellets were analyzed by Western blotting (Figure 3.18).

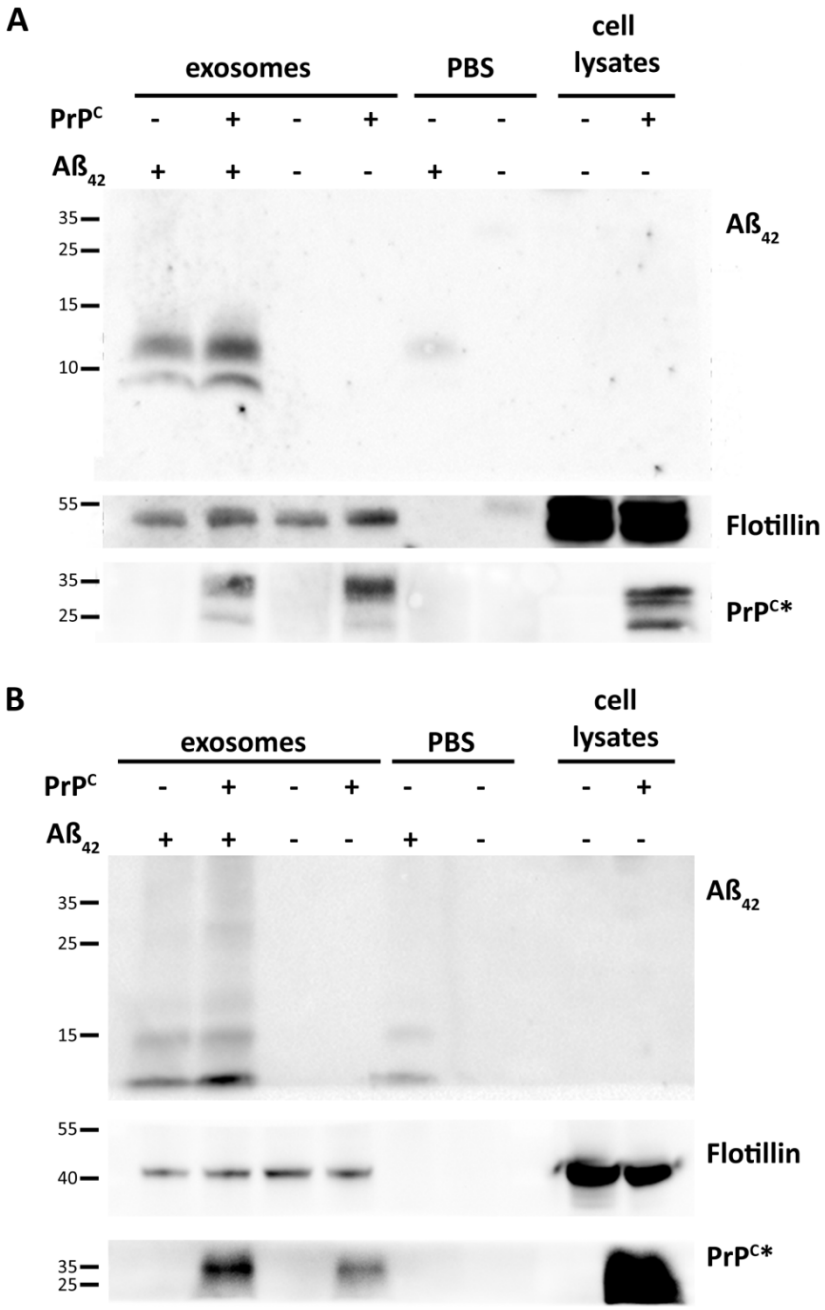

Figure 3.18: Western blot analysis of exosome-mediated Aβ_{42} pulldown.

(A) Western blot analysis of Aβ_{42} bound to exosomes isolated from N2a-PrP$^{0/0}$ and N2a-WT cells after a pull-down experiment. (B) Western blot analysis of Aβ_{42} bound to exosomes isolated from SH-SY5Y-PrP(-) and SH-SY5Y-PrP(+) cells after a pull-down experiment. *PrP^{C} was run on replica gels since it was not detectable using gradient gels.

Quantification revealed that PrP^{C}-containing exosomes were able to pull down a significantly higher amount of Aβ_{42} compared to PrP^{C}-deficient exosomes (Figure 3.19; N2a-WT vs N2a-PrP$^{0/0}$, unpaired t-test, p=0.0164, n=3; SH-SY5Y-PrP(+) vs SH-SY5Y-PrP(-), p=0.0304, n=3). Aβ_{42} binding capacity of N2a-WT exosomes was 2.8 times higher compared to N2a-PrP$^{0/0}$

exosomes and SH-SY5Y-PrP(+) exosomes pulled down 2 times more Aβ_{42} compared to SH-SY5Y-PrP(-) exosomes.

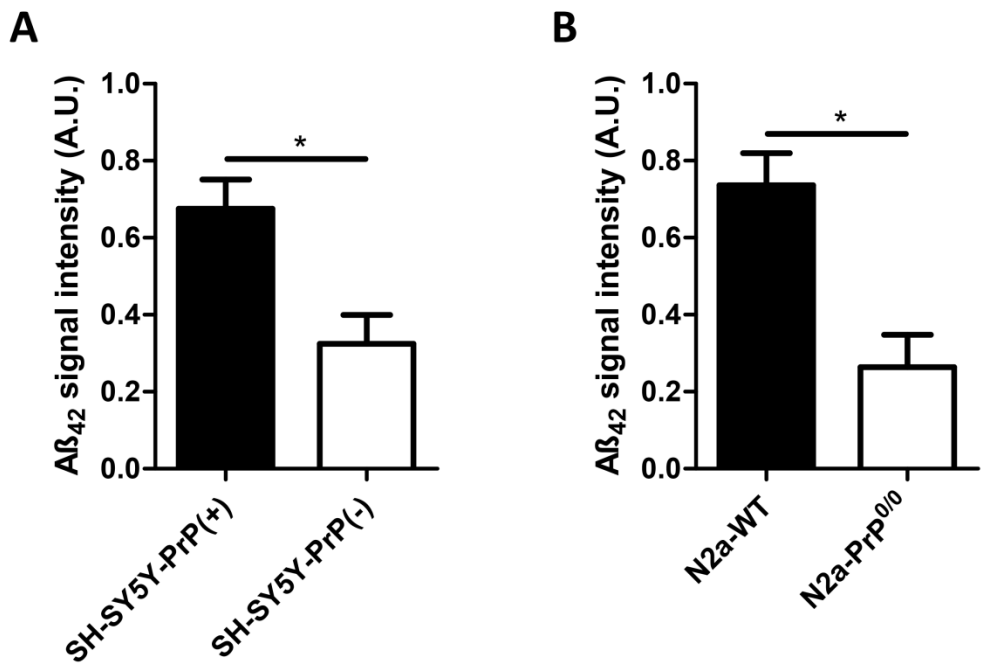

Figure 3.19: Quantification of exosome mediated Aβ_{42} pulldown.

(A) Binding of Aβ_{42} to N2a-WT exosomes is 2.8-fold higher compared to Aβ_{42} binding to $PrP^{0/0}$ exosomes (*p=0.0164, n=3). (B) Binding of Aβ_{42} to SH-SY5Y-PrP(+) exosomes is 2-fold higher compared to Aβ_{42} binding to SH-SY5Y-PrP(-) exosomes (*p=0.0304, n=3). *PrP^{C} was run on replica gels since it was not detectable using gradient gels.

3.4 Influence of exosomes on Aβ aggregation

Since it has been shown previously that exosomes promote Aβ fibrillization[210], this experiment was designed to identify a putative influence of exosomal PrP^{C} on Aβ aggregation. To achieve this, a kinetic Thioflavin T (ThT) time course experiment was performed. ThT is a fluorescent dye that binds β-sheet rich structures and changes its emission spectrum upon binding. Hence, ThT signal is a direct correlate of protein aggregation. Measurements were done in a Tecan Safire^{2} microplate reader. To assure measurement accuracy a calibration test was carried out. Different amounts of aged Aβ_{42} (0µM-8µM, n=3) were incubated with ThT and 9 measurements were taken during a time period of 27min (Figure 3.20).

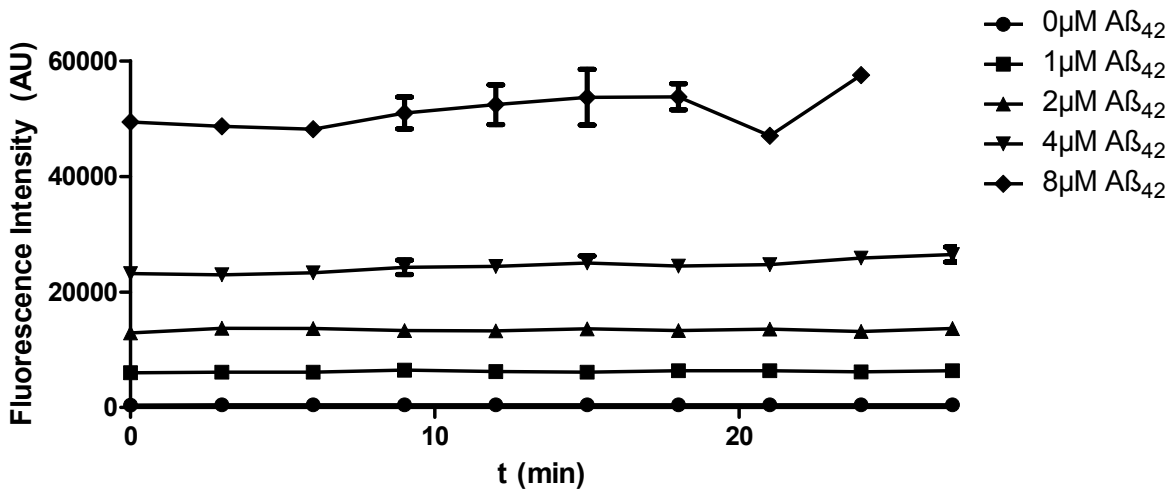

Figure 3.20: Calibration test of the Tecan Safire² microplate reader.

Different amounts of aggregated Aβ42 (0-8µM; n=3) were incubated with ThT and fluorescent signal was measured over a time period of 27min.

A linear regression of the obtained values revealed a correlation of 99.91% between $A\beta_{42}$ concentration and fluorescence intensity (Figure 3.21, r^2=0,9991, p<0.0001, n=21-30).

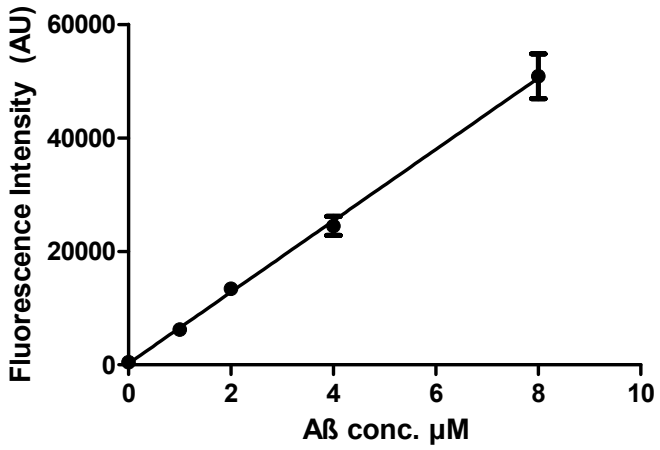

Figure 3.21: Linear regression of all values acquired during the Tecan Safire² calibration test.

An r^2 value of 0.9991 indicates that the measurement is highly reliable (0µM $A\beta_{42}$ n=30; 1µM $A\beta_{42}$ n=30; 2µM $A\beta_{42}$ n=30; 4µM $A\beta_{42}$ n=30; 8µM $A\beta_{42}$ n=21).

Exosomes derived from N2a-WT and N2a-$PrP^{0/0}$ cells as well as PBS as a control were each incubated with $A\beta_{42}$ over a time period of 54h in a fluorescence plate reader. There was no observable influence of N2a-$PrP^{0/0}$ exosomes on $A\beta_{42}$ aggregation compared to the PBS control containing only $A\beta_{42}$ ($A\beta_{42}$ only). N2a-WT exosomes lead to a significant increase in ThT fluorescence compared to the control (Figure 3.22; N2a-$PrP^{0/0}$ vs $A\beta_{42}$ only, Two-way ANOVA, p=0.8248, n=3; N2a-WT vs $A\beta_{42}$ only, Two-way ANOVA, p=0.0076, n=3).

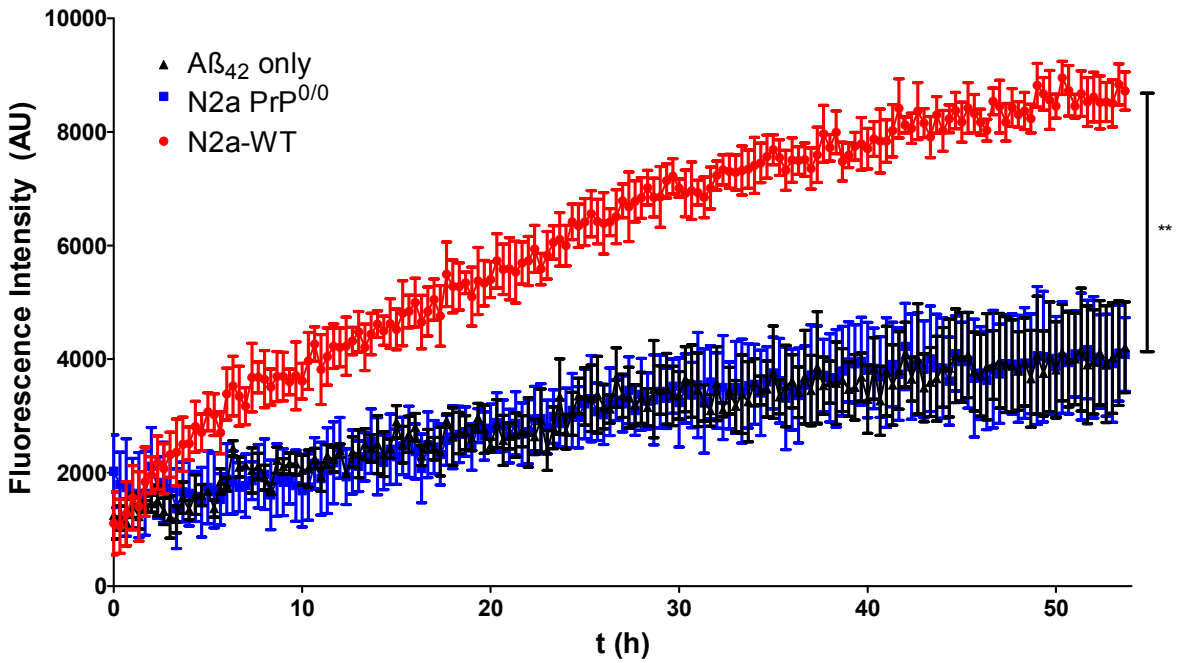

Figure 3.22: ThT time course of N2a exosomes incubated with Aβ$_{42}$.

Quantitation of a ThT time course experiment showed that N2a-WT exosomes significantly accelerate Aβ$_{42}$ aggregation, whereas N2a-PrP$^{0/0}$ had no impact on Aβ$_{42}$ aggregation (N2a-PrP$^{0/0}$ vs Aβ$_{42}$ only, p=0.8248, n=3; N2a-WT vs Aβ$_{42}$ only, **p=0.0076, n=3).

Statistical significance between N2a-WT and Aβ$_{42}$ only fluorescence signal was reached after 7h incubation. After ~50h the signal plateaued with a 1.43 fold increase in ThT signal. Nevertheless, Aβ$_{42}$ significantly increased over the time course of 54h. But this was drastically increased by addition of N2a-WT exosomes (Aβ$_{42}$ only t=0 vs Aβ$_{42}$ only t=54h, unpaired t-test, p=0.0219, n=3; N2a-WT t=0 vs N2a-WT t=54h, unpaired t-test, p=0.0003, n=3).

Neither exosomes isolated from SH-SY5Y-PrP(-) nor SH-SY5Y-PrP(+) cells could significantly alter Aβ$_{42}$ aggregation compared to Aβ$_{42}$ only over a time course of 57h. However, if compared to each other, a statistically significant difference between SH-SY5Y-PrP(-) and SH-SY5Y-PrP(+) exosomes concerning their influence on Aβ$_{42}$ aggregation over the time course was observable (Figure 3.23; SH-SY5Y-PrP(-) vs Aβ$_{42}$ only, Two-way ANOVA, p=0.1849, n=3; SH-SY5Y-PrP(+) vs Aβ$_{42}$ only, Two-way ANOVA, p=0.0506, n=3; SH-SY5Y-PrP(+) vs SH-SY5Y-PrP(-) only, Two-way ANOVA, p=0.0226, n=3).

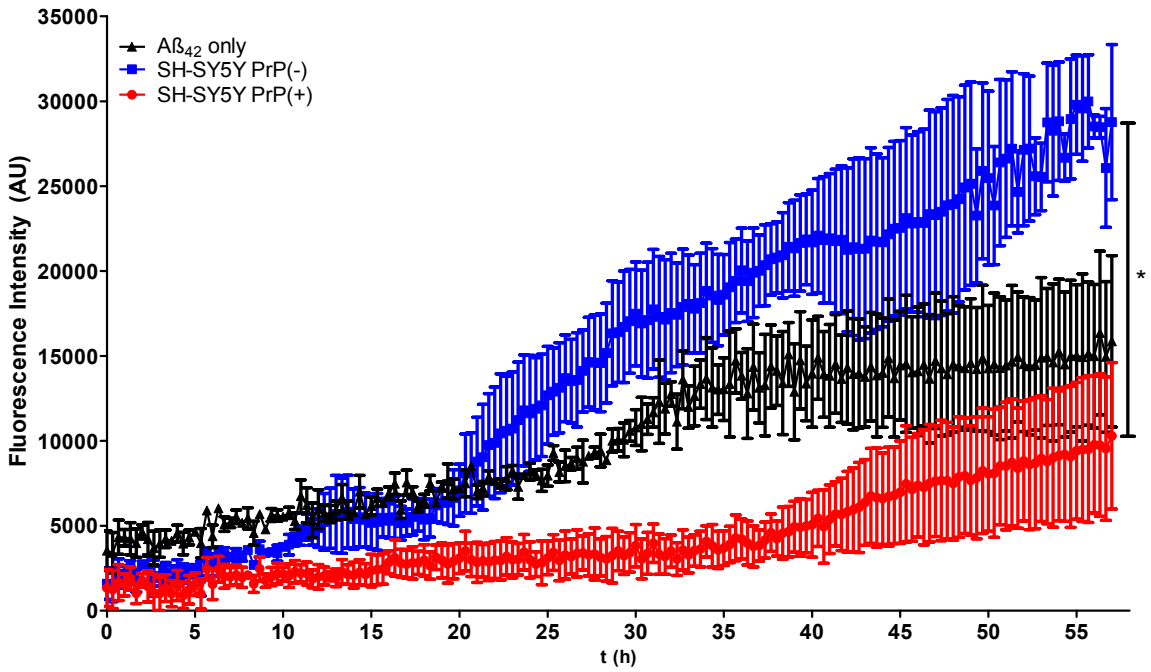

Figure 3.23: ThT time course of SH-SY5Y exosomes incubated with Aβ_{42}.

Over the time course of 57h SH-SY5Y-PrP(-) and SH-SY5Y-PrP(+) exosomes did not influence Aβ_{42} aggregation (SH-SY5Y-PrP(-) vs Aβ_{42} only, p=0.1849, n=3; SH-SY5Y-PrP(+) vs Aβ_{42} only, p=0.0506, n=3; SH-SY5Y-PrP(+) vs SH-SY5Y-PrP(-) only, *p=0.0226, n=3). Between t=48-57h SH-SY5Y-PrP(-) exosomes significantly accelerated Aβ_{42} aggregation. SH-SY5Y-PrP(-) significantly decelerated Aβ_{42} aggregation between t=20-45h.

It is noteworthy, that SH-SY5Y-PrP(+) exosomes inhibit Aβ_{42} aggregation, whereas exosomes derived from SH-SY5Y-PrP(-) cells accelerate aggregation. Furthermore, significant exosome mediated effects on Aβ_{42} aggregation compared to Aβ_{42} only were observable at various time points employing an unpaired t-test (e.g. SH-SY5Y-PrP(+) vs Aβ_{42} only, t=20-45h; SH-SY5Y-PrP(-) vs Aβ_{42} only, t=48-57h).

In summary, contradictory data was acquired using two different cell lines. While N2a-WT exosomes accelerated the fibrillization of Aβ_{42}, SH-SY5Y-PrP(+) exosomes inhibited Aβ_{42} aggregation. Furthermore, exosomes derived from N2a-PrP$^{0/0}$ cells did not alter Aβ_{42} aggregation kinetics over time, whereas a slight increase was observable in the case of SH-SY5Y-PrP(-) exosomes.

In addition the effects of SH-SY5Y exosomes on the aggregation of another Aβ isoform, Aβ_{40}, were assessed in a non-automated experiment using a Perkin-Elmer LS50 spectrofluorometer. The results are depicted in Figure 3.24.

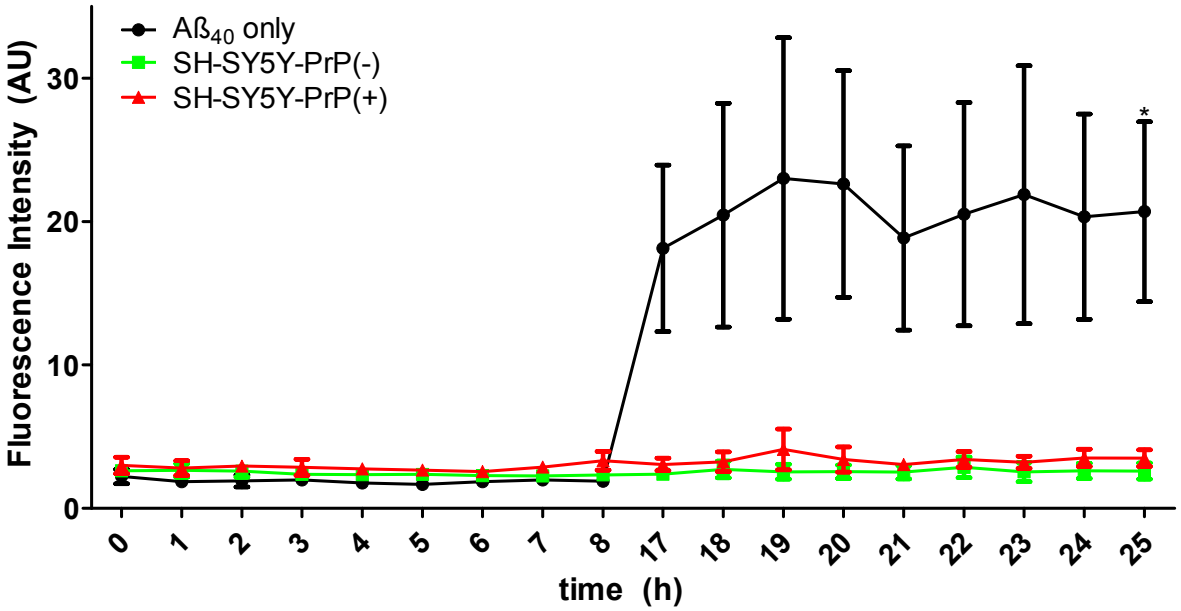

Figure 3.24: ThT time course of SH-SY5Y exosomes incubated with Aβ$_{40}$.

Exosomes isolated from SH-SY5Y-PrP(-) and SH-SY5Y-PrP(+) cells inhibited Aβ$_{40}$ aggregation over a time course of 25h independent of their PrP^{C} content. Lack of time points t=9-16 and the high standard deviation of Aβ$_{40}$ only hampered statistical analysis (SH-SY5Y-PrP(-) vs Aβ$_{42}$ only, p=0.0872, n=3; SH-SY5Y-PrP(+) vs Aβ$_{42}$ only, p=0.1042, n=3; SH-SY5Y-PrP(+) vs SH-SY5Y-PrP(-) only, p=0.3633, n=3; SH-SY5Y-PrP(-) t=25 vs Aβ$_{40}$ only t=25, *p=0.0455, n=3; SH-SY5Y-PrP(+) t=25 vs Aβ$_{40}$ only t=25, p=0.0526, n=3; SH-SY5Y-PrP(+) t=25 vs SH-SY5Y-PrP(-) t=25, p=0.3314, n=3).

Over the time course of 25h no statistical significant differences between the experimental groups were observable (SH-SY5Y-PrP(-) vs Aβ$_{40}$ only, Two-way ANOVA, p=0.0872, n=3; SH-SY5Y-PrP(+) vs Aβ$_{40}$ only, Two-way ANOVA, p= 0.1042, n=3; SH-SY5Y-PrP(+) vs SH-SY5Y-PrP(-) only, Two-way ANOVA, p=0.3633, n=3). Looking at single time points no significant differences could be found at t=17, whereas at t=25 exosomes derived from SH-SY5Y-PrP(-) significantly inhibited Aβ$_{40}$ aggregation (SH-SY5Y-PrP(-) t=25 vs Aβ$_{40}$ only t=25, unpaired t-test, p=0.0455, n=3; SH-SY5Y-PrP(+) t=25 vs Aβ$_{40}$ only t=25, unpaired t-test, p=0.0526, n=3; SH-SY5Y-PrP(+) t=25 vs SH-SY5Y-PrP(-) t=25, unpaired t-test, p=0.3314, n=3). Statistical analysis of the data set was exacerbated by the lack of time points t=9-16h and the high standard deviation of the positive control, Aβ$_{40}$ only (Figure 3.25).

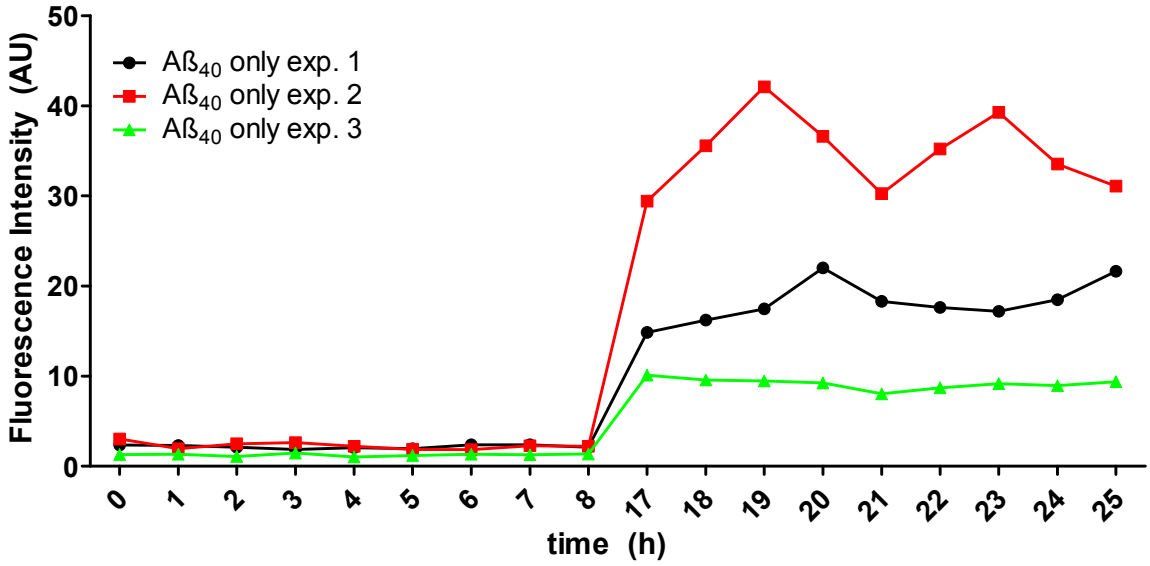

Figure 3.25: Single measurements of the aggregation properties of $A\beta_{40}$ only.

Strong scatter of values resulted in high standard deviations, which made statistical analysis of the data set difficult.

3.5 Exosomes and Aβ neurotoxicity

According to the current state of knowledge, small pre-fibrillar soluble $A\beta_{42}$ oligomers are the most deleterious Aβ species in AD. Hence, the already described protective effect of exosomes towards $A\beta_{42}$ conferred toxicity might be explainable by their ability to catalyze $A\beta_{42}$ fibrillization. Employing two different cell viability assays, we tested if exosomal PrP^{C} plays a putative role in this regard. In a flow cytometry based cell viability assay N2a-WT cells were incubated with freshly dissolved $A\beta_{42}$ in combination with exosomes for 24h and subsequently stained using propidium iodide (Figure 3.26).

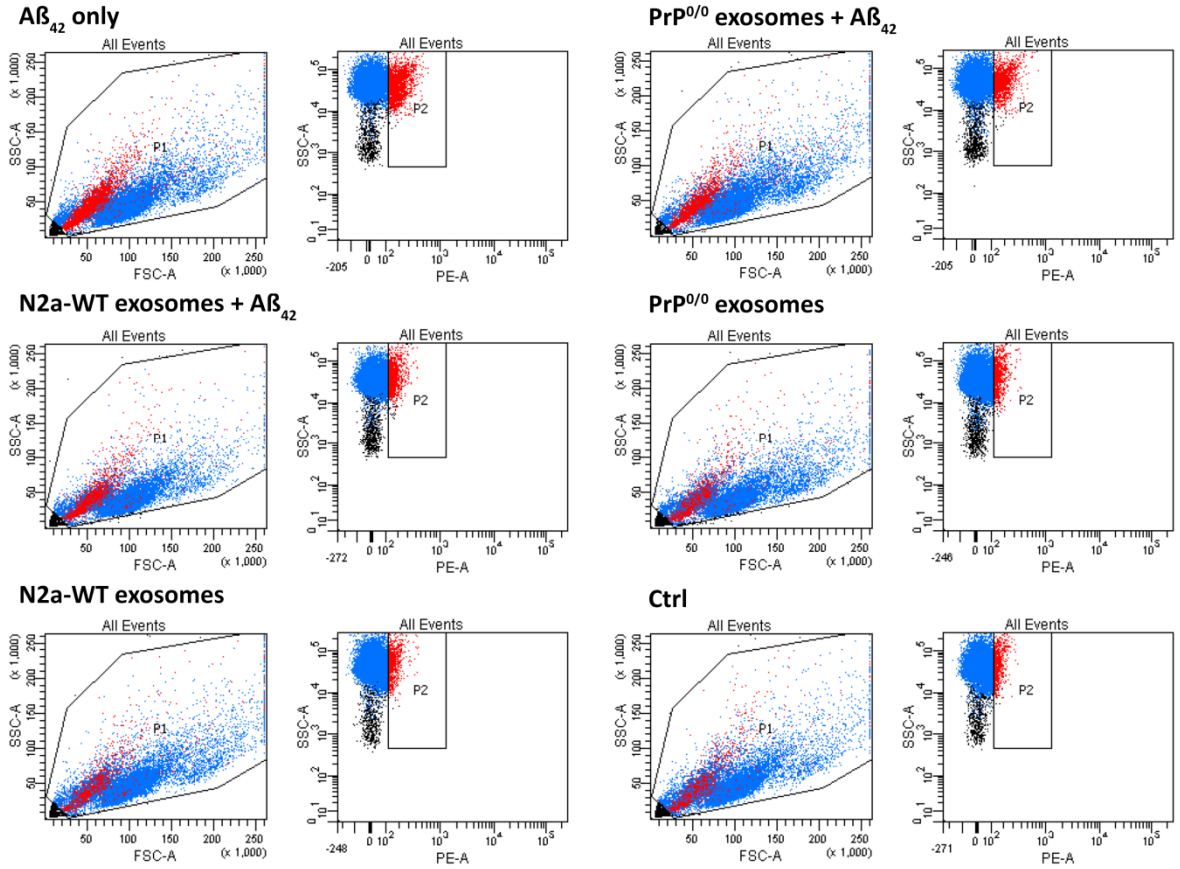

Figure 3.26: Flow cytometric cell viability assay of N2a-WT cells after 24h exposure to different combinations of exosomes and Aβ42.

N2a-WT cells were exposed to $A\beta_{42}$, N2a-$PrP^{0/0}$ exosomes + $A\beta_{42}$, N2a-WT exosomes + $A\beta_{42}$, N2a-$PrP^{0/0}$ exosomes, N2a-WT exosomes, and PBS (Ctrl) for 24h and a cell viability assay after propidium iodide staining was done by flow cytometric analysis.

In this assay N2a-WT exosomes were able to rescue N2a-WT cells from $A\beta_{42}$ mediated toxic effects (Figure 3.27; N2a-WT+ $A\beta_{42}$ vs $A\beta_{42}$, unpaired t-test, p=0.0415, n=3). $PrP^{0/0}$ exosomes had no significant impact on $A\beta_{42}$ mediated toxicity (Figure 3.27; N2a-$PrP^{0/0}$+ $A\beta_{42}$ vs $A\beta_{42}$, unpaired t-test, p=0.1069, n=3). Exosomes per se did not show any toxic effects in the absence of $A\beta_{42}$(Figure 3.27; N2a-WT vs Ctrl, unpaired t-test, p=0.0721, n=3; N2a-$PrP^{0/0}$ vs Ctrl, unpaired t-test, p=0.0636, n=3).

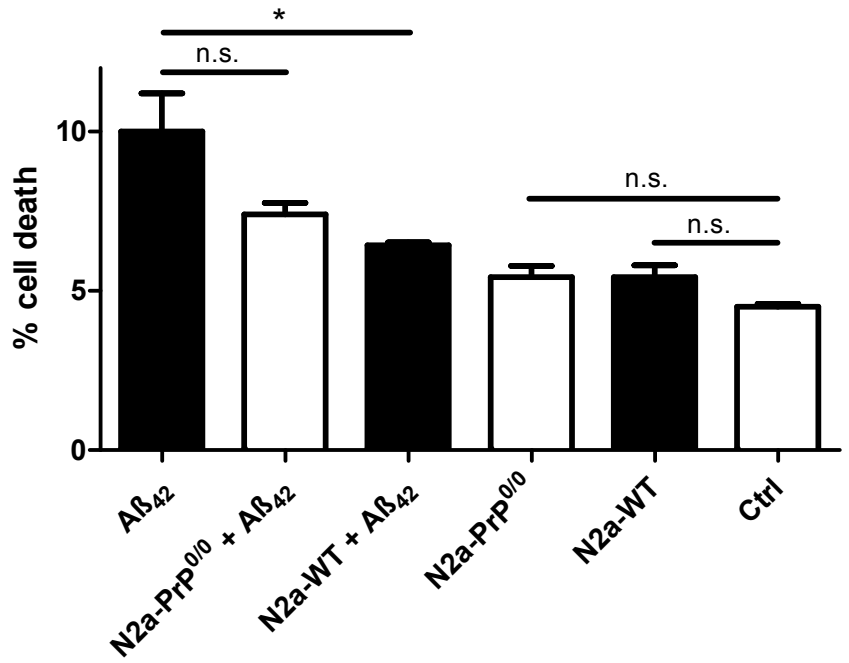

Figure 3.27: Statistical analysis of a cell viability assay of N2a-WT cells after 24h exposure to different combinations of exosomes and Aβ_{42}.

N2a-WT exosomes were able to rescue Aβ_{42} mediated cell death, whereas N2a-PrP$^{0/0}$ exosomes did not have an impact on Aβ_{42} toxicity. Further, exosomes per se did not influence cell viability in N2a-WT cells (N2a-WT+ Aβ_{42} vs Aβ_{42}, *p=0.0415, n=3; N2a-PrP$^{0/0}$+ Aβ_{42} vs Aβ_{42}, p=0.1069, n=3; N2a-WT vs Ctrl, p=0.0721, n=3; N2a-PrP$^{0/0}$ vs Ctrl, p=0.0636, n=3).

The influence of exosomes isolated from SH-SY5Y cells on Aβ_{42} toxicity was measured by live cell imaging. Aggregated Aβ_{42} was preincubated with exosomes O/N and incubated with SH-SY5Y-PrP(+) cells for 24 h. Dead cells were stained with propidium iodide, viable cells were stained using calcein AM and nuclei were stained with Hoechst 33342. Propidium iodide positive cells as well as calcein negative cells were considered dead or apoptotic. Exemplary microscopic pictures of the analyzed groups are depicted in Figure 3.28.

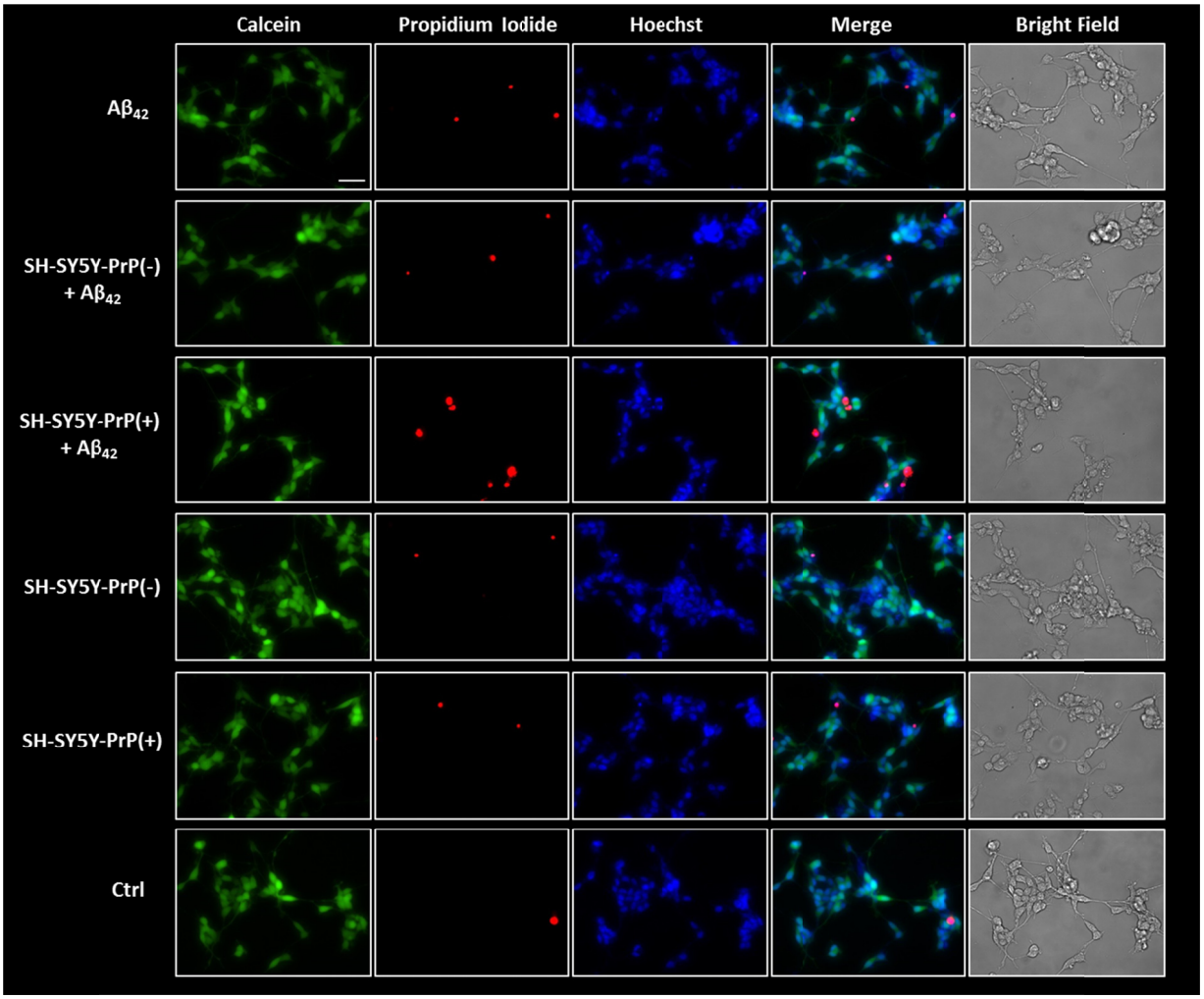

Figure 3.28: Life cell imaging cell viability assay of SH-SY5Y-PrP(+) cells after 24h exposure to different combinations of preincubated exosomes and aggregated $A\beta_{42}$.

Viable cells were stained with calcein, dead cells were stained with propidium idodide and nuclei were stained using Hoechst. Ten fields of view were analyzed per experiment (n=3, scale bar=50µm).

Analysis of live cell imaging data revealed that exosomes from SH-SY5Y-PrP(+) convert aggregated $A\beta_{42}$ into a neurotoxic species when compared to the untreated control (Figure 3.29; SH-SY5Y-PrP(+) + $A\beta_{42}$ vs Ctrl, unpaired t-test, p=0.0110, n=3). SH-SY5Y-PrP(-) exosomes did not significantly alter $A\beta_{42}$ toxicity (Figure 3.29; SH-SY5Y-PrP(-) + $A\beta_{42}$ vs Ctrl, unpaired t-test, p=0.7082, n=3) and aggregated $A\beta_{42}$ as well as exosomes alone were both not toxic (Figure 3.29; $A\beta_{42}$ vs Ctrl, unpaired t-test, p=0.5182, n=3; SH-SY5Y-PrP(-) vs Ctrl, unpaired t-test, p=0.9820, n=3; SH-SY5Y-PrP(+) vs Ctrl, unpaired t-test, p=0.6397, n=3).

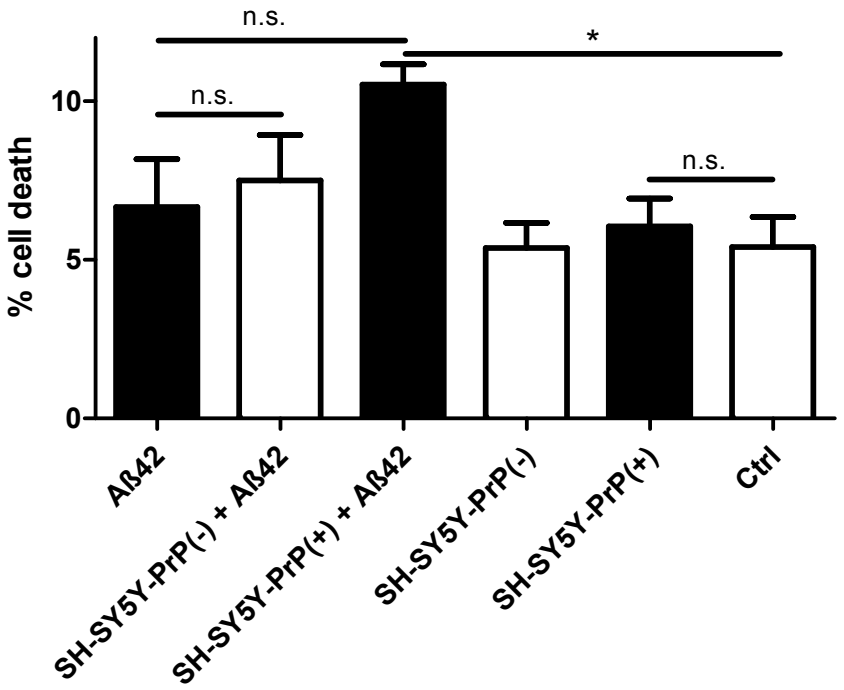

Figure 3.29: Statistical analysis of a life cell imaging cell viability assay of SH-SY5Y-PrP(+) cells after 24h exposure to different combinations of preincubated exosomes and aggregated Aβ_{42}.

SH-SY5Y-PrP(+) exosomes converted aggregated Aβ_{42} into a neurotoxic species. Exosomes derived from SH-SY5Y-PrP(-) cells did not influence the toxicity of aggregated Aβ_{42}. Aggregated Aβ_{42} and exosomes per se were not toxic (SH-SY5Y-PrP(+) + Aβ_{42} vs Ctrl, p=0.0110, n=3; SH-SY5Y-PrP(-) + Aβ_{42} vs Ctrl, p=0.7082, n=3; Aβ_{42} vs Ctrl, p=0.5182, n=3; SH-SY5Y-PrP(-) vs Ctrl, p=0.9820, n=3; SH-SY5Y-PrP(+) vs Ctrl, p=0.6397, n=3)

4 Discussion

The aim of this study was to clarify the role of exosomal PrP^C in molecular mechanisms of AD. Very few studies have addressed the involvement of exosomes in AD pathogenesis so far and mechanistic insights from these studies has revealed that exosomes might have a protective effect *in vitro* and *in vivo*[208,210,213,214]. Independent of exosome research a general connection between PrP^C and AD has been established over the last decade. Colocalization of PrP^C with amyloid plaques[118] and a modulating function of PrP^C in amyloid plaque formation[119] have been described. Furthermore, data are accumulating, which implicate PrP^C as a receptor for toxic Aβ oligomers[102,103]. This PrP^C Aβ interaction at the cell membrane is thought to activate a toxic signaling cascade by activation of Fyn kinase[133-135]. This line of evidence as well as the relative enrichment of PrP^C on exosomes isolated from neuronal cell lines (Figure 3.16-3.17) led to the investigation of a putative functional role of PrP^C on exosomes in AD mechanisms in this study.

4.1 Generation of an N2a *Prnp* knockout cell line

In order to have a reliable and stable neuronal PrP^C knockout cell model to study exosome biology, TALENs were utilized to knockout the *Prnp* gene. In a first attempt, N2a cells were transfected with TALEN pair mPrP-TALEN01 and PrP^C negative clones were isolated by antibody labeling and subsequent FACS (Table 3.1, Appendix 1). Immunofluorescent staining and Western blotting of obtained clones revealed that PrP^C was still expressed in all analyzed clones (Figure 3.3-3.4). A major weakness of this first approach is the lack of a selection marker for TALEN activity. This should have been compensated by antibody staining against cell-surface PrP^C. Antibody labeling obviously led to the selection of clones, which intrinsically express low amounts of PrP^C. PrP^C expression levels of these clones were beneath the detection level of the FACS device. Furthermore, the amount of TALEN DNA used for transfection might not have been sufficient to induce a DNA DSB, as discussed later in this section. Another explanation for low efficiency of mPrP-TALEN01 are the binding sites of the TALEN pair (Figure 3.6). The start codon is located at position +3 of the DNA binding region of the 3' TALEN and therefore the coding region of *Prnp* is located 3' of the spacer region, where cleavage of the *Fok*I nuclease dimer is less likely. TALEN cleavage positions were analyzed by Cermak *et al.* in human embryonic kidney cells targeting the *HPRT1* gene

and they showed that only 6 out of 14 knockout clones analyzed carried deletions as far as position +3 of the 3' TALEN binding site[217]. In conclusion, all the factors mentioned most likely contributed to failure of the first approach to generate a *Prnp* knockout cell line.

In a second approach to achieve a *Prnp* knockout in N2a cells a knockout cassette containing an EGFP-Zeo fusion protein as a selection marker was constructed. Upon cotransfection with a TALEN pair this mPrP-KO-Cas should be inserted into the genome via homologous recombination and replace the start codon of the *Prnp* gene (Figure 3.5). To increase TALEN-cleavage efficiency two additional TALEN pairs were designed, assembled and expressed (see Section 3.1). Different combinations of vectors and DNA amount ratios revealed that only mPrP-TALEN01 was able to produce EGFP positive clones (Figure 3.7). This is a rather surprising result because mPrP-TALEN01 was designed with Golden Gate TALEN and TAL Effector Kit 1.0[217], which lacks the newly introduced RVD NH. NH has a medium affinity to guanine, whereas NN has a high affinity to both guanine and adenine, which may lead to unspecific binding of adenine bases in close proximity to the target base[234]. Since the genomic target sites of mPrP-TALEN01 contain four neighboring guanine-adenine nucleotides, the Golden Gate TALEN and TAL Effector Kit 2.0, containing the RVD NH, was used for the design of mPrP-TALEN03 and mPrP-TALEN04. In case of neighboring guanine-adenine nucleotides, the RVD NH was used to target guanine (Figure 3.6). Hence, a better DNA-binding ability of mPrP-TALEN03 and mPrP-TALEN04 in comparison to mPrP-TALEN01 was expected. The binding sites of both mPrP-TALEN03 and mPrP-TALEN04 are shifted 14-17bp in 3' direction compared to mPrP-TALEN01. gDNA may be less accessible at these positions due to secondary structures, which could explain the lack of EGFP positive clones after transfection of mPrP-TALEN03 and mPrP-TALEN04. Remarkably high amounts of TALEN DNA and homologous recombination template DNA as well as lipofection agent were required to produce EGFP positive clones. It is known that high amounts of transfected plasmid DNA are required for successful genomic editing by TALENs[235]. A requirement for high amounts of knockin template vector is explainable by its lack of a nuclear localization signal (NLS). The DNA concentration inside the cell has to be high enough to ensure a sufficient distribution of plasmid DNA into the nucleus. Thus, introduction of a NLS into pCDNA3.1-mPrP-Ko-Cas might have enhanced recombination frequency by promoting the targeting of plasmid DNA in to the nucleus. The low frequency of EGFP positive clones after transfection indicates that the probability of simultaneous TALEN induced DNA DSBs on two

chromosomes and the presence of KO-Cas DNA in the vicinity of these DNA DSBs might be very low. Hence, to achieve higher knockout frequencies lipofection may not be the most suitable way to introduce DNA into mammalian cells since the system was already pushed to its limit in this study. Electroporation leads to higher frequencies of transfected cells in many mammalian and other cell types[236] and therefore poses a more reliable method for TALEN facilitated gene knockouts in mammalian cells[237].

Multiple EGFP positive clones could be derived from transfection N2a-TAL6.11 (Figure 3.7). All clones that were further expanded in cell culture were less adherent to the polystyrene surface of the culture flask, compared to N2a-WT cells. This is either an effect of the *Prnp* knockout or the EGFP expression under the *Prnp* promoter. Ultimately the three most adherent EGFP positive clones (clone C2, clone D4 and clone E4) were chosen for further analysis. There was no PrP^C detectable by Western blotting or immunofluorescent staining and *Prnp* mRNA was also absent in these clones. This sufficiently proofs that *Prnp* is knocked out in clones C2, D4 and E4. However, analysis of gDNA (Figure 3.11-3.12) showed that the expected homologous recombination event (Figure 3.5) has not taken place. PCR analysis revealed that on one chromosome a 793bp deletion has taken place, which comprises adenine and thymine of the *Prnp* start codon, hence disrupting *Prnp* gene expression from this chromosome. On the other chromosome the analyzed region of the *Prnp* locus comprising position -1500 to +400 is still intact. pCDNA.3.1-KO-Cas does not contain a promoter. Hence, the EGFP-Zeo fusion per se cannot be expressed if randomly integrated in to the genome. Since the cells are EGFP positive and PrP^C negative, integration of mPrP-KO-Cas in the regulatory region of *Prnp* is highly likely.

4.2 Comparison of exosomes isolated from different neuronal cells

In this work four different cell lines were used to study PrP^C-dependent functions of neuronal exosomes. SH-SY5Y is a human neuroblastoma cell line derived from a bone marrow biopsy. SH-SY5Y cells do not express detectable levels of PrP^C and were therefore used as a model for PrP^C deficient neurons[238]. Perera *et al.* transfected SH-SY5Y cells with a vector containing murine PrP^C (SH-SY5Y-PrP(+)) and as a control with an empty vector (SH-SY5Y-PrP(-))[218]. N2a cells were the second neuronal cell system that was deployed in this study. N2a cells were derived from a spontaneous brain tumor in an albino strain A

mouse[239]. Exosomes derived from SH-SY5Y-PrP(+) and SH-SY5Y-PrP(-) were compared to exosomes isolated from N2a-WT and N2a-$PrP^{0/0}$ cells, which were created in this study. Immediately after exosome purification vesicles were always analyzed and quantified by NTA. NTA revealed that all mode values of exosomal preparations were in the size range of 50-150nm described for exosomal vesicles[136]. PrP^C expression did not have a significant impact on exosome size (Figure 3.14-3.15) and differences in exosome production of PrP^C deficient compared to PrP^C expressing cells were not noticeable. Hence, an involvement of PrP^C in exosome biogenesis or release is unlikely. Exosomes released by SH-SY5Y cell lines were significantly smaller compared to N2a exosomes, irrespective of PrP^C expression (Figure 3.14-3.15). SH-SY5Y cells exhibited a noticeable high rate of apoptosis, probably due to high passage numbers. Apoptotic cells are known to shed membrane vesicles that represent a vesicle population (apoptotic vesicles, AVs) distinct from exosomes[240,241]. These AVs range from 50-500nm in size, float at a similar sucrose density to exosomes and sediment at centrifugal forces of 1,200g, 10,000g or 100,000g[242]. Hence, AVs in the range of 50-100nm are inevitably copurified with exosomes to an extent that may not be neglected. AVs are loaded with nuclear, cytosolic, and ER-derived proteins[243] and have the same membrane topology as exosomes[241] making it difficult to differentiate AVs from exosomes. A contamination of SH-SY5Y exosomes with AVs might explain the size discrepancy between SH-SY5Y and N2a exosomes. Purity of exosome preparations was further investigated by Western blotting (Figure 3.16). Absence of the cis-Golgi marker GM130 ruled out contamination with intracellular components and Flotillin served as a well-established exosomal marker[143]. As expected exosomes isolated from SH-SY5Y-PrP(-) and N2a-$PrP^{0/0}$ cells did not contain PrP^C. Concerning PrP^C amounts on exosomes, both SH-SY5Y-PrP(+) and N2a-WT derived vesicles show a 10-fold enrichment of PrP^C compared to cell lysates when Flotillin is used for normalization (Figure 3.16- 3.17). There is no standardized marker to compare exosomes with cells. Flotillin was used because both PrP^C and Flotillin are localized in lipid rafts, which are incorporated into endosome upon invagination of the cell membrane during endosome biogenesis. Based on the assumption that undirected incorporation of PrP^C and Flotillin into exosomes during MVE formation would not change the ratio of PrP^C to Flotillin, the results presented here suggest an active sorting of PrP^C into exosomes. Together with the fact that PrP^C is enriched on exosomes derived from ovine CSF[193], this line of

argumentation strongly suggests that PrP^C on exosomes plays functional roles in the mammalian nervous system.

4.3 Exosomal PrP^C in Aβ-dependent AD mechanisms

A growing body of evidence lends support to the idea that extracellular vesicles are mechanistically involved in AD and other neurodegenerative diseases (reviewed in Kalani 2014)[244]. For example, Rajendran *et al.* were the first to show the presence of Aβ on exosomes secreted from N2a-swAPP cells and they concluded that exosomes serve as a vehicle for Aβ to exit the cell. Further, they found exosomal markers Alix and Flotillin to colocalize with amyloid plaques, which led them to the conclusion that exosomes promote amyloid plaque formation[208]. To clarify if PrP^C, located on the outer leaflet of exosomes[214], is required for the association of $A\beta_{42}$ to exosomes a pull-down experiment was carried out. Presence of PrP^C on exosomes from neuronal cells led to significantly higher amounts of bound $A\beta_{42}$ after O/N incubation (Figure 3.18-3.19). While this study was carried out, the PrP^C-dependent binding of $A\beta_{42}$ to exosomes was shown by An *et al.*, but in a less convincing experimental setup[214]. First of all, the PrP^C wild type and PrP^C knockout cell lines used in this study, namely HW8-1 and Hpl3-4, were not derived from the same origin[223]. This might lead to experimental differences like general protein composition or the ratio between exosomes and other vesicles or particles, which will be discussed later in this section. Furthermore, different cell types exhibit different exosomal protein compositions[161]. Consequently, this makes the already inaccurate quantification of exosomes by protein content less reliable, which was overcome in this study by using NTA to quantify exosomes, which eliminates potential bias attributable to protein-based quantification methods[245]. Thus, the approach presented here, comparing a TALEN generated N2a PrP^C knockout cell line to its parental cell line as well as SH-SY5Y cells, with no detectable expression of PrP^C, to SH-SY5Y cells transfected with PrP^C, provides a more reliable experimental outcome. The data presented here suggest that binding of Aβ is largely facilitated by PrP^C on the surface of exosomes (Figure 3.18-3.19). Nevertheless, exosomes derived from SH-SY5Y-PrP(-) and N2a-$PrP^{0/0}$ cells also show Aβ binding capacity, which may be facilitated by GSLs on the exosomal surface. GSLs are a type of glycolipid found in cell membranes, consisting of a sphingolipid core with an attached carbohydrate moiety. Yuyama *et al.* presented experimental evidence that

exosomal GSLs are involved in the association of Aβ with exosomes and the subsequent uptake and degradation of these exosome-Aβ complexes in microglia cells[213]. GSLs have been shown to promote Aβ fibril formation[211] and to associate with PrP^C when present on synthetic liposomes[212]. Hence, PrP^C could act as an adaptor that keeps Aβ molecules spatially close to GSLs to facilitate exosome driven fibrillization of Aβ, as discussed later in this section. A link between GSLs and the neuropathology of AD was presented by Ariga *et al.* who showed that GSLs on the plasma membrane promote amyloid plaque formation[246]. Although the authors concluded that GSLs have a disease promoting function in AD, the current consensus of Aβ oligomers being the most neurotoxic species[90] rather suggests that GSLs exhibit protective functions in AD.

A connection between exosomes and Aβ aggregation has already been established. Exosomes isolated from N2a cells and primary neurons accelerate fibrillization of $A\beta_{42}$[210], which could be confirmed in this study (Figure 3.22). The results presented here point to PrP^C as the main contributor to exosome mediated aggregation of $A\beta_{42}$, which seems to be an exclusive function of PrP^C on exosomes since soluble GPI-anchorless PrP^C was shown to inhibit $A\beta_{42}$ aggregation[247] and may even disaggregate Aβ fibrils towards oligomeric forms[248]. N2a exosomes devoid of PrP^C had no impact on $A\beta_{42}$ aggregation (Figure 3.22). However, contradictory data has been acquired using SH-SY5Y cell lines. SH-SY5Y-PrP(+) exosomes inhibited aggregation of $A\beta_{42}$, whereas SH-SY5Y-PrP(-) exosomes accelerated $A\beta_{42}$ fibrillization (Figure 3.23). Although SH-SY5Y-PrP(-) cells do not contain detectable amounts of PrP^C, it is not a knockout cell line. Hence, traces of PrP^C might still be present on SH-SY5Y-PrP(-) exosomes that are sufficient to accelerate the fibrillization of $A\beta_{42}$. The aggregation inhibiting properties of SH-SY5Y-PrP(+) exosomes might be caused by a stronger contamination of the vesicle preparations with AVs. SH-SY5Y-PrP(+) are noticeably more apoptotic than SH-SY5Y-PrP(-) cells and therefore might shed larger quantities of AVs into the culture medium. This line of argumentation is emphasized by the observation that MVs, which are shed from the plasma membrane in a similar manner to AVs, inhibit $A\beta_{42}$ aggregation and even disaggregate fibrillar $A\beta_{42}$[215]. Joshi *et al.* showed that the lipids of MVs are sufficient to inhibit $A\beta_{42}$ aggregation. Based on the assumption that MVs and AVs might be similar in lipid composition, inhibition of $A\beta_{42}$ aggregation by SH-SY5Y-PrP(+) exosomes can be explained by contamination of the exosomal preparation with AVs. $A\beta_{40}$ seems to

behave differently than $A\beta_{42}$ in the presence of SH-SY5Y exosomes. A clear increase of $A\beta_{40}$ aggregation over a time course of 25h was observable, whereas SH-SY5Y exosomes irrespective of their PrP^{C} content prevented $A\beta_{40}$ aggregation (Figure 3.24). Hence, differences in nucleation behavior and aggregation kinetics for $A\beta_{40}$ and $A\beta_{42}$[249], as reported by Meisl *et al.*, may also apply to the influence of exosomes on $A\beta_{40}$ and $A\beta_{42}$ aggregation kinetics. Meisl *et al.* have shown that the aggregation of $A\beta_{40}$ is a "fibril-catalyzed nucleation process" that requires only a small concentration of fibrils to favor the formation of new aggregates. Nonetheless, aggregation of $A\beta_{40}$ requires a much higher peptide concentration to reach a level of aggregation similar to $A\beta_{42}$, which was attributed to its higher hydrophobicity conferred by aa 41 (isoleucine) and 42(alanine). Hence, exosomes might only catalyze aggregation processes that depend on hydrophobicity, as in the case of $A\beta_{42}$[249]. Furthermore, higher peptide concentrations of $A\beta_{40}$ may be required to see exosome dependent effects similar to $A\beta_{42}$. Yuyama *et al.* used a concentration of $A\beta_{40}$ five times higher compared to this study, to show an aggregation promoting effect upon the addition of exosomes[210].

Soluble pre-fibrillar $A\beta_{42}$ oligomers are considered to be the most neurotoxic Aβ species. Hence, the results obtained in cell viability assays (see Section 3.5) reflect the exosome-dependent Aβ-aggregation states that could be measured by ThT assays. N2a-WT exosomes significantly accelerated aggregation of freshly dissolved $A\beta_{42}$ (Figure 3.22). During 24h exposition of $A\beta_{42}$ to N2a-WT cells, only the presence of N2a-WT exosomes led to a rescue from $A\beta_{42}$ conferred neurotoxicity (Figure 3.26-3.27). N2a-$PrP^{0/0}$ exosomes had no impact on $A\beta_{42}$ aggregation (Figure 3.22) and were accordingly not able to counteract $A\beta_{42}$ mediated toxic effects (Figure 3.26-3.27). To test the influence of SH-SY5Y exosomes on $A\beta_{42}$ toxicity, aggregated $A\beta_{42}$ was incubated with exosomes O/N prior 24h exposition to SH-SY5Y-PrP(+) cells. The results also correlate with the data on the influence of SH-SY5Y exosomes on $A\beta_{42}$ aggregation states (Figure 3.23). Contamination of SH-SY5Y-PrP(+) exosomes with AVs may have led to inhibition of further aggregation and/or disassembly of $A\beta_{42}$ aggregates leading to the production of neurotoxic $A\beta_{42}$ species, which was observable in the cell viability assay (Figure 3.28-3.29). Since the data obtained with SH-SY5Y cells may not be reliable they will not be further discussed. The data obtained with N2a cells confirm the results by Yuyama *et al.*, who showed that addition of N2a-WT exosomes to neurotoxic oligomeric $A\beta_{42}$, reduces

neurotoxic effects. This study strongly suggests that exosomal PrP^C is the main contributor to this protective effect of neuronal exosomes. Via binding to PrP^C exosomes could work as a scavenger of toxic oligomeric Aβ. Exosomes may detoxify Aβ oligomers through GSL and PrP^C aided catalyzation of Aβ fibril formation and may ultimately promote amyloid plaque formation (Figure 4.1).

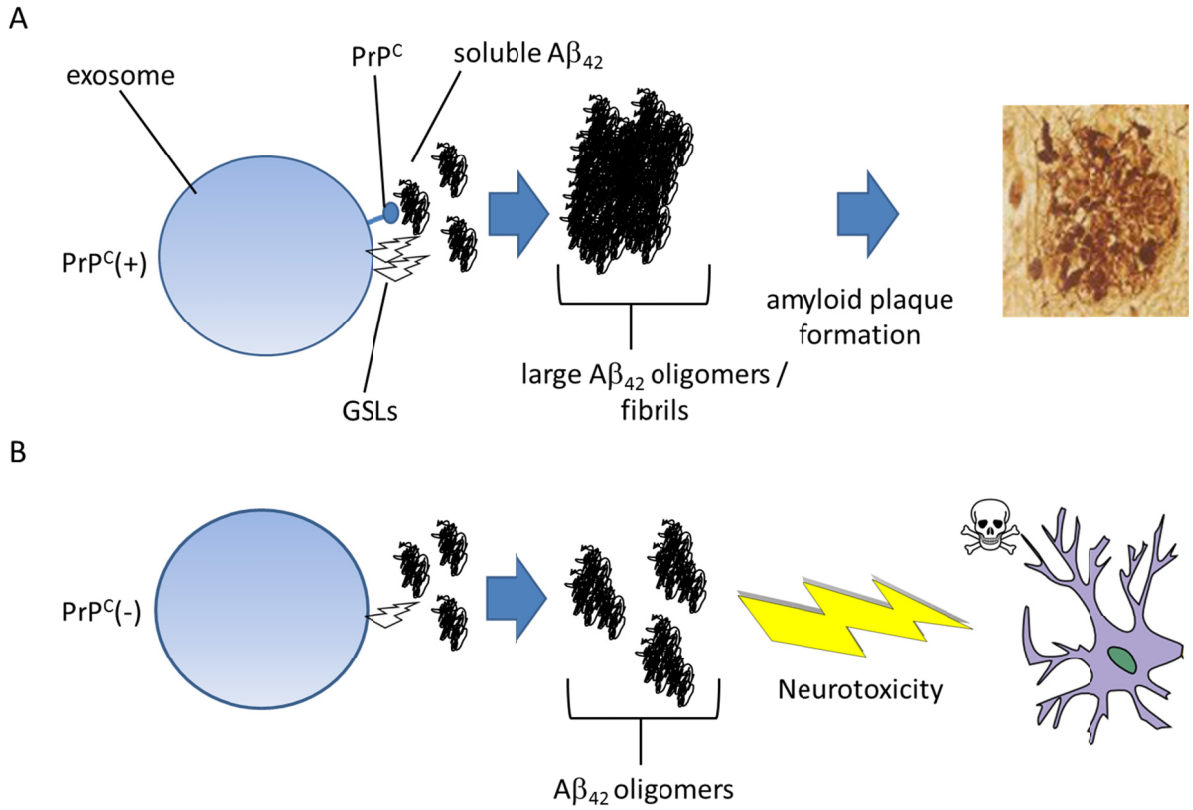

Figure 4.1: Schematic drawing of the PrP^C-dependent effect of exosomes on Aβ aggregation and toxicity.
(A) Exosomes containing PrP^C on the outer membrane leaflet bind soluble Aβ molecules and promote their fibrillization, which may be aided by GSLs. This exosome driven Aβ-fibrillization may ultimately lead to amyloid plaque formation in the brain. (B) PrP^C deficient exosomes do not significantly influence Aβ aggregation and therefore don not detoxify Aβ oligomers. GSLs only may not be sufficient to prevent Aβ mediated neurotoxicity.

On the contrary, MVs produced by microglial cells were shown to inhibit $A\beta_{42}$ aggregation. Furthermore, MVs convert fibrillar $A\beta_{42}$ into a neurotoxic species[215]. Hence, MVs secreted by microglia could be necessary for disassembly of already highly aggregated $A\beta_{42}$ states, giving rise to more soluble toxic forms. The production of MVs is elevated in AD patients compared to healthy individuals[215] and correlates with markers of degeneration and hippocampal atrophy[250]. In summary, these results indicate that the effects conferred by extracellular vesicles may depend on the cell type of origin and vary between distinct vesicle populations. Concerning AD pathogenesis, MVs and exosomes might present a regulatory circuit that

enables the organisms to regulate Aβ aggregation states to maintain an equilibrium of non-toxic Aβ species in healthy individuals, which might be out of balance in AD.

The results presented here add to the list of neuroprotective functions that have been described for fragments of PrP^C that have been released to the extracellular space (reviewed in Altmeppen 2013)[251]. Despite its release via exosomes, GPI-anchorless PrP^C can also be released from the plasma membrane by a proteolytic cleavage event termed shedding[252]. α-cleavage of PrP^C leads to the release of an N-terminal part of the protein (N1) leaving the C-terminal part (C1) attached to the plasma membrane[253]. According to the current state of knowledge β-cleavage of PrP^C does not produce physiologically relevant PrP^C fragments and will therefore not be further discussed[254,255]. Shed PrP^C was shown to reduce neurotoxicity of Aβ peptides[129,247] and N1 is reportedly neuroprotective in general[255,256]. Supported by this line of evidence and the data acquired during this study, extracellular versions of PrP^C can be interpreted as protective entities in health and disease. This stands in contrast to the controversial function of PrP^C as a receptor that activates a toxic signaling cascade upon binding of β-sheet rich protein conformers (see Section 1.2.2). Hence, PrP^C might exhibit divergent roles, depending on its localization.

5 Summary

Alzheimer's disease (AD) is a common neurodegenerative, progressive and fatal disorder and one of the leading causes of death in the elderly in western countries. According to the Amyloid Hypothesis, generation and deposition of amyloid beta (Aβ) in the brain is correlated with disease initiation and progression. Aβ, the aggregation-prone product of sequential proteolytic processing of the amyloid precursor protein, is released to the extracellular space. Small soluble pre-fibrillar Aβ species show the most pronounced neurotoxic effects and Aβ peptides of 42 amino acids length ($A\beta_{42}$) are thought to represent the major neurotoxic entity causing synaptic dysfunction, dendritic spine loss, and ultimately neuronal death. The molecular pathways leading to neurodegeneration in AD are not yet fully understood. Recent findings have highlighted the role of exosomes, small extracellular vesicles of endosomal origin, in promoting Aβ fibrillization and uptake by microglial cells, thus extenuating disease progression in a murine AD model. Furthermore, the cellular prion protein (PrP^C), a glycosylphosphatidylinositol (GPI)-anchored surface glycoprotein, highly expressed in neurons, was shown to bind oligomeric $A\beta_{42}$ with high affinity via its flexible N-terminus. It is widely accepted that membrane-attached PrP^C is required for Aβ-mediated synaptotoxicity and suppression of long term potentiation as well as toxic signaling via Fyn kinase activation.

To study the involvement of exosomal PrP^C in molecular mechanisms of AD, a murine neuroblastoma Neuro 2a (N2a) *Prnp* knockout cell line was generated using transcription activator-like effector nucleases (TALENs). Using this cell line and its parental wild type cell line, as well as human SH-SY5Y neuroblastoma cells devoid of PrP^C and SH-SY5Y cells transfected with PrP^C, it was possible to demonstrate that PrP^C is highly enriched on exosomes and that PrP^C expression does not influence exosome size. Differences in exosome size however were detectable when comparing exosomes derived from N2a cell lines to SH-SY5Y exosomes irrespective of their PrP^C content. Furthermore, it could be shown that binding of $A\beta_{42}$ to exosomes is largely facilitated by PrP^C. It was previously described that neuronal exosomes accelerate $A\beta_{42}$ aggregation, which could be confirmed in this study. The data presented here point to exosomal PrP^C as a main contributor in exosome driven $A\beta_{42}$ fibrillization. In the absence of PrP^C, N2a exosomes did not alter $A\beta_{42}$ aggregation kinetics. This exosome induced $A\beta_{42}$ aggregation reduced neurotoxic effects on N2a cells imparted by

oligomeric $A\beta_{42}$. In summary, the data acquired in this study suggest that PrP^C on exosomes might play a central role in exosome-mediated protective effects in AD pathology, which raises interesting questions about potential therapeutic applications that could be addressed by examining the role of PrP^C on exosomes in vivo.

6 Zusammenfassung

Alzheimer (AD, Alzheimer´s disease, Alzheimer-Erkrankung) ist eine weit verbreitete neurodegenerative, progressive und tödliche Erkrankung und eine der häufigsten Todesursachen älterer Menschen in der westlichen Welt. Gemäß der Amyloid-Hypothese korreliert Entstehung und Fortschreiten der Krankheit mit der Generierung und extrazellulären Ablagerung von Amyloid β (Aβ) Peptiden im Gehirn. Aβ entsteht durch sequenzielle proteolytische Spaltung des Amyloidvorläuferproteins, wird in den extrazellulären Raum abgegeben und tendiert stark zur Aggregation. Kleine, lösliche pre-fibrilläre Aβ Spezies mit einer Länge von 42 Aminosäuren ($A\beta_{42}$) weisen die stärksten neurotoxischen Eigenschaften auf und wurden mit synaptischer Dysfunktion, dem Verlust dendritischer Dornenfortsätze und letztendlich dem Niedergang von Neuronen in Verbindung gebracht. Die genauen molekularen Vorgänge, die zur Neurodegeneration führen sind noch nicht vollständig geklärt. Exosomen, kleine extrazelluläre Vesikel endosomalen Ursprungs, wurden kürzlich mit AD in Verbindung gebracht. Es konnte gezeigt werden, dass Exosomen die Aggregation von Aβ beschleunigen, welches anschließend von Mikrogliazellen aufgenommen wird. In einem Mausmodell führte dies zu einem milderen Krankheitsverlauf. Unabhängig von diesen Erkenntnissen wurde gezeigt, dass das zelluläre Prion-Protein (PrP^C), welches über einen Glycosylphosphatidylinositol-Anker an der Oberfläche Zellmembran verankert ist, oligomere Aβ Spezies hochaffin über seinen flexiblen Amino-Terminus bindet. Es ist überwiegend Konsens, dass membranständiges PrP^C notwendig ist für Aβ-vermittelte Synaptotoxizität und Verminderung der Langzeit-Potenzierung sowie für eine toxische Signalkaskade über die Fyn-Kinase.

Um herauszufinden ob PrP^C auf Exosomen an molekularen Mechanismen der AD beteiligt ist, wurde mithilfe von transcription activator-like effector nucleases (TALENs) eine murine Neuro 2a (N2a) *Prnp* knockout Neuroblastoma Zell-Linie hergestellt. Unter Verwendung dieser und der parentalen Wildtyp Zell-Linie, sowie der humanen SH-SY5Y Neuroblastoma Zell-Linie, welche keine detektierbaren Mengen an PrP^C exprimiert, verglichen zu SH-SY5Y Zellen die mit PrP^C stabil transfiziert wurden, konnte in dieser Studie gezeigt werden, dass PrP^C auf Exosomen angereichert ist und dass PrP^C die Größe von Exosomen nicht beeinflusst. PrP^C-unabhängige Größenunterschiede zwischen N2a und SH-SY5Y Exosomen konnten jedoch festgestellt werden. Ferner konnte gezeigt werden, dass die Bindung von $A\beta_{42}$ an

Exosomen vorwiegend durch PrP^C auf Exosomen vermittelt wird. Außerdem konnte bestätigt werden, dass neuronale Exosomen die Aggregation von $A\beta_{42}$ katalysieren. Die hier vorliegenden Daten implizieren exosomales PrP^C als treibende Kraft der Exosomen-induzierten Aβ Aggregation. Exosomen ohne PrP^C hatten keinen Einfluss auf die Reaktionskinetic der $A\beta_{42}$ Aggregation. Diese Exosomen-induzierte Aggregation von $A\beta_{42}$ führte zu einer Reduzierung $A\beta_{42}$ vermittelter Toxizität in N2a Zellen. Zusammenfassend deuten die hier erarbeiteten Daten darauf hin, dass exosomales PrP^C zentral an Exosomen-vermittelten protektiven Effekten in der Alzheimer Pathologie beteiligt ist. Dies wirft interessante Fragen über mögliche therapeutische Interventionen auf, die durch *in vivo* Studien zur weiteren Klärung der Funktion von exosomalem PrP^C beantwortet werden könnten.

7 References

1 Brookmeyer, R., Johnson, E., Ziegler-Graham, K. & Arrighi, H. M. Forecasting the global burden of Alzheimer's disease. *Alzheimers Dement* **3**, 186-191, doi:10.1016/j.jalz.2007.04.381S1552-5260(07)00475-X [pii] (2007).

2 Ashford, J. W. APOE genotype effects on Alzheimer's disease onset and epidemiology. *J Mol Neurosci* **23**, 157-165, doi:JMN:23:3:157 [pii]10.1385/JMN:23:3:157 (2004).

3 Blessed, G., Tomlinson, B. E. & Roth, M. The association between quantitative measures of dementia and of senile change in the cerebral grey matter of elderly subjects. *Br J Psychiatry* **114**, 797-811 (1968).

4 Braak, H. & Braak, E. Demonstration of amyloid deposits and neurofibrillary changes in whole brain sections. *Brain Pathol* **1**, 213-216 (1991).

5 Glenner, G. G. & Wong, C. W. Alzheimer's disease: initial report of the purification and characterization of a novel cerebrovascular amyloid protein. *Biochem Biophys Res Commun* **120**, 885-890, doi:S0006-291X(84)80190-4 [pii] (1984).

6 Iwatsubo, T. *et al.* Visualization of A beta 42(43) and A beta 40 in senile plaques with end-specific A beta monoclonals: evidence that an initially deposited species is A beta 42(43). *Neuron* **13**, 45-53, doi:0896-6273(94)90458-8 [pii] (1994).

7 Klöppel, G., Kreipe, H. H., Remmele, W., Paulus, W. & Schröder, J. M. Pathologie - Neuropathologie. *Springer-Verlag Berlin Heidelberg* (2012).

8 Capell, A. *et al.* Maturation and pro-peptide cleavage of beta-secretase. *J Biol Chem* **275**, 30849-30854, doi:10.1074/jbc.M003202200M003202200 [pii] (2000).

9 Katzman, R. Alzheimer's disease. *N Engl J Med* **314**, 964-973, doi:10.1056/NEJM198604103141506 (1986).

10 Budson, A. E. & Price, B. H. Memory dysfunction. *N Engl J Med* **352**, 692-699, doi:352/7/692 [pii]10.1056/NEJMra041071 (2005).

11 Walsh, D. M. & Selkoe, D. J. A beta Oligomers - a decade of discovery. *Journal of Neurochemistry* **101**, 1172-1184, doi:DOI 10.1111/j.1471-4159.2006.04426.x (2007).

12 McLean, C. A. *et al.* Soluble pool of Abeta amyloid as a determinant of severity of neurodegeneration in Alzheimer's disease. *Ann Neurol* **46**, 860-866 (1999).

13 Alzheimer, A. Über eine eigenartige Erkrankung der Hirnrinde. *Allgemeine Zeitschrift für Psychiatrie und psychisch-gerichtliche Medizin* **64** (1907).

14 Greenson, L. J. a. H. About a peculiar disease of the cerebral cortex. By Alois Alzheimer, 1907 (Translated by L. Jarvik and H. Greenson). *Alzheimer Dis Assoc Disord* **1**, 3-8 (1987).

15 Alzheimer's-Association. *Major Milestones in Alzheimer's and Brain Research*, <http://www.alz.org/research/science/major_milestones_in_alzheimers.asp> (2014).

16 Marinesco, G. & Blocq, P. Lésions des cordons postérieurs d'origine exogène. *Atlas d'histopathologie du système nerveux* **12**, 445 (1892).

17 Measures of dementia and senile change. *Lancet* **1**, 88-89, doi:S0140-6736(69)91100-3 [pii] (1969).

18 Kraepelin, E. Psychiatrie. Ein Lehrbuch für Studierende und Ärzte. *Barth Verlag, Leipzig* (1910).

19 Weintraub, S., Wicklund, A. H. & Salmon, D. P. The neuropsychological profile of Alzheimer disease. *Cold Spring Harb Perspect Med* **2**, a006171, doi:10.1101/cshperspect.a006171a006171 [pii] (2012).

20 Perrin, R. J., Fagan, A. M. & Holtzman, D. M. Multimodal techniques for diagnosis and prognosis of Alzheimer's disease. *Nature* **461**, 916-922, doi:10.1038/nature08538nature08538 [pii] (2009).

21 Weintraub, S. & Mesulam, M. With or without FUS, it is the anatomy that dictates the dementia phenotype. *Brain* **132**, 2906-2908, doi:10.1093/brain/awp286awp286 [pii] (2009).

22 Braak, H. & Braak, E. Neuropathological stageing of Alzheimer-related changes. *Acta Neuropathol* **82**, 239-259 (1991).

23 Morris, J. C. *et al.* Cerebral amyloid deposition and diffuse plaques in "normal" aging: Evidence for presymptomatic and very mild Alzheimer's disease. *Neurology* **46**, 707-719 (1996).

24 Buckner, R. L., Andrews-Hanna, J. R. & Schacter, D. L. The brain's default network: anatomy, function, and relevance to disease. *Ann N Y Acad Sci* **1124**, 1-38, doi:10.1196/annals.1440.0111124/1/1 [pii] (2008).

25 Sperling, R. A. *et al.* Amyloid deposition is associated with impaired default network function in older persons without dementia. *Neuron* **63**, 178-188, doi:10.1016/j.neuron.2009.07.003S0896-6273(09)00505-4 [pii] (2009).

26 Baddeley, A. Working memory and language: an overview. *J Commun Disord* **36**, 189-208, doi:S0021992403000194 [pii] (2003).

27 Baddeley, A. D., Bressi, S., Della Sala, S., Logie, R. & Spinnler, H. The decline of working memory in Alzheimer's disease. A longitudinal study. *Brain* **114 (Pt 6)**, 2521-2542 (1991).

28 Rocca, W. A. *et al.* Frequency and distribution of Alzheimer's disease in Europe: a collaborative study of 1980-1990 prevalence findings. The EURODEM-Prevalence Research Group. *Ann Neurol* **30**, 381-390, doi:10.1002/ana.410300310 (1991).

29 Campion, D. *et al.* Early-onset autosomal dominant Alzheimer disease: prevalence, genetic heterogeneity, and mutation spectrum. *Am J Hum Genet* **65**, 664-670, doi:S0002-9297(07)62317-9 [pii]10.1086/302553 (1999).

30 Bekris, L. M., Yu, C. E., Bird, T. D. & Tsuang, D. W. Genetics of Alzheimer disease. *J Geriatr Psychiatry Neurol* **23**, 213-227, doi:10.1177/089198871038357123/4/213 [pii] (2010).

31 Ferri, C. P. *et al.* Global prevalence of dementia: a Delphi consensus study. *Lancet* **366**, 2112-2117, doi:S0140-6736(05)67889-0 [pii]10.1016/S0140-6736(05)67889-0 (2005).

32 Qiu, C., Kivipelto, M. & von Strauss, E. Epidemiology of Alzheimer's disease: occurrence, determinants, and strategies toward intervention. *Dialogues Clin Neurosci* **11**, 111-128 (2009).

33 Bertram, L. & Tanzi, R. E. Alzheimer's disease: one disorder, too many genes? *Hum Mol Genet* **13 Spec No 1**, R135-141, doi:10.1093/hmg/ddh077ddh077 [pii] (2004).

34 Castellano, J. M. *et al.* Human apoE isoforms differentially regulate brain amyloid-beta peptide clearance. *Sci Transl Med* **3**, 89ra57, doi:10.1126/scitranslmed.30021563/89/89ra57 [pii] (2011).

35 Cerf, E., Gustot, A., Goormaghtigh, E., Ruysschaert, J. M. & Raussens, V. High ability of apolipoprotein E4 to stabilize amyloid-beta peptide oligomers, the pathological entities responsible for Alzheimer's disease. *FASEB J* **25**, 1585-1595, doi:10.1096/fj.10-175976fj.10-175976 [pii] (2011).

36 Daw, E. W. *et al.* The number of trait loci in late-onset Alzheimer disease. *Am J Hum Genet* **66**, 196-204, doi:S0002-9297(07)62247-2 [pii]10.1086/302710 (2000).

37 Cruchaga, C. *et al.* Rare coding variants in the phospholipase D3 gene confer risk for Alzheimer's disease. *Nature* **505**, 550-554, doi:10.1038/nature12825nature12825 [pii] (2014).

38 Bertram, L., Parrado, A. R. & Tanzi, R. E. TREM2 and neurodegenerative disease. *N Engl J Med* **369**, 1565, doi:10.1056/NEJMc1306509#SA2 (2013).

39 Guerreiro, R. & Hardy, J. TREM2 and neurodegenerative disease. *N Engl J Med* **369**, 1569-1570 (2013).

40 De Strooper, B. Proteases and proteolysis in Alzheimer disease: a multifactorial view on the disease process. *Physiol Rev* **90**, 465-494, doi:10.1152/physrev.00023.200990/2/465 [pii] (2010).

41 alzforum.org. *MUTATIONS database*, <http://www.alzforum.org/mutations> (2014).

42 Nilsberth, C. *et al.* The 'Arctic' APP mutation (E693G) causes Alzheimer's disease by enhanced Abeta protofibril formation. *Nat Neurosci* **4**, 887-893, doi:10.1038/nn0901-887nn0901-887 [pii] (2001).

43 Tomiyama, T. *et al.* A new amyloid beta variant favoring oligomerization in Alzheimer's-type dementia. *Ann Neurol* **63**, 377-387, doi:10.1002/ana.21321 (2008).

44 Theuns, J. *et al.* Genetic variability in the regulatory region of presenilin 1 associated with risk for Alzheimer's disease and variable expression. *Hum Mol Genet* **9**, 325-331, doi:ddd036 [pii] (2000).

45 Sherrington, R. *et al.* Alzheimer's disease associated with mutations in presenilin 2 is rare and variably penetrant. *Hum Mol Genet* **5**, 985-988, doi:6w0044 [pii] (1996).

46 Cummings, J. L. Treatment of Alzheimer's disease: current and future therapeutic approaches. *Rev Neurol Dis* **1**, 60-69 (2004).

47 Huang, Y. & Mucke, L. Alzheimer mechanisms and therapeutic strategies. *Cell* **148**, 1204-1222, doi:10.1016/j.cell.2012.02.040S0092-8674(12)00278-4 [pii] (2012).

48 Kang, J. *et al.* The precursor of Alzheimer's disease amyloid A4 protein resembles a cell-surface receptor. *Nature* **325**, 733-736, doi:10.1038/325733a0 (1987).

49 Dyrks, T. *et al.* Identification, transmembrane orientation and biogenesis of the amyloid A4 precursor of Alzheimer's disease. *EMBO J* **7**, 949-957 (1988).

50 Muller-Hill, B. & Beyreuther, K. Molecular biology of Alzheimer's disease. *Annu Rev Biochem* **58**, 287-307, doi:10.1146/annurev.bi.58.070189.001443 (1989).

51 Wasco, W. *et al.* Identification of a mouse brain cDNA that encodes a protein related to the Alzheimer disease-associated amyloid beta protein precursor. *Proc Natl Acad Sci U S A* **89**, 10758-10762 (1992).

52 Masters, C. L. *et al.* Amyloid plaque core protein in Alzheimer disease and Down syndrome. *Proc Natl Acad Sci U S A* **82**, 4245-4249 (1985).

53 Dawkins, E. & Small, D. H. Insights into the physiological function of the beta-amyloid precursor protein: beyond Alzheimer's disease. *J Neurochem* **129**, 756-769, doi:10.1111/jnc.12675 (2014).

54 Salbaum, J. M., Weidemann, A., Lemaire, H. G., Masters, C. L. & Beyreuther, K. The promoter of Alzheimer's disease amyloid A4 precursor gene. *EMBO J* **7**, 2807-2813 (1988).

55 Izumi, R. *et al.* Positive and negative regulatory elements for the expression of the Alzheimer's disease amyloid precursor-encoding gene in mouse. *Gene* **112**, 189-195 (1992).

56 Quitschke, W. W. & Goldgaber, D. The amyloid beta-protein precursor promoter. A region essential for transcriptional activity contains a nuclear factor binding domain. *J Biol Chem* **267**, 17362-17368 (1992).

57 Clarris, H. J., Key, B., Beyreuther, K., Masters, C. L. & Small, D. H. Expression of the amyloid protein precursor of Alzheimer's disease in the developing rat olfactory system. *Brain Res Dev Brain Res* **88**, 87-95, doi:016538069500083P [pii] (1995).

58 Zheng, H. *et al.* beta-Amyloid precursor protein-deficient mice show reactive gliosis and decreased locomotor activity. *Cell* **81**, 525-531, doi:0092-8674(95)90073-X [pii] (1995).

59 Selkoe, D. J. Alzheimer's disease: genes, proteins, and therapy. *Physiol Rev* **81**, 741-766 (2001).

60 Bhattacharyya, R., Barren, C. & Kovacs, D. M. Palmitoylation of amyloid precursor protein regulates amyloidogenic processing in lipid rafts. *J Neurosci* **33**, 11169-11183, doi:10.1523/JNEUROSCI.4704-12.201333/27/11169 [pii] (2013).

61 Koo, E. H., Squazzo, S. L., Selkoe, D. J. & Koo, C. H. Trafficking of cell-surface amyloid beta-protein precursor. I. Secretion, endocytosis and recycling as detected by labeled monoclonal antibody. *J Cell Sci* **109 (Pt 5)**, 991-998 (1996).

62 Yamazaki, T., Koo, E. H. & Selkoe, D. J. Trafficking of cell-surface amyloid beta-protein precursor. II. Endocytosis, recycling and lysosomal targeting detected by immunolocalization. *J Cell Sci* **109 (Pt 5)**, 999-1008 (1996).

63 Haass, C., Koo, E. H., Mellon, A., Hung, A. Y. & Selkoe, D. J. Targeting of cell-surface beta-amyloid precursor protein to lysosomes: alternative processing into amyloid-bearing fragments. *Nature* **357**, 500-503, doi:10.1038/357500a0 (1992).

64 Shoji, M. *et al.* Production of the Alzheimer amyloid beta protein by normal proteolytic processing. *Science* **258**, 126-129 (1992).

65 Haass, C. *et al.* Amyloid beta-peptide is produced by cultured cells during normal metabolism. *Nature* **359**, 322-325, doi:10.1038/359322a0 (1992).

66 Haass, C., Kaether, C., Thinakaran, G. & Sisodia, S. Trafficking and proteolytic processing of APP. *Cold Spring Harb Perspect Med* **2**, a006270, doi:10.1101/cshperspect.a006270a006270 [pii] (2012).

67 Esch, F. S. *et al.* Cleavage of amyloid beta peptide during constitutive processing of its precursor. *Science* **248**, 1122-1124 (1990).

68 Haass, C., Hung, A. Y., Schlossmacher, M. G., Teplow, D. B. & Selkoe, D. J. beta-Amyloid peptide and a 3-kDa fragment are derived by distinct cellular mechanisms. *J Biol Chem* **268**, 3021-3024 (1993).

69 Sastre, M. *et al.* Presenilin-dependent gamma-secretase processing of beta-amyloid precursor protein at a site corresponding to the S3 cleavage of Notch. *EMBO Rep* **2**, 835-841, doi:10.1093/embo-reports/kve180kve180 [pii] (2001).

70 Lammich, S. *et al.* Constitutive and regulated alpha-secretase cleavage of Alzheimer's amyloid precursor protein by a disintegrin metalloprotease. *Proc Natl Acad Sci U S A* **96**, 3922-3927 (1999).

71 Nitsch, R. M., Slack, B. E., Wurtman, R. J. & Growdon, J. H. Release of Alzheimer amyloid precursor derivatives stimulated by activation of muscarinic acetylcholine receptors. *Science* **258**, 304-307 (1992).

72 von Rotz, R. C. *et al.* The APP intracellular domain forms nuclear multiprotein complexes and regulates the transcription of its own precursor. *J Cell Sci* **117**, 4435-4448, doi:10.1242/jcs.01323117/19/4435 [pii] (2004).

73 Haass, C. Take five--BACE and the gamma-secretase quartet conduct Alzheimer's amyloid beta-peptide generation. *EMBO J* **23**, 483-488, doi:10.1038/sj.emboj.76000617600061 [pii] (2004).

74 Thinakaran, G. & Koo, E. H. Amyloid precursor protein trafficking, processing, and function. *J Biol Chem* **283**, 29615-29619, doi:10.1074/jbc.R800019200R800019200 [pii] (2008).

75 Choy, R. W., Cheng, Z. & Schekman, R. Amyloid precursor protein (APP) traffics from the cell surface via endosomes for amyloid beta (Abeta) production in the trans-Golgi network. *Proc Natl Acad Sci U S A* **109**, E2077-2082, doi:10.1073/pnas.12086351091208635109 [pii] (2012).

76 Brown, M. S., Ye, J., Rawson, R. B. & Goldstein, J. L. Regulated intramembrane proteolysis: a control mechanism conserved from bacteria to humans. *Cell* **100**, 391-398, doi:S0092-8674(00)80675-3 [pii] (2000).

77 Hussain, I. *et al.* Identification of a novel aspartic protease (Asp 2) as beta-secretase. *Mol Cell Neurosci* **14**, 419-427, doi:S1044-7431(99)90811-4 [pii]10.1006/mcne.1999.0811 (1999).

78 Hong, L. *et al.* Structure of the protease domain of memapsin 2 (beta-secretase) complexed with inhibitor. *Science* **290**, 150-153, doi:8888 [pii] (2000).

79 Cai, H. *et al.* BACE1 is the major beta-secretase for generation of Abeta peptides by neurons. *Nat Neurosci* **4**, 233-234, doi:10.1038/8506485064 [pii] (2001).

80 Steiner, H., Fluhrer, R. & Haass, C. Intramembrane proteolysis by gamma-secretase. *J Biol Chem* **283**, 29627-29631, doi:10.1074/jbc.R800010200R800010200 [pii] (2008).

81 Lichtenthaler, S. F., Haass, C. & Steiner, H. Regulated intramembrane proteolysis--lessons from amyloid precursor protein processing. *J Neurochem* **117**, 779-796, doi:10.1111/j.1471-4159.2011.07248.x (2011).

82 Chavez-Gutierrez, L. *et al.* The mechanism of gamma-Secretase dysfunction in familial Alzheimer disease. *EMBO J* **31**, 2261-2274, doi:10.1038/emboj.2012.79emboj201279 [pii] (2012).

83 Haass, C. & Selkoe, D. J. Soluble protein oligomers in neurodegeneration: lessons from the Alzheimer's amyloid beta-peptide. *Nat Rev Mol Cell Biol* **8**, 101-112, doi:nrm2101 [pii]10.1038/nrm2101 (2007).

84 Hardy, J. & Selkoe, D. J. The amyloid hypothesis of Alzheimer's disease: progress and problems on the road to therapeutics. *Science* **297**, 353-356, doi:10.1126/science.1072994297/5580/353 [pii] (2002).

85 Fandrich, M. On the structural definition of amyloid fibrils and other polypeptide aggregates. *Cell Mol Life Sci* **64**, 2066-2078, doi:10.1007/s00018-007-7110-2 (2007).

86 Kumar, S. & Walter, J. Phosphorylation of amyloid beta (Abeta) peptides - a trigger for formation of toxic aggregates in Alzheimer's disease. *Aging (Albany NY)* **3**, 803-812, doi:100362 [pii] (2011).

87 Roth, M., Tomlinson, B. E. & Blessed, G. Correlation between scores for dementia and counts of 'senile plaques' in cerebral grey matter of elderly subjects. *Nature* **209**, 109-110 (1966).

88 Serrano-Pozo, A., Frosch, M. P., Masliah, E. & Hyman, B. T. Neuropathological alterations in Alzheimer disease. *Cold Spring Harb Perspect Med* **1**, a006189, doi:10.1101/cshperspect.a006189a006189 [pii] (2011).

89 Campioni, S. *et al.* A causative link between the structure of aberrant protein oligomers and their toxicity. *Nat Chem Biol* **6**, 140-147, doi:10.1038/nchembio.283nchembio.283 [pii] (2010).

90 Benilova, I., Karran, E. & De Strooper, B. The toxic Abeta oligomer and Alzheimer's disease: an emperor in need of clothes. *Nat Neurosci* **15**, 349-357, doi:10.1038/nn.3028nn.3028 [pii] (2012).

91 Pike, C. J., Walencewicz, A. J., Glabe, C. G. & Cotman, C. W. In vitro aging of beta-amyloid protein causes peptide aggregation and neurotoxicity. *Brain Res* **563**, 311-314 (1991).

92 Harper, J. D., Wong, S. S., Lieber, C. M. & Lansbury, P. T. Observation of metastable Abeta amyloid protofibrils by atomic force microscopy. *Chem Biol* **4**, 119-125, doi:S1074-5521(97)90255-6 [pii] (1997).

93 Walsh, D. M., Lomakin, A., Benedek, G. B., Condron, M. M. & Teplow, D. B. Amyloid beta-protein fibrillogenesis. Detection of a protofibrillar intermediate. *J Biol Chem* **272**, 22364-22372 (1997).

94 Oda, T. *et al.* Clusterin (apoJ) alters the aggregation of amyloid beta-peptide (A beta 1-42) and forms slowly sedimenting A beta complexes that cause oxidative stress. *Exp Neurol* **136**, 22-31, doi:S0014488685710801 [pii] (1995).

95 Lambert, M. P. *et al.* Diffusible, nonfibrillar ligands derived from Abeta1-42 are potent central nervous system neurotoxins. *Proc Natl Acad Sci U S A* **95**, 6448-6453 (1998).

96 Walsh, D. M. *et al.* Naturally secreted oligomers of amyloid beta protein potently inhibit hippocampal long-term potentiation in vivo. *Nature* **416**, 535-539, doi:10.1038/416535a416535a [pii] (2002).

97 Mc Donald, J. M. *et al.* The presence of sodium dodecyl sulphate-stable Abeta dimers is strongly associated with Alzheimer-type dementia. *Brain* **133**, 1328-1341, doi:10.1093/brain/awq065awq065 [pii] (2010).

98 Dohler, F. *et al.* High molecular mass assemblies of amyloid-beta oligomers bind prion protein in patients with Alzheimer's disease. *Brain* **137**, 873-886, doi:10.1093/brain/awt375awt375 [pii] (2014).

99 Bezprozvanny, I. Amyloid goes global. *Sci Signal* **2**, pe16, doi:10.1126/scisignal.263pe16scisignal.263pe16 [pii] (2009).

100 Aguzzi, A., Baumann, F. & Bremer, J. The prion's elusive reason for being. *Annu Rev Neurosci* **31**, 439-477, doi:10.1146/annurev.neuro.31.060407.125620 (2008).

101 Altmeppen, H. C. *et al.* Proteolytic processing of the prion protein in health and disease. *Am J Neurodegener Dis* **1**, 15-31 (2012).

102 Lauren, J., Gimbel, D. A., Nygaard, H. B., Gilbert, J. W. & Strittmatter, S. M. Cellular prion protein mediates impairment of synaptic plasticity by amyloid-beta oligomers. *Nature* **457**, 1128-1132, doi:10.1038/nature07761nature07761 [pii] (2009).

103 Gimbel, D. A. *et al.* Memory impairment in transgenic Alzheimer mice requires cellular prion protein. *J Neurosci* **30**, 6367-6374, doi:10.1523/JNEUROSCI.0395-10.201030/18/6367 [pii] (2010).

104 Prusiner, S. B. Novel proteinaceous infectious particles cause scrapie. *Science* **216**, 136-144 (1982).

105 Bueler, H. *et al.* Normal development and behaviour of mice lacking the neuronal cell-surface PrP protein. *Nature* **356**, 577-582, doi:10.1038/356577a0 (1992).

106 Steele, A. D., Lindquist, S. & Aguzzi, A. The prion protein knockout mouse: a phenotype under challenge. *Prion* **1**, 83-93, doi:4346 [pii] (2007).

107 Le Pichon, C. E. *et al.* Olfactory behavior and physiology are disrupted in prion protein knockout mice. *Nat Neurosci* **12**, 60-69, doi:10.1038/nn.2238nn.2238 [pii] (2009).

108 Bremer, J. *et al.* Axonal prion protein is required for peripheral myelin maintenance. *Nat Neurosci* **13**, 310-318, doi:10.1038/nn.2483nn.2483 [pii] (2010).

109 Graner, E. *et al.* Cellular prion protein binds laminin and mediates neuritogenesis. *Brain Res Mol Brain Res* **76**, 85-92, doi:S0169328X99003344 [pii] (2000).

110 Hajj, G. N. *et al.* Cellular prion protein interaction with vitronectin supports axonal growth and is compensated by integrins. *J Cell Sci* **120**, 1915-1926, doi:jcs.03459 [pii]10.1242/jcs.03459 (2007).

111 Chen, S., Mange, A., Dong, L., Lehmann, S. & Schachner, M. Prion protein as trans-interacting partner for neurons is involved in neurite outgrowth and neuronal survival. *Mol Cell Neurosci* **22**, 227-233, doi:S1044743102000143 [pii] (2003).

112 Moya, K. L. *et al.* Immunolocalization of the cellular prion protein in normal brain. *Microsc Res Tech* **50**, 58-65, doi:10.1002/1097-0029(20000701)50:1<58::AID-JEMT9>3.0.CO;2-5 [pii]10.1002/1097-0029(20000701)50:1<58::AID-JEMT9>3.0.CO;2-5 (2000).

113 Kanaani, J., Prusiner, S. B., Diacovo, J., Baekkeskov, S. & Legname, G. Recombinant prion protein induces rapid polarization and development of synapses in embryonic rat

hippocampal neurons in vitro. *J Neurochem* **95**, 1373-1386, doi:JNC3469 [pii]10.1111/j.1471-4159.2005.03469.x (2005).

114 Gillessen, T., Budd, S. L. & Lipton, S. A. Excitatory amino acid neurotoxicity. *Adv Exp Med Biol* **513**, 3-40 (2002).

115 Khosravani, H. *et al.* Prion protein attenuates excitotoxicity by inhibiting NMDA receptors. *J Cell Biol* **181**, 551-565, doi:10.1083/jcb.200711002jcb.200711002 [pii] (2008).

116 Kellett, K. A. & Hooper, N. M. Prion protein and Alzheimer disease. *Prion* **3**, 190-194, doi:9980 [pii] (2009).

117 Hainfellner, J. A. *et al.* Coexistence of Alzheimer-type neuropathology in Creutzfeldt-Jakob disease. *Acta Neuropathol* **96**, 116-122 (1998).

118 Voigtlander, T. *et al.* Marked increase of neuronal prion protein immunoreactivity in Alzheimer's disease and human prion diseases. *Acta Neuropathol* **101**, 417-423 (2001).

119 Schwarze-Eicker, K. *et al.* Prion protein (PrPc) promotes beta-amyloid plaque formation. *Neurobiol Aging* **26**, 1177-1182, doi:S0197-4580(04)00335-5 [pii]10.1016/j.neurobiolaging.2004.10.004 (2005).

120 Del Bo, R. *et al.* Is M129V of PRNP gene associated with Alzheimer's disease? A case-control study and a meta-analysis. *Neurobiol Aging* **27**, 770 e771-770 e775, doi:S0197-4580(05)00161-2 [pii]10.1016/j.neurobiolaging.2005.05.025 (2006).

121 Berr, C. *et al.* Polymorphism of the codon 129 of the prion protein (PrP) gene and neuropathology of cerebral ageing. *Acta Neuropathol* **106**, 71-74, doi:10.1007/s00401-003-0700-7 (2003).

122 Parkin, E. T. *et al.* Cellular prion protein regulates beta-secretase cleavage of the Alzheimer's amyloid precursor protein. *Proc Natl Acad Sci U S A* **104**, 11062-11067, doi:0609621104 [pii]10.1073/pnas.0609621104 (2007).

123 Chen, X. H., Johnson, V. E., Uryu, K., Trojanowski, J. Q. & Smith, D. H. A lack of amyloid beta plaques despite persistent accumulation of amyloid beta in axons of long-term survivors of traumatic brain injury. *Brain Pathol* **19**, 214-223, doi:10.1111/j.1750-3639.2008.00176.xBPA176 [pii] (2009).

124 Chung, E. *et al.* Anti-PrPC monoclonal antibody infusion as a novel treatment for cognitive deficits in an Alzheimer's disease model mouse. *BMC Neurosci* **11**, 130, doi:10.1186/1471-2202-11-1301471-2202-11-130 [pii] (2010).

125 Freir, D. B. *et al.* Interaction between prion protein and toxic amyloid beta assemblies can be therapeutically targeted at multiple sites. *Nat Commun* **2**, 336, doi:10.1038/ncomms1341ncomms1341 [pii] (2011).

126 Barry, A. E. *et al.* Alzheimer's disease brain-derived amyloid-beta-mediated inhibition of LTP in vivo is prevented by immunotargeting cellular prion protein. *J Neurosci* **31**, 7259-7263, doi:10.1523/JNEUROSCI.6500-10.201131/20/7259 [pii] (2011).

127 Balducci, C. *et al.* Synthetic amyloid-beta oligomers impair long-term memory independently of cellular prion protein. *Proc Natl Acad Sci U S A* **107**, 2295-2300, doi:10.1073/pnas.0911829107 0911829107 [pii] (2010).

128 Cisse, M. *et al.* Ablation of cellular prion protein does not ameliorate abnormal neural network activity or cognitive dysfunction in the J20 line of human amyloid precursor protein

transgenic mice. *J Neurosci* **31**, 10427-10431, doi:10.1523/JNEUROSCI.1459-11.201131/29/10427 [pii] (2011).

129 Calella, A. M. *et al.* Prion protein and Abeta-related synaptic toxicity impairment. *EMBO Mol Med* **2**, 306-314, doi:10.1002/emmm.201000082 (2010).

130 Kessels, H. W., Nguyen, L. N., Nabavi, S. & Malinow, R. The prion protein as a receptor for amyloid-beta. *Nature* **466**, E3-4; discussion E4-5, doi:10.1038/nature09217nature09217 [pii] (2010).

131 Benilova, I. & De Strooper, B. Prion protein in Alzheimer's pathogenesis: a hot and controversial issue. *EMBO Mol Med* **2**, 289-290, doi:10.1002/emmm.201000088 (2010).

132 Biasini, E., Turnbaugh, J. A., Unterberger, U. & Harris, D. A. Prion protein at the crossroads of physiology and disease. *Trends Neurosci* **35**, 92-103, doi:10.1016/j.tins.2011.10.002S0166-2236(11)00173-1 [pii] (2012).

133 Um, J. W. *et al.* Alzheimer amyloid-beta oligomer bound to postsynaptic prion protein activates Fyn to impair neurons. *Nat Neurosci* **15**, 1227-1235, doi:10.1038/nn.3178nn.3178 [pii] (2012).

134 Larson, M. *et al.* The complex PrP(c)-Fyn couples human oligomeric Abeta with pathological tau changes in Alzheimer's disease. *J Neurosci* **32**, 16857-16871a, doi:10.1523/JNEUROSCI.1858-12.201232/47/16857 [pii] (2012).

135 Resenberger, U. K., Winklhofer, K. F. & Tatzelt, J. Cellular prion protein mediates toxic signaling of amyloid beta. *Neurodegener Dis* **10**, 298-300, doi:10.1159/000332596000332596 [pii] (2012).

136 Raposo, G. & Stoorvogel, W. Extracellular vesicles: exosomes, microvesicles, and friends. *J Cell Biol* **200**, 373-383, doi:10.1083/jcb.201211138jcb.201211138 [pii] (2013).

137 Thery, C., Zitvogel, L. & Amigorena, S. Exosomes: composition, biogenesis and function. *Nat Rev Immunol* **2**, 569-579, doi:10.1038/nri855nri855 [pii] (2002).

138 Harding, C., Heuser, J. & Stahl, P. Receptor-mediated endocytosis of transferrin and recycling of the transferrin receptor in rat reticulocytes. *J Cell Biol* **97**, 329-339 (1983).

139 Pan, B. T., Teng, K., Wu, C., Adam, M. & Johnstone, R. M. Electron microscopic evidence for externalization of the transferrin receptor in vesicular form in sheep reticulocytes. *J Cell Biol* **101**, 942-948 (1985).

140 Johnstone, R. M., Adam, M., Hammond, J. R., Orr, L. & Turbide, C. Vesicle formation during reticulocyte maturation. Association of plasma membrane activities with released vesicles (exosomes). *J Biol Chem* **262**, 9412-9420 (1987).

141 Katzmann, D. J., Babst, M. & Emr, S. D. Ubiquitin-dependent sorting into the multivesicular body pathway requires the function of a conserved endosomal protein sorting complex, ESCRT-I. *Cell* **106**, 145-155, doi:S0092-8674(01)00434-2 [pii] (2001).

142 Stuffers, S., Sem Wegner, C., Stenmark, H. & Brech, A. Multivesicular endosome biogenesis in the absence of ESCRTs. *Traffic* **10**, 925-937, doi:10.1111/j.1600-0854.2009.00920.xTRA920 [pii] (2009).

143 Trajkovic, K. *et al.* Ceramide triggers budding of exosome vesicles into multivesicular endosomes. *Science* **319**, 1244-1247, doi:10.1126/science.1153124319/5867/1244 [pii] (2008).

144 van Niel, G. *et al.* The tetraspanin CD63 regulates ESCRT-independent and -dependent endosomal sorting during melanogenesis. *Dev Cell* **21**, 708-721, doi:10.1016/j.devcel.2011.08.019S1534-5807(11)00357-1 [pii] (2011).

145 Escola, J. M. *et al.* Selective enrichment of tetraspan proteins on the internal vesicles of multivesicular endosomes and on exosomes secreted by human B-lymphocytes. *J Biol Chem* **273**, 20121-20127 (1998).

146 Nazarenko, I. *et al.* Cell surface tetraspanin Tspan8 contributes to molecular pathways of exosome-induced endothelial cell activation. *Cancer Res* **70**, 1668-1678, doi:10.1158/0008-5472.CAN-09-24700008-5472.CAN-09-2470 [pii] (2010).

147 Mobius, W. *et al.* Immunoelectron microscopic localization of cholesterol using biotinylated and non-cytolytic perfringolysin O. *J Histochem Cytochem* **50**, 43-55 (2002).

148 Buschow, S. I. *et al.* MHC II in dendritic cells is targeted to lysosomes or T cell-induced exosomes via distinct multivesicular body pathways. *Traffic* **10**, 1528-1542, doi:10.1111/j.1600-0854.2009.00963.xTRA963 [pii] (2009).

149 McNew, J. A. *et al.* Compartmental specificity of cellular membrane fusion encoded in SNARE proteins. *Nature* **407**, 153-159, doi:10.1038/35025000 (2000).

150 Rao, S. K., Huynh, C., Proux-Gillardeaux, V., Galli, T. & Andrews, N. W. Identification of SNAREs involved in synaptotagmin VII-regulated lysosomal exocytosis. *J Biol Chem* **279**, 20471-20479, doi:10.1074/jbc.M400798200M400798200 [pii] (2004).

151 Matsuo, H. *et al.* Role of LBPA and Alix in multivesicular liposome formation and endosome organization. *Science* **303**, 531-534, doi:10.1126/science.1092425303/5657/531 [pii] (2004).

152 Brouwers, J. F. *et al.* Distinct lipid compositions of two types of human prostasomes. *Proteomics* **13**, 1660-1666, doi:10.1002/pmic.201200348 (2013).

153 Laulagnier, K. *et al.* Mast cell- and dendritic cell-derived exosomes display a specific lipid composition and an unusual membrane organization. *Biochem J* **380**, 161-171, doi:10.1042/BJ20031594BJ20031594 [pii] (2004).

154 Llorente, A. *et al.* Molecular lipidomics of exosomes released by PC-3 prostate cancer cells. *Biochim Biophys Acta* **1831**, 1302-1309 (2013).

155 Wubbolts, R. *et al.* Proteomic and biochemical analyses of human B cell-derived exosomes. Potential implications for their function and multivesicular body formation. *J Biol Chem* **278**, 10963-10972, doi:10.1074/jbc.M207550200M207550200 [pii] (2003).

156 Laulagnier, K. *et al.* PLD2 is enriched on exosomes and its activity is correlated to the release of exosomes. *FEBS Lett* **572**, 11-14, doi:10.1016/j.febslet.2004.06.082S0014579304008518 [pii] (2004).

157 Ikonen, E. Roles of lipid rafts in membrane transport. *Curr Opin Cell Biol* **13**, 470-477, doi:S0955-0674(00)00238-6 [pii] (2001).

158 Tan, S. S. *et al.* Therapeutic MSC exosomes are derived from lipid raft microdomains in the plasma membrane. *J Extracell Vesicles* **2**, doi:10.3402/jev.v2i0.2261422614 [pii] (2013).

159 Fang, Y. *et al.* Higher-order oligomerization targets plasma membrane proteins and HIV gag to exosomes. *PLoS Biol* **5**, e158, doi:06-PLBI-RA-2411R2 [pii]10.1371/journal.pbio.0050158 (2007).

160 Van Niel, G. *et al.* Intestinal epithelial exosomes carry MHC class II/peptides able to inform the immune system in mice. *Gut* **52**, 1690-1697 (2003).

161 Simpson, R. J., Jensen, S. S. & Lim, J. W. Proteomic profiling of exosomes: current perspectives. *Proteomics* **8**, 4083-4099, doi:10.1002/pmic.200800109 (2008).

162 Kharaziha, P., Ceder, S., Li, Q. & Panaretakis, T. Tumor cell-derived exosomes: a message in a bottle. *Biochim Biophys Acta* **1826**, 103-111, doi:10.1016/j.bbcan.2012.03.006S0304-419X(12)00020-0 [pii] (2012).

163 Ratajczak, J., Wysoczynski, M., Hayek, F., Janowska-Wieczorek, A. & Ratajczak, M. Z. Membrane-derived microvesicles: important and underappreciated mediators of cell-to-cell communication. *Leukemia* **20**, 1487-1495, doi:2404296 [pii]10.1038/sj.leu.2404296 (2006).

164 Valadi, H. *et al.* Exosome-mediated transfer of mRNAs and microRNAs is a novel mechanism of genetic exchange between cells. *Nat Cell Biol* **9**, 654-659, doi:ncb1596 [pii]10.1038/ncb1596 (2007).

165 Harding, C., Heuser, J. & Stahl, P. Endocytosis and intracellular processing of transferrin and colloidal gold-transferrin in rat reticulocytes: demonstration of a pathway for receptor shedding. *Eur J Cell Biol* **35**, 256-263 (1984).

166 Raposo, G. *et al.* B lymphocytes secrete antigen-presenting vesicles. *J Exp Med* **183**, 1161-1172 (1996).

167 Zitvogel, L. *et al.* Eradication of established murine tumors using a novel cell-free vaccine: dendritic cell-derived exosomes. *Nat Med* **4**, 594-600 (1998).

168 Taylor, D. D. & Gercel-Taylor, C. Tumour-derived exosomes and their role in cancer-associated T-cell signalling defects. *Br J Cancer* **92**, 305-311, doi:6602316 [pii]10.1038/sj.bjc.6602316 (2005).

169 Sims, P. J., Faioni, E. M., Wiedmer, T. & Shattil, S. J. Complement proteins C5b-9 cause release of membrane vesicles from the platelet surface that are enriched in the membrane receptor for coagulation factor Va and express prothrombinase activity. *J Biol Chem* **263**, 18205-18212 (1988).

170 Skokos, D. *et al.* Mast cell-dependent B and T lymphocyte activation is mediated by the secretion of immunologically active exosomes. *J Immunol* **166**, 868-876 (2001).

171 Faure, J. *et al.* Exosomes are released by cultured cortical neurones. *Mol Cell Neurosci* **31**, 642-648, doi:S1044-7431(05)00302-7 [pii]10.1016/j.mcn.2005.12.003 (2006).

172 Kramer-Albers, E. M. *et al.* Oligodendrocytes secrete exosomes containing major myelin and stress-protective proteins: Trophic support for axons? *Proteomics Clin Appl* **1**, 1446-1461, doi:10.1002/prca.200700522 (2007).

173 Lopez-Verrilli, M. A., Picou, F. & Court, F. A. Schwann cell-derived exosomes enhance axonal regeneration in the peripheral nervous system. *Glia* **61**, 1795-1806, doi:10.1002/glia.22558 (2013).

174 Mallegol, J. *et al.* T84-intestinal epithelial exosomes bear MHC class II/peptide complexes potentiating antigen presentation by dendritic cells. *Gastroenterology* **132**, 1866-1876, doi:S0016-5085(07)00402-7 [pii]10.1053/j.gastro.2007.02.043 (2007).

175 Ronquist, G. & Hedstrom, M. Restoration of detergent-inactivated adenosine triphosphatase activity of human prostatic fluid with concanavalin A. *Biochim Biophys Acta* **483**, 483-486 (1977).

176 Caby, M. P., Lankar, D., Vincendeau-Scherrer, C., Raposo, G. & Bonnerot, C. Exosomal-like vesicles are present in human blood plasma. *Int Immunol* **17**, 879-887, doi:dxh267 [pii]10.1093/intimm/dxh267 (2005).

177 Pisitkun, T., Shen, R. F. & Knepper, M. A. Identification and proteomic profiling of exosomes in human urine. *Proc Natl Acad Sci U S A* **101**, 13368-13373, doi:10.1073/pnas.04034531010403453101 [pii] (2004).

178 Ogawa, Y. *et al.* Proteomic analysis of two types of exosomes in human whole saliva. *Biol Pharm Bull* **34**, 13-23, doi:JST.JSTAGE/bpb/34.13 [pii] (2011).

179 Admyre, C. *et al.* Exosomes with immune modulatory features are present in human breast milk. *J Immunol* **179**, 1969-1978, doi:179/3/1969 [pii] (2007).

180 Asea, A. *et al.* Heat shock protein-containing exosomes in mid-trimester amniotic fluids. *J Reprod Immunol* **79**, 12-17, doi:10.1016/j.jri.2008.06.001S0165-0378(08)00069-7 [pii] (2008).

181 Andre, F. *et al.* Malignant effusions and immunogenic tumour-derived exosomes. *Lancet* **360**, 295-305, doi:S0140-6736(02)09552-1 [pii]10.1016/S0140-6736(02)09552-1 (2002).

182 Vella, L. J. *et al.* Packaging of prions into exosomes is associated with a novel pathway of PrP processing. *J Pathol* **211**, 582-590, doi:10.1002/path.2145 (2007).

183 Masyuk, A. I. *et al.* Biliary exosomes influence cholangiocyte regulatory mechanisms and proliferation through interaction with primary cilia. *Am J Physiol Gastrointest Liver Physiol* **299**, G990-999, doi:10.1152/ajpgi.00093.2010ajpgi.00093.2010 [pii] (2010).

184 Rana, S., Yue, S., Stadel, D. & Zoller, M. Toward tailored exosomes: the exosomal tetraspanin web contributes to target cell selection. *Int J Biochem Cell Biol* **44**, 1574-1584, doi:10.1016/j.biocel.2012.06.018S1357-2725(12)00217-8 [pii] (2012).

185 Hemler, M. E. Tetraspanin proteins mediate cellular penetration, invasion, and fusion events and define a novel type of membrane microdomain. *Annu Rev Cell Dev Biol* **19**, 397-422, doi:10.1146/annurev.cellbio.19.111301.153609 (2003).

186 Ronquist, G. & Brody, I. The prostasome: its secretion and function in man. *Biochim Biophys Acta* **822**, 203-218, doi:0304-4157(85)90008-5 [pii] (1985).

187 van Niel, G. *et al.* Intestinal epithelial cells secrete exosome-like vesicles. *Gastroenterology* **121**, 337-349, doi:S001650850128055X [pii] (2001).

188 Zeelenberg, I. S. *et al.* Targeting tumor antigens to secreted membrane vesicles in vivo induces efficient antitumor immune responses. *Cancer Res* **68**, 1228-1235, doi:10.1158/0008-5472.CAN-07-316368/4/1228 [pii] (2008).

189 Zhang, H. G. & Grizzle, W. E. Exosomes and cancer: a newly described pathway of immune suppression. *Clin Cancer Res* **17**, 959-964, doi:10.1158/1078-0432.CCR-10-14891078-0432.CCR-10-1489 [pii] (2011).

190 Kang, D., Oh, S., Ahn, S. M., Lee, B. H. & Moon, M. H. Proteomic analysis of exosomes from human neural stem cells by flow field-flow fractionation and nanoflow liquid chromatography-tandem mass spectrometry. *J Proteome Res* **7**, 3475-3480, doi:10.1021/pr800225z (2008).

191 Guescini, M., Genedani, S., Stocchi, V. & Agnati, L. F. Astrocytes and Glioblastoma cells release exosomes carrying mtDNA. *J Neural Transm* **117**, 1-4, doi:10.1007/s00702-009-0288-8 (2010).

192 Lachenal, G. *et al.* Release of exosomes from differentiated neurons and its regulation by synaptic glutamatergic activity. *Mol Cell Neurosci* **46**, 409-418, doi:10.1016/j.mcn.2010.11.004S1044-7431(10)00255-1 [pii] (2011).

193 Vella, L. J., Greenwood, D. L., Cappai, R., Scheerlinck, J. P. & Hill, A. F. Enrichment of prion protein in exosomes derived from ovine cerebral spinal fluid. *Vet Immunol Immunopathol* **124**, 385-393, doi:10.1016/j.vetimm.2008.04.002S0165-2427(08)00165-7 [pii] (2008).

194 Wang, S. *et al.* Synapsin I is an oligomannose-carrying glycoprotein, acts as an oligomannose-binding lectin, and promotes neurite outgrowth and neuronal survival when released via glia-derived exosomes. *J Neurosci* **31**, 7275-7290, doi:10.1523/JNEUROSCI.6476-10.201131/20/7275 [pii] (2011).

195 Bakhti, M., Winter, C. & Simons, M. Inhibition of myelin membrane sheath formation by oligodendrocyte-derived exosome-like vesicles. *J Biol Chem* **286**, 787-796, doi:10.1074/jbc.M110.190009M110.190009 [pii] (2011).

196 Ecroyd, H., Sarradin, P., Dacheux, J. L. & Gatti, J. L. Compartmentalization of prion isoforms within the reproductive tract of the ram. *Biol Reprod* **71**, 993-1001, doi:10.1095/biolreprod.104.029801biolreprod.104.029801 [pii] (2004).

197 Robertson, C. *et al.* Cellular prion protein is released on exosomes from activated platelets. *Blood* **107**, 3907-3911, doi:2005-02-0802 [pii]10.1182/blood-2005-02-0802 (2006).

198 Lacroux, C. *et al.* Impact of leucocyte depletion and prion reduction filters on TSE blood borne transmission. *PLoS One* **7**, e42019, doi:10.1371/journal.pone.0042019PONE-D-12-17441 [pii] (2012).

199 Mironov, A., Jr. *et al.* Cytosolic prion protein in neurons. *J Neurosci* **23**, 7183-7193, doi:23/18/7183 [pii] (2003).

200 Vella, L. J., Sharples, R. A., Nisbet, R. M., Cappai, R. & Hill, A. F. The role of exosomes in the processing of proteins associated with neurodegenerative diseases. *Eur Biophys J* **37**, 323-332, doi:10.1007/s00249-007-0246-z (2008).

201 Fevrier, B. *et al.* Cells release prions in association with exosomes. *Proc Natl Acad Sci U S A* **101**, 9683-9688, doi:10.1073/pnas.03084131010308413101 [pii] (2004).

202 Alais, S. *et al.* Mouse neuroblastoma cells release prion infectivity associated with exosomal vesicles. *Biol Cell* **100**, 603-615, doi:10.1042/BC20080025BC20080025 [pii] (2008).

203 Arellano-Anaya, Z. E. *et al.* Prion strains are differentially released through the exosomal pathway. *Cell Mol Life Sci*, doi:10.1007/s00018-014-1735-8 (2014).

204 Taylor, D. R. & Hooper, N. M. The prion protein and lipid rafts. *Mol Membr Biol* **23**, 89-99, doi:U2058T5U3JP63H07 [pii]10.1080/09687860500449994 (2006).

205 Baron, G. S., Wehrly, K., Dorward, D. W., Chesebro, B. & Caughey, B. Conversion of raft associated prion protein to the protease-resistant state requires insertion of PrP-res (PrP(Sc)) into contiguous membranes. *EMBO J* **21**, 1031-1040, doi:10.1093/emboj/21.5.1031 (2002).

206 Deleault, N. R., Harris, B. T., Rees, J. R. & Supattapone, S. Formation of native prions from minimal components in vitro. *Proc Natl Acad Sci U S A* **104**, 9741-9746, doi:0702662104 [pii]10.1073/pnas.0702662104 (2007).

207 Wang, F. *et al.* Lipid interaction converts prion protein to a PrPSc-like proteinase K-resistant conformation under physiological conditions. *Biochemistry* **46**, 7045-7053, doi:10.1021/bi700299h (2007).

208 Rajendran, L. *et al.* Alzheimer's disease beta-amyloid peptides are released in association with exosomes. *Proc Natl Acad Sci U S A* **103**, 11172-11177, doi:0603838103 [pii]10.1073/pnas.0603838103 (2006).

209 Sharples, R. A. *et al.* Inhibition of gamma-secretase causes increased secretion of amyloid precursor protein C-terminal fragments in association with exosomes. *FASEB J* **22**, 1469-1478, doi:10.1096/fj.07-9357comfj.07-9357com [pii] (2008).

210 Yuyama, K., Sun, H., Mitsutake, S. & Igarashi, Y. Sphingolipid-modulated exosome secretion promotes clearance of amyloid-beta by microglia. *J Biol Chem* **287**, 10977-10989, doi:10.1074/jbc.M111.324616M111.324616 [pii] (2012).

211 Utsumi, M. *et al.* Up-and-down topological mode of amyloid beta-peptide lying on hydrophilic/hydrophobic interface of ganglioside clusters. *Glycoconj J* **26**, 999-1006, doi:10.1007/s10719-008-9216-7 (2009).

212 Sanghera, N. *et al.* Deciphering the molecular details for the binding of the prion protein to main ganglioside GM1 of neuronal membranes. *Chem Biol* **18**, 1422-1431, doi:10.1016/j.chembiol.2011.08.016S1074-5521(11)00345-0 [pii] (2011).

213 Yuyama, K. *et al.* Decreased Amyloid-beta Pathologies by Intracerebral Loading of Glycosphingolipid-enriched Exosomes in Alzheimer Model Mice. *J Biol Chem*, doi:jbc.M114.577213 [pii]M114.577213 [pii]10.1074/jbc.M114.577213 (2014).

214 An, K. *et al.* Exosomes neutralize synaptic-plasticity-disrupting activity of Abeta assemblies in vivo. *Mol Brain* **6**, 47, doi:10.1186/1756-6606-6-471756-6606-6-47 [pii] (2013).

215 Joshi, P. *et al.* Microglia convert aggregated amyloid-beta into neurotoxic forms through the shedding of microvesicles. *Cell Death Differ* **21**, 582-593, doi:10.1038/cdd.2013.180cdd2013180 [pii] (2014).

216 Doyle, E. L. *et al.* TAL Effector-Nucleotide Targeter (TALE-NT) 2.0: tools for TAL effector design and target prediction. *Nucleic Acids Res* **40**, W117-122, doi:10.1093/nar/gks608gks608 [pii] (2012).

217 Cermak, T. *et al.* Efficient design and assembly of custom TALEN and other TAL effector-based constructs for DNA targeting. *Nucleic Acids Res* **39**, e82, doi:10.1093/nar/gkr218gkr218 [pii] (2011).

218 Perera, W. S. & Hooper, N. M. Ablation of the metal ion-induced endocytosis of the prion protein by disease-associated mutation of the octarepeat region. *Curr Biol* **11**, 519-523, doi:S0960-9822(01)00147-6 [pii] (2001).

219 Segura, E. *et al.* ICAM-1 on exosomes from mature dendritic cells is critical for efficient naive T-cell priming. *Blood* **106**, 216-223, doi:2005-01-0220 [pii]10.1182/blood-2005-01-0220 (2005).

220 Ostrowski, M. *et al.* Rab27a and Rab27b control different steps of the exosome secretion pathway. *Nat Cell Biol* **12**, 19-30; sup pp 11-13, doi:10.1038/ncb2000ncb2000 [pii] (2010).

221 Fitzner, D. *et al.* Selective transfer of exosomes from oligodendrocytes to microglia by macropinocytosis. *J Cell Sci* **124**, 447-458, doi:10.1242/jcs.074088124/3/447 [pii] (2011).

222 Du, D. *et al.* A kinetic aggregation assay allowing selective and sensitive amyloid-beta quantification in cells and tissues. *Biochemistry* **50**, 1607-1617, doi:10.1021/bi1013744 (2011).

223 Kuwahara, C. *et al.* Prions prevent neuronal cell-line death. *Nature* **400**, 225-226, doi:10.1038/22241 (1999).

224 Nakamura, Y. *et al.* Transfection of prion protein gene suppresses coxsackievirus B3 replication in prion protein gene-deficient cells. *J Gen Virol* **84**, 3495-3502 (2003).

225 Goold, R. *et al.* Rapid cell-surface prion protein conversion revealed using a novel cell system. *Nat Commun* **2**, 281, doi:10.1038/ncomms1282ncomms1282 [pii] (2011).

226 Christian, M. *et al.* Targeting DNA double-strand breaks with TAL effector nucleases. *Genetics* **186**, 757-761, doi:10.1534/genetics.110.120717genetics.110.120717 [pii] (2010).

227 Bogdanove, A. J., Schornack, S. & Lahaye, T. TAL effectors: finding plant genes for disease and defense. *Curr Opin Plant Biol* **13**, 394-401, doi:10.1016/j.pbi.2010.04.010S1369-5266(10)00053-1 [pii] (2010).

228 Boch, J. & Bonas, U. Xanthomonas AvrBs3 family-type III effectors: discovery and function. *Annu Rev Phytopathol* **48**, 419-436, doi:10.1146/annurev-phyto-080508-081936 (2010).

229 Moscou, M. J. & Bogdanove, A. J. A simple cipher governs DNA recognition by TAL effectors. *Science* **326**, 1501, doi:10.1126/science.11788171178817 [pii] (2009).

230 Boch, J. *et al.* Breaking the code of DNA binding specificity of TAL-type III effectors. *Science* **326**, 1509-1512, doi:10.1126/science.11788111178811 [pii] (2009).

231 Weterings, E. & van Gent, D. C. The mechanism of non-homologous end-joining: a synopsis of synapsis. *DNA Repair (Amst)* **3**, 1425-1435, doi:10.1016/j.dnarep.2004.06.003S156878640400179X [pii] (2004).

232 Sung, P. & Klein, H. Mechanism of homologous recombination: mediators and helicases take on regulatory functions. *Nat Rev Mol Cell Biol* **7**, 739-750, doi:nrm2008 [pii]10. 1038/nrm2008 (2006).

233 Landry, J. J. *et al.* The genomic and transcriptomic landscape of a HeLa cell line. *G3 (Bethesda)* **3**, 1213-1224, doi:10.1534/g3.113.005777g3.113.005777 [pii] (2013).

234 Streubel, J., Blucher, C., Landgraf, A. & Boch, J. TAL effector RVD specificities and efficiencies. *Nat Biotechnol* **30**, 593-595, doi:10.1038/nbt.2304nbt.2304 [pii] (2012).

235 Juillerat, A. *et al.* Comprehensive analysis of the specificity of transcription activator-like effector nucleases. *Nucleic Acids Res* **42**, 5390-5402, doi:10.1093/nar/gku155gku155 [pii] (2014).

236 Potter, H. & Heller, R. Transfection by electroporation. *Curr Protoc Cell Biol* **Chapter 20**, Unit20 25, doi:10.1002/0471143030.cb2005s52 (2011).

237 Ding, Q. *et al.* A TALEN genome-editing system for generating human stem cell-based disease models. *Cell Stem Cell* **12**, 238-251, doi:10.1016/j.stem.2012.11.011S1934-5909(12)00645-5 [pii] (2013).

238 Rushworth, J. V., Griffiths, H. H., Watt, N. T. & Hooper, N. M. Prion protein-mediated toxicity of amyloid-beta oligomers requires lipid rafts and the transmembrane LRP1. *J Biol Chem* **288**, 8935-8951, doi:10.1074/jbc.M112.400358M112.400358 [pii] (2013).

239 Olmsted, J. B., Carlson, K., Klebe, R., Ruddle, F. & Rosenbaum, J. Isolation of microtubule protein from cultured mouse neuroblastoma cells. *Proc Natl Acad Sci U S A* **65**, 129-136 (1970).

240 Aupeix, K. *et al.* The significance of shed membrane particles during programmed cell death in vitro, and in vivo, in HIV-1 infection. *J Clin Invest* **99**, 1546-1554, doi:10.1172/JCI119317 (1997).

241 Thery, C. *et al.* Proteomic analysis of dendritic cell-derived exosomes: a secreted subcellular compartment distinct from apoptotic vesicles. *J Immunol* **166**, 7309-7318 (2001).

242 Thery, C., Ostrowski, M. & Segura, E. Membrane vesicles as conveyors of immune responses. *Nat Rev Immunol* **9**, 581-593, doi:10.1038/nri2567nri2567 [pii] (2009).

243 Majno, G. & Joris, I. Apoptosis, oncosis, and necrosis. An overview of cell death. *Am J Pathol* **146**, 3-15 (1995).

244 Kalani, A., Tyagi, A. & Tyagi, N. Exosomes: mediators of neurodegeneration, neuroprotection and therapeutics. *Mol Neurobiol* **49**, 590-600, doi:10.1007/s12035-013-8544-1 (2014).

245 Amel, S. *et al.* Renal physiology. *Nephrology Dialysis Transplantation* **27**, ii3-ii4, doi:10.1093/ndt/gfs196 (2012).

246 Ariga, T., McDonald, M. P. & Yu, R. K. Role of ganglioside metabolism in the pathogenesis of Alzheimer's disease--a review. *J Lipid Res* **49**, 1157-1175, doi:10.1194/jlr.R800007-JLR200R800007-JLR200 [pii] (2008).

247 Nieznanski, K., Choi, J. K., Chen, S., Surewicz, K. & Surewicz, W. K. Soluble prion protein inhibits amyloid-beta (Abeta) fibrillization and toxicity. *J Biol Chem* **287**, 33104-33108, doi:C112.400614 [pii]10.1074/jbc.C112.400614 (2012).

248 Younan, N. D., Sarell, C. J., Davies, P., Brown, D. R. & Viles, J. H. The cellular prion protein traps Alzheimer's Abeta in an oligomeric form and disassembles amyloid fibers. *FASEB J* **27**, 1847-1858, doi:10.1096/fj.12-222588fj.12-222588 [pii] (2013).

249 Meisl, G. *et al.* Differences in nucleation behavior underlie the contrasting aggregation kinetics of the Abeta40 and Abeta42 peptides. *Proc Natl Acad Sci U S A* **111**, 9384-9389, doi:10.1073/pnas.14015641111401564111 [pii] (2014).

250 Agosta, F. *et al.* Myeloid microvesicles in cerebrospinal fluid are associated with myelin damage and neuronal loss in mild cognitive impairment and Alzheimer disease. *Ann Neurol*, doi:10.1002/ana.24235 (2014).

251 Altmeppen, H. C. *et al.* Roles of endoproteolytic alpha-cleavage and shedding of the prion protein in neurodegeneration. *FEBS J* **280**, 4338-4347, doi:10.1111/febs.12196 (2013).

252 Altmeppen, H. C. *et al.* Lack of a-disintegrin-and-metalloproteinase ADAM10 leads to intracellular accumulation and loss of shedding of the cellular prion protein in vivo. *Mol Neurodegener* **6**, 36, doi:10.1186/1750-1326-6-361750-1326-6-36 [pii] (2011).

253 Mange, A. *et al.* Alpha- and beta- cleavages of the amino-terminus of the cellular prion protein. *Biol Cell* **96**, 125-132, doi:10.1016/j.biolcel.2003.11.007S0248490004000061 [pii] (2004).

254 Sunyach, C., Cisse, M. A., da Costa, C. A., Vincent, B. & Checler, F. The C-terminal products of cellular prion protein processing, C1 and C2, exert distinct influence on p53-dependent staurosporine-induced caspase-3 activation. *J Biol Chem* **282**, 1956-1963, doi:M609663200 [pii]10.1074/jbc.M609663200 (2007).

255 Guillot-Sestier, M. V., Sunyach, C., Druon, C., Scarzello, S. & Checler, F. The alpha-secretase-derived N-terminal product of cellular prion, N1, displays neuroprotective function in vitro and in vivo. *J Biol Chem* **284**, 35973-35986, doi:10.1074/jbc.M109.051086M109.051086 [pii] (2009).

256 Turnbaugh, J. A., Westergard, L., Unterberger, U., Biasini, E. & Harris, D. A. The N-terminal, polybasic region is critical for prion protein neuroprotective activity. *PLoS One* **6**, e25675, doi:10.1371/journal.pone.0025675PONE-D-11-08356 [pii] (2011).

Acknowledgments

I want to thank Prof. Dr. Markus Glatzel for the supervision of my doctoral thesis and the opportunity to work in his research group.

I also want to express my gratitude to my supervisor Dr. Susanne Krasemann who always supported me in every possible way to solve problems of any kind.

I thank Prof. Dr. Thorsten Burmester for his consent to be referee of my thesis.

Further, I would like to thank the whole Institute of Neuropathology for the great experience over the last three years and I hope to keep in touch.

Special thanks go to Dr. Jonathan Gilthorpe for proof reading and scientific advice.

Finally, I thank my family and my soon to be wife Astrid for the never ending support.

Appendix

Appendix 1: FACS sorting of putative Prnp knockout cells after transfection with mPrP-TALEN01 and labelling with a fluorescent antibody complex against PrP^{C}.

(A) Control of 1st TALEN transfection were unlabeled N2a-WT cells. (B) N2a cells 7 days post transfection with mPrP-TALEN01 labeled with Pom1 and Alexa555. (C) N2a cells 7 days post transfection with mPrP-TALEN01 labeled with Pom2 and Alexa555. (D) Control of 2nd TALEN transfection were unlabeled N2a-WT cells. (E) N2a cells 7 days post transfection with mPrP-TALEN01 labeled with Pom1 and Alexa555.

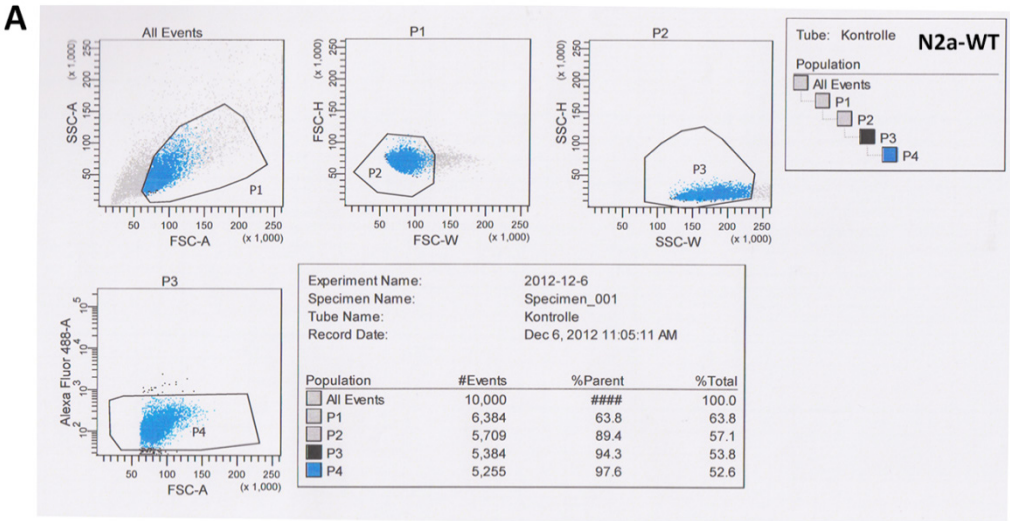

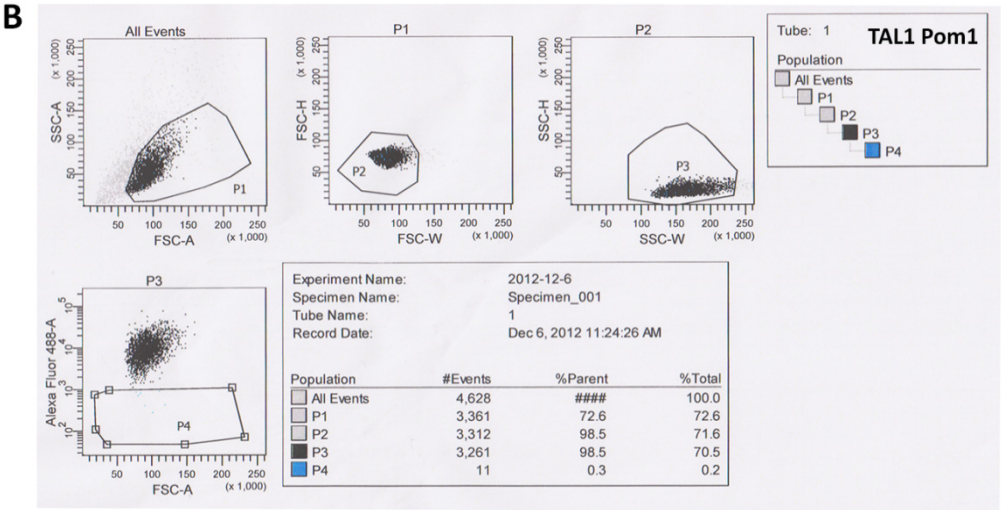

C

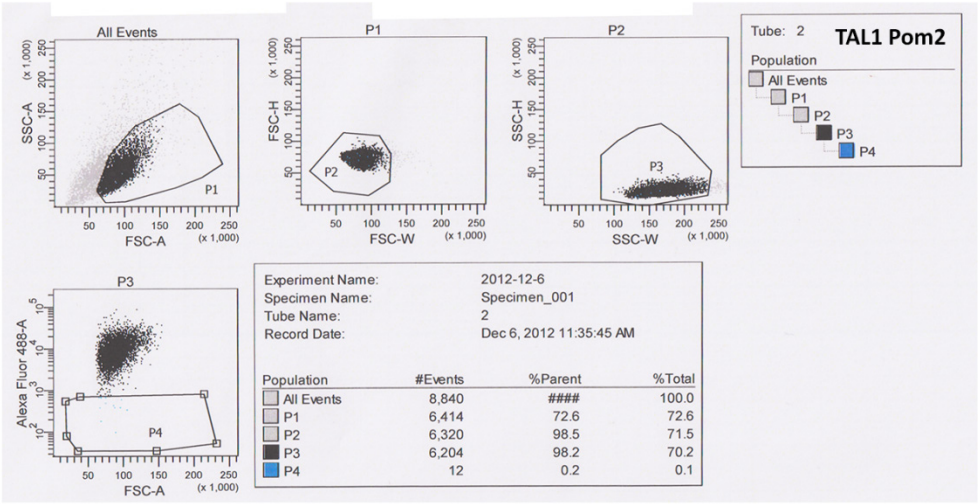
All Events
P1
P2
P3
P4
SSC-A
FSC-A
FSC-H
FSC-W
SSC-H
SSC-W
Alexa Fluor 488-A
(x 1,000)
Tube: 2
TAL1 Pom2
Population
All Events
Experiment Name: 2012-12-6
Specimen Name: Specimen_001
Tube Name: 2
Record Date: Dec 6, 2012 11:35:45 AM
Population #Events %Parent %Total
All Events 8,840 #### 100.0
P1 6,414 72.6 72.6
P2 6,320 98.5 71.5
P3 6,204 98.2 70.2
P4 12 0.2 0.1

D

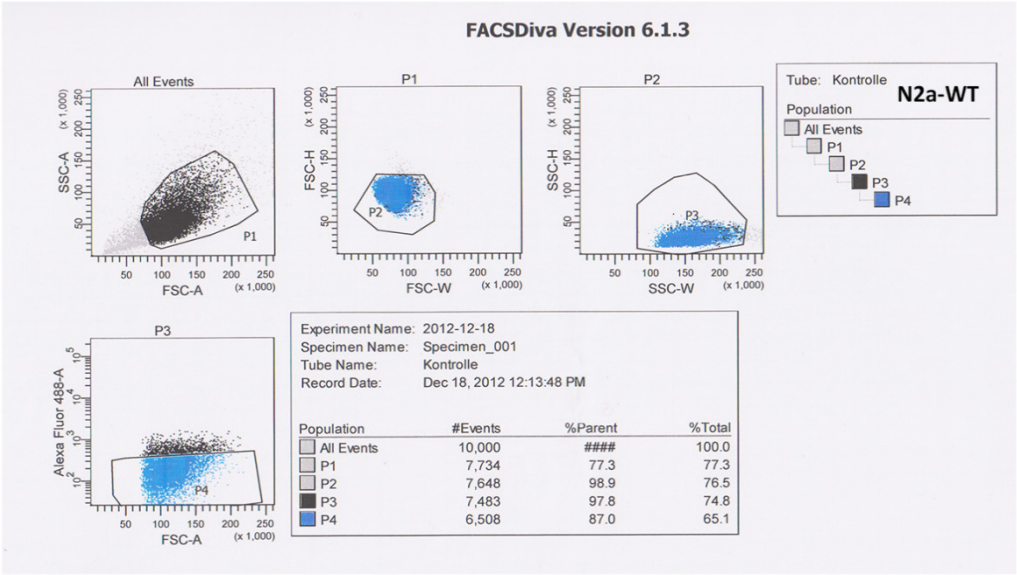
FACSDiva Version 6.1.3
All Events
P1
P2
P3
P4
SSC-A
FSC-A
FSC-H
FSC-W
SSC-H
SSC-W
Alexa Fluor 488-A
(x 1,000)
Tube: Kontrolle
N2a-WT
Population
All Events
Experiment Name: 2012-12-18
Specimen Name: Specimen_001
Tube Name: Kontrolle
Record Date: Dec 18, 2012 12:13:48 PM
Population #Events %Parent %Total
All Events 10,000 #### 100.0
P1 7,734 77.3 77.3
P2 7,648 98.9 76.5
P3 7,483 97.8 74.8
P4 6,508 87.0 65.1

E

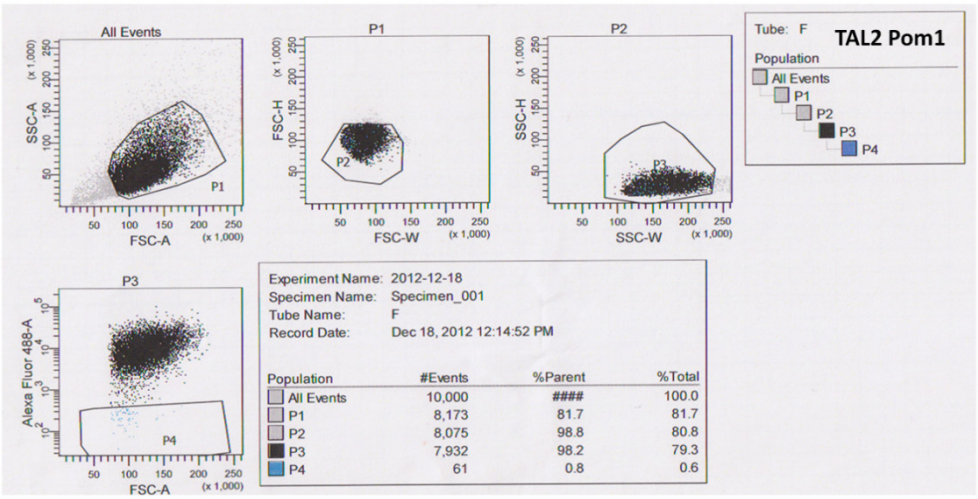
All Events
P1
P2
P3
P4
SSC-A
FSC-A
FSC-H
FSC-W
SSC-H
SSC-W
Alexa Fluor 488-A
(x 1,000)
Tube: F
TAL2 Pom1
Population
All Events
Experiment Name: 2012-12-18
Specimen Name: Specimen_001
Tube Name: F
Record Date: Dec 18, 2012 12:14:52 PM
Population #Events %Parent %Total
All Events 10,000 #### 100.0
P1 8,173 81.7 81.7
P2 8,075 98.8 80.8
P3 7,932 98.2 79.3
P4 61 0.8 0.6

Appendix 2: DNA sequence alignment of N2a-WT gDNA and the 1kb amplicon resulting from clone D4 gDNA using the primer combination mPrP-KO-F1 and mPrP-seq-R2.

Prnp start codon is highlighted in red.

```
N2a             ATGGCCTACTGGCATTTTGGTGTGTATGTTTTGACCTAGGGTGTGGTAATACTGCTCAAT 60
TAL_D4_1kb      ATGGCCTACTGGCATTTTGGTGTGTATGTTTTGACCTAGGGTGTGGTAATACTGCTCAAT 60
                ************************************************************

N2a             CGTCACTGTTGTCCTTAGCCTCTGCCCAGGGATCTCGTCTCAGGGTGAGTGAGGTCACTG 120
TAL_D4_1kb      CGTCACTGTTGTCCTTAGCCTCTGCCCAGGGATCTCGTCTCAGGGTGAGTGAGGTCACTG 120
                ************************************************************

N2a             ATCTGAAATGTTATATTTGATGAAGGCACACACTCATCGGAGGGTCGGAACTTGTGGGCG 180
TAL_D4_1kb      ATCTGAAATGTTATATTTGATGAAGGCACACACTCATCGGAGGGTCGGAACTAGTGGGCG 180
                *************************************************** *******

N2a             AGGCTGTTTGGTGTGTTTGCTGTTTTCTAAACTGTACTACCCCTTCTGTACAGAAAATCA 240
TAL_D4_1kb      AGGCTGTTTGGTGTGTTTGCTGTTTTCTAAACTGTACTACCCCTTCTGTACAGAAAATCA 240
                ************************************************************

N2a             AAAGGAAAAAACCACCCAAATACTAATACTAGCTGGTACATATCTATGATCTGAGTATTA 300
TAL_D4_1kb      AAAGGAAAAAACCACCCAAATACTAATACTAGCTGGTACATATCTATGATCTGAGTATTA 300
                ************************************************************

N2a             AAGAGGCTGAGTCAGGAGGATTGCCATGAGTTCAAAGCAAACCCAAGCTTCAAAGTAAAA 360
TAL_D4_1kb      AAGAGGCTGAGTCAGGAGGATTGCCATGAGTTCAAAGCAAACCCAAGCTTCAAAGTAAAA 360
                ************************************************************

N2a             CCCTATCTCCCTGACCCCTCAAAAAAAGCATTCATGCTGAACTCAAACTCACCACGTGTG 420
TAL_D4_1kb      CCCTATCTCCCTGACCCCTCAAAAAAAGCATTCATGCTGAACTCAAACTCACCACGTGTG 420
                ************************************************************

N2a             TGAGACTGCCGCACTTCTTGTGAATGCAGCTAGATGTATCTCAGCAGCCCAGCCCGCCCG 480
TAL_D4_1kb      TGAGACTGCCGCACTTCTTGTGAATGCAGCTAGATGTATCTCAGCAGCCCAGCCCGCCCG 480
                ************************************************************

N2a             GCTCTCTTGTCTATGGAGAGAGTGAGGAATTCTCAAGTGAGCCTGCCAAAACTCTAGATG 540
TAL_D4_1kb      GCTCTTTTGTCTATGGAGAGAGTGAGGAATTCTCAAGTGAGCCTGCCAAAACTCTAGATG 540
                ***** ******************************************************

N2a             TTTCCTGTCTCTGATAAACTTAGGTTGAAAATTCCCTCAAGGAGATTCTTGGCTTTGTGC 600
TAL_D4_1kb      TTTCCTGTCTCTGATAAACTTAGGTTGAAAATTCCCTCAAGGAGATTCTTGGCTTTGTGC 600
                ************************************************************

N2a             TTAGGGGATGTTAATTCCGTCACTTGACAGCTGTGTTGTGTCCTCCTCTGTGCCAGGCAC 660
TAL_D4_1kb      TTAGGGGATGTTAATTCCGTCACTTGACAGCTGTGTTGTGTCCTCCTT------------ 648
                **********************************************

N2a             TGCCCTTACCCATAAAATATGGCAACGAAACAGAGGCTCTTGGTTTGGTTTGGATTCTGG 720
TAL_D4_1kb      ------------------------------------------------------------


N2a             GGCATGAGCTGTAAAGCCCAGATGTATTAGAACTCACAGCCGTCCTGTTTCAGCCTCTAC 780
TAL_D4_1kb      ------------------------------------------------------------


N2a             TTCCCAAGTGCTGGGGCACCAACGTGCACTTCCTCATGCCTGGCTCTGGAGACCTACTGC 840
TAL_D4_1kb      ------------------------------------------------------------


N2a             TTGTCTCCAGGGCTCAAACACTGAGTCAGCTTTCTTCAAGTCCTTGCTCCTGCTGTAGCC 900
TAL_D4_1kb      ------------------------------------------------------------

N2a             ACTCAGGAGCCCTCCTGACTAGACCATGACTCAGGCCCTTGTGGTGTTACGGTTACTCAG 960
TAL_D4_1kb      ---------------------------------------------------GGCTACT--- 655
                                                                  ** ****
```

```
N2a             GACCAGTGTACTCACAGCTACCCCTGCAGGTGACTTTCTGCATTCTGGGGAATGAAGCCT 1020
TAL_D4_1kb      ------------------------------------------------------------

N2a             ACATCCGTGGATAAAGGTTCTCCTCTGTGTAGAGGCTCACACCCCACAGGACCCTGGGGC 1080
TAL_D4_1kb      ------------------------------------------------------------

N2a             CATTATAGCAGCCTTATAGTACAGCTGCCAGGCTCCCCACAAGATCATGCCCATTTCCAA 1140
TAL_D4_1kb      ------------------------------------------------------------

N2a             ATTCCACTACATTGTTAAAGCTCAAAGCCATGGCGTAACAACCATGCAATATCACCTAGA 1200
TAL_D4_1kb      ------------------------------------------------------------

N2a             CCAGACGTGGTTTACCAGTTGGGGTAACTCTTGTCAAATCTGTCCTCAGAGGATGGGATG 1260
TAL_D4_1kb      ------------------------------------------------------------

N2a             AGCTGTGTGTTTTTGATTTACTTTTTTCCTGAAGGAAAAGCTACGGGGGGGGGGGGGGGG 1320
TAL_D4_1kb      ------------------------------------------------------------

N2a             CGGGGGGGAGGGTTGACGCCATGACTTTCATACATTTGCTTTGTAGATAGATGTCAAGGA 1380
TAL_D4_1kb      ------------------------------------------------------------

N2a             CCTTCAGCCTAAATACTGGGCACTGATACCTTGTTCCTCATTTTGCAGATCAGTCATCAT 1440
TAL_D4_1kb      ------------------------------------------------------------

N2a             GGCGAACCTTGGCTACTGGCTGCTGGCCCTCTTTGTGACTATGTGGACTGATGTCGGCCT 1500
TAL_D4_1kb      GGCGAACCTTGGCTACTGGCTGCTGGCCCTCTTTGTGACTATGTGGACTGATGTCGGCCT 715
                ************************************************************

N2a             CTGCAAAAAGCGGCCAAAGCCTGGAGGGTGGAACACCGGTGGAAGCCGGTATCCCGGGCA 1560
TAL_D4_1kb      CTGCAAAAAGCGGCCAAAGCCTGGAGGGTGGAACACCGGTGGAAGCCGGTATCCCGGGCA 775
                ************************************************************

N2a             GGGAAGCCCTGGAGGCAACCGTTACCCACCTCAGGGTGGCACCTGGGGGCAGCCCCACGG 1620
TAL_D4_1kb      GGTAAGCCCTGGAGGCAACCGTTACCCACCTCAGGGTGGCACCTGGGGGCAGCCCCACGG 835
                ** *********************************************************

N2a             TGGTGGCTGGGGACAACCCCATGGGGGCAGCTGGGGACAACCTCATGGTGGTAGTTGGGG 1680
TAL_D4_1kb      TGGTGGCTGGGGACAACCCCATGGGGGCAGCTGGGGACAACCTCATGGTGGTAGTTGGGG 895
                ************************************************************

N2a             TCAGCCCCATGGCGGTGGATGGGGCCAAGGAGGGGGTACCCATAATCAGTGGAACAAGCC 1740
TAL_D4_1kb      TCAGCCCCATGGCGGTGGATGGGGCCAAGGAGGGGGTACCCATAATCAGTGGAACAAGCC 955
                ************************************************************

N2a             CAGCAAACCAAAAACCAACCTCAAGCATGTGGCAGGGGCTGCGGCAGCTGGGGCAGTAGT 1800
TAL_D4_1kb      CAGCAAACCAAAAACCAACCTCAAGCATGTGGCAGGGGCTGCGGCAGCTGGG-------- 1007
                **************************************************
```

Appendix 3: DNA sequence alignment of N2a-WT gDNA and the 1.8kb amplicon resulting from clone D4 gDNA using the primer combination mPrP-KO-F1 and mPrP-seq-R2.

Prnp start codon is highlighted in red.

```
N2a                 CACGTGTGGTCTAGAGCTAGCCTAGGCTCGAGAAGCTTGTCGACGAATTCAGATTATGGC 60
TAL_D4_1.8kb_cl1    CACGTGTGGTCTAGAGCTAGCCTAGGCTCGAGAAGCTTGTCGACGAATTCAGATTATGGC 60
                    ************************************************************

N2a                 CTACTGGCATTTTGGTGTGTATGTTTTGACCTAGGGTGTGGTAATATTGCTCAATCGTCA 120
TAL_D4_1.8kb_cl1    CTACTGGCATTTTGGTGTGTATGTTTTGACCTAGGGTGTGGTAATATTGCTCAATCGTCA 120
                    ************************************************************

N2a                 CTGTTGTCCTTAGCCTCTGCCCAGGGATCTCGTCTCAGGGTGAGTGAGGTCACTGATCTG 180
TAL_D4_1.8kb_cl1    CTGTTGTCCTTAGCCTCTGCCCAGGGATCTCGTCTCAGGGTGAGTGAGGTCACTGATCTG 180
                    ************************************************************

N2a                 AAATGTTATATTTGATGAAGGCACACACTCATCGGAGGGTCGGAACTTGTGGGCGAGGCT 240
TAL_D4_1.8kb_cl1    AAATGTTATATTTGATGAAGGCACACACTCATCGGAGGGTCGGAACTTGTGGGCGAGGCT 240
                    ************************************************************

N2a                 GTTTGGTGTGTTTGCTGTTTTCTAAACTGTACTACCCCTTCTGTACAGAAAATCAAAAGG 300
TAL_D4_1.8kb_cl1    GTTTGGTGTGTTTGCTGTTTTCTAAACTGTACTACCCCTTCTGTACAGAAAATCAAAAGG 300
                    ************************************************************

N2a                 AAAAAACCACCCAAATACTAATACTAGCTGGTACATATCTATGATCTGAGTATTAAAGAG 360
TAL_D4_1.8kb_cl1    AAAAAACCACCCAAATACTAATACTAGCTGGTACATATCTATGATCTGAGTATTAAAGAG 360
                    ************************************************************

N2a                 GCTGAGTCAGGAGGATTGCCATGAGTTCAAAGCAAACCCAAGCTTCAAAGTAAAACCCTA 420
TAL_D4_1.8kb_cl1    GCTGAGTCAGGAGGATTGCCATGAGTTCAAAGCAAACCCAAGCTTCAAAGTAAAACCCTA 420
                    ************************************************************

N2a                 TCTCCCTGACCCCTCAAAAAAAGCATTCATGCTGAACTCAAACTCACCACGTGTGTGAGA 480
TAL_D4_1.8kb_cl1    TCTCCCTGACCCCTCAAAAAAAGCATTCATGCTGAACTCAAACTCACCACGTGTGTGAGA 480
                    ************************************************************

N2a                 CTGCCGCACTTCTTGTGAATGCAGCTAGATGTATCTCAGCAGCCCAGCCCGCCCGGCTCT 540
TAL_D4_1.8kb_cl1    CTGCCGCACTTCTTGTGAATGCAGCTAGATGTATCTCAGCAGCCCAGCCCGCCCGGCTCT 540
                    ************************************************************

N2a                 CTTGTCTATGGAGAGAGTGAGGAATTCTCAAGTGAGCCTGCCAAAACTCTAGATGTTTCC 600
TAL_D4_1.8kb_cl1    CTTGTCTATGGAGAGAGTGAGGAATTCTCAAGTGAGCCTGCCAAAACTCTAGATGTTTCC 600
                    ************************************************************

N2a                 TGTCTCTGATAAACTTAGGTTGAAAATTCCCTCAAAGAGATTCTTGGCTTTGTGCTTAGG 660
TAL_D4_1.8kb_cl1    TGTCTCTGATAAACTTAGGTTGAAAATTCCCTCAAAGAGATTCTTGGCTTTGTGCTTAGG 660
                    ************************************************************

N2a                 GGATGTTAATTCCGTCACTTGACAGCTGTGTTGTGTCCTCCTCTGTGCCAGGCACTGCCC 720
TAL_D4_1.8kb_cl1    GGATGTTAATTCCGTCACTTGACAGCTGTGTTGTGTCCTCCTCTGTGCCAGGCACTGCCC 720
                    ************************************************************

N2a                 TTACCCATAAAATATGGCAACGAAACAGAGGCTCTTGGTTTGGTTTGGATTCTGGGGCAT 780
TAL_D4_1.8kb_cl1    TTACCCATAAAATATGGCAACGAAACAGAGGCTCTTGGTTTGGTTTGGATTCTGGGGCAT 780
                    ************************************************************

N2a                 GAGCTGTAAAGCCCAGATGTATTAGAACTCACAGCCGTCCTGTTTCAGCCTCTACTTCCC 840
TAL_D4_1.8kb_cl1    GAGCTGTAAAGCCCAGATGTATTAGAACTCACAGCCGTCCTGTTTCAGCCTCTACTTCCC 840
                    ************************************************************

N2a                 AAGTGCTGGGGCACCAACGTGCACTTCCTCATGCCTGGCTCTGGGGACCTACTGCTTGTC 900
TAL_D4_1.8kb_cl1    AAGTGCTGGGGCACCAACGTGCACTTCCTCATGCCTGGCTCTGGGGACCTACTGCTTGTC 900
                    ************************************************************

N2a                 TCCAGGGCTCAAACACTGAGTCAGCTTTCTTCAAGTCCTTGCTCCTGCTGTAGCCACTCA 960
TAL_D4_1.8kb_cl1    TCCAGGGCTCAAACACTGAGTCAGCTTTCTTCAAGTCCTTGCTCCTGCTGTAGCCACTCA 960
                    ************************************************************


N2a                 GGAGCCCTCCTGACTAGACCATGACTCGGCCCTTGTGGTGTTACGGTTACTCAGGACCAG 1020
TAL_D4_1.8kb_cl1    GGAGCCCTCCTGACTAGACCATGACTCGGCCCTTGTGGTGTTACGGTTACTCAGGACCAG 1020
                    ************************************************************

N2a                 TGTACTCACAGCTACCCCTGCAGGTGACTTTCTGCATTCTGGGGAATGAAGCCTACATCC 1080
TAL_D4_1.8kb_cl1    TGTACTCACAGCTACCCCTGCAGGTGACTTTCTGCATTCTGGGGAATGAAGCCTACATCC 1080
                    ************************************************************
```

```
N2a                 GTGGATAAAGGTTCTCCTCTGTGTAGAGGCTCACACCCCACAGGACCCTGGGGCCATTAT 1140
TAL_D4_1.8kb_cl1    GTGGATAAAGGTTCTCCTCTGTGTAGAGGCTCACACCCCACAGGACCCTGGGGCCATTAT 1140
                    ************************************************************

N2a                 AGCAGCCTTATAGTACAGCTGCCAGGCTCCCCACAAGATCATGCCCATTTCCAAATTCCA 1200
TAL_D4_1.8kb_cl1    AGCAGCCTTATAGTACAGCTGCCAGGCTCCCCACAAGATCATGCCCATTTCCAAATTCCA 1200
                    ************************************************************

N2a                 CTACATTGTTAAAGCTCAAAGCCATGGCGTAACAACCATGCAATATCACCTAGACCAGAC 1260
TAL_D4_1.8kb_cl1    CTACATTGTTAAAGCTCAAAGCCATGGCGTAACAACCATGCAATATCACCTAGACCAGAC 1260
                    ************************************************************

N2a                 GTGGTTTACCAGTTGGGGTAACTCTTGTCAAATCTGTCCTCAGAGGATGGGATGAGCTGT 1320
TAL_D4_1.8kb_cl1    GTGGTTTACCAGTTGGGGTAACTCTTGTCAAATCTGTCCTCAGAGGATGGGATGAGCTGT 1320
                    ************************************************************

N2a                 GTGTTTTTGATTTACTTTTTTCCTGAAGGAAAAGCTACGGGGGGGGGGGGGCGGGGGGGA 1380
TAL_D4_1.8kb_cl1    GTGTTTTTGATTTACTTTTTTCCTGAAGGAAAAGCTACGGGGGGGGGGGGGCGGGGGGGA 1380
                    ************************************************************

N2a                 GGGTTGACGCCATGACTTTCATACATTTGCTTTGTAGATAGATGTCAAGGACCTTCAGCC 1440
TAL_D4_1.8kb_cl1    GGGTTGACGCCATGACTTTCATACATTTGCTTTGTAGATAGATGTCAAGGACCTTCAGCC 1440
                    ************************************************************

N2a                 TAAATACTGGGCACTGATACCTTGTTCCTCATTTTGCAGGTCAGTCATCATGGCGAACCT 1500
TAL_D4_1.8kb_cl1    TAAATACTGGGCACTGATACCTTGTTCCTCATTTTGCAGGTCAGTCATCATGGCGAACCT 1500
                    ************************************************************

N2a                 TGGCTACTGGCTGCTGGCCCTCTTTGTGACTATGTGGACTGATGTCGGCCTCTGCAAAAA 1560
TAL_D4_1.8kb_cl1    TGGCTACTGGCTGCTGGCCCTCTTTGTGACTATGTGGACTGATGTCGGCCTCTGCAAAAA 1560
                    ************************************************************

N2a                 GCGGCCAAAGCCTGGAGGGTGGAACACCGGTGGAAGCCGGTATCCCGGGCAGGGAAGCCC 1620
TAL_D4_1.8kb_cl1    GCGGCCAAAGCCTGGAGGGTGGAACACCGGTGGAAGCCGGTATCCCGGGCAGGGAAGCCC 1620
                    ************************************************************

N2a                 TGGAGGCAACCGTTACCCACCTCAGGGTGGCACCTGGGGGCAGCCCCACGGTGGTGGCTG 1680
TAL_D4_1.8kb_cl1    TGGAGGCAACCGTTACCCACCTCAGGGTGGCACCTGGGGGCAGCCCCACGGTGGTGGCTG 1680
                    ************************************************************

N2a                 GGGACAACCCCATGGGGGCAGCTGGGGACAACCTCATGGTGGTAGTTGGGGTCAGCCCCA 1740
TAL_D4_1.8kb_cl1    GGGACAACCCCATGGGGGCAGCTGGGGACAACCTCATGGTGGTAGTTGGGGTCAGCCCCA 1740
                    ************************************************************

N2a                 TGGCGGTGGATGGGGCCAAGGAGGGGGTACCCATAATCAGTGGAACAAGCCCAGCAAACC 1800
TAL_D4_1.8kb_cl1    TGGCGGTGGATGGGGCCAAGGAGGGGGTACCCATAATCAGTGGAACAAGCCCAGCAAACC 1800
                    ************************************************************

N2a                 AAAAACCAACCTCAAGCATGTGGCAGGGGCTGCGGCAGCTGGGGCAGTAGTGGAATCACG 1860
TAL_D4_1.8kb_cl1    AAAAACCAACCTCAAGCATGTGGCAGGGGCTGCGGCAGCTGGGGCAGTAGTGGAATCACG 1860
                    ************************************************************

N2a                 AATTCTGGATCCGATACGTAACG 1883
TAL_D4_1.8kb_cl1    AATTCTGGATCCGATACGTAACG 1883
                    ***********************
```

Eidesstattliche Versicherung

Sehr geehrte Damen und Herren,

hiermit erkläre ich an Eides statt, dass ich die vorliegende Dissertationsschrift selbst verfasst und keine anderen als die angegebenen Quellen und Hilfsmittel verwendet habe.

Ich versichere außerdem, dass ich die beigefügte Dissertation nur in diesem und keinem anderen Promotionsverfahren eingereicht habe und, dass diesem Promotionsverfahren keine endgültig gescheiterten Promotionsverfahren vorausgegangen sind.

Hamburg, den 17. Dezember 2014

_____
Unterschrift